UNCERTAINTY ANALYSIS FOR ROCKET-BASED COMBINED CYCLE (RBCC) SYSTEMS TESTING

By

Boon-Chuan Law

A Thesis
Submitted to Faculty of
Mississippi State University
in Partial Fulfillment of the Requirement
for the Degree of Master of Science
in Mechanical Engineering
in the Department of Mechanical Engineering

Mississippi State, Mississippi

August 2003

UNCERTAINTY ANALYSIS FOR ROCKET-BASED COMBINED CYCLE (RBCC) SYSTEMS TESTING

By

Boon-Chuan Law

Approved:

Susan T. Hudson Adjunct Assistant Professor of Mechanical Engineering (Director of Thesis)	Rogelio Luck Graduate Coordinator Department of Mechanical Engineering
B. K. Hodge Professor of Mechanical Engineering (Committee Member)	W. Glenn Steele Professor and Head of Mechanical Engineering (Committee Member)
A. Wayne Bennett Dean of the College of Engineering	

Name: Boon-Chuan Law

Date of Degree: August 2, 2003

Institution: Mississippi State University

Major Field: Mechanical Engineering

Major Professor: Dr. Susan T. Hudson

Title of Study: UNCERTAINTY ANALYSIS FOR ROCKET-BASED COMBINED CYCLE (RBCC) SYSTEMS TESTING

Pages in Study: 138

Candidate for Degree of Master of Science

General uncertainty analysis was used to evaluate the performance of a Rocket-Based Combined Cycle (RBCC) engine system. To estimate the uncertainties of test results, uncertainties of basic measurements such as temperature, pressure, mass flow rate, and thrust were determined. The desired test results of interest included specific impulse and characteristic velocity. Various possible test facilities were reviewed to obtain background information and example test run conditions. Based on the test run conditions, five methods of determining specific impulse were evaluated. Also, theoretical and actual characteristic velocities were analyzed to evaluate C* efficiency. Initially, general uncertainty analyses were completed relative to 1% accuracy for each measured variable. Then, cases were run using more realistic uncertainty estimates. The relative contributions of the different variables' uncertainties to the overall uncertainty of the selected performance parameters were also calculated. This process helps to identify

the critical measurements from an uncertainty standpoint and can be a significant guide in the cost effective use of resources to reduce the test uncertainty.

ACKNOWLEDGEMENTS

Words cannot describe how grateful I am for those who helped me in the process of completing my research work. I will always remember the sincere help and guidance from my major professor, Dr. Susan T. Hudson. Indeed, I appreciate her patience in guiding and assisting me throughout the master's program. She is an excellent teacher and a great boss as well. Moreover, I would like to address my special thanks to both Dr. W. Glenn Steele and Dr. B. K. Hodge for their help and guidance that have motivated me to pursue my master's degree.

Last but not least, I would not have completed my master's degree if not for the support, guidance, and love from my family members, especially my parents and my beloved wife. I will always cherish every moment spent in the process of completing my research work.

TABLE OF CONTENTS

CHAPTER Page

APPENDIX Page

LIST OF TABLES

TABLE Page

LIST OF FIGURES

FIGURE Page

LIST OF SYMBOLS AND VARIABLES

VARIABLE		DEFINITION
C_d	=	Discharge coefficient
C_F	=	Thrust coefficient
Cp_{eff}	=	Effective specific heat
C*	=	Characteristic velocity
D	=	Meter inside diameter
d	=	Diameter
F_a	=	Thermal expansion factor
F	=	Thrust force
Isp	=	Specific impulse
M	=	Molecular weight
P	=	Pressure
ΔP	=	Pressure difference
Q	=	Volumetric flow rate
Rc	=	Specific gas constant
T	=	Temperature
w	=	Mass flow rate
Y	=	Expansion factor
β	=	Ratio of throat to pipe diameter

VARIABLE		DEFINITION
γ	=	Specific heat ratio
λ	=	Nozzle divergence factor
ρ	=	Density
θ	=	Nozzle divergence angle

Subscript

1, c	=	Chamber or pipe inlet
2, t	=	Throat (applied to nozzle and mass flow devices)
e	=	Nozzle exit
3	=	Atmospheric condition
f	=	Fuel
o	=	Oxidizer

CHAPTER I

INTRODUCTION

Uncertainty analyses are developed in this study to realize the greatest benefit of Rocket Based Combined Cycle (RBCC) engine testing. This research work describes the methods used to evaluate the basic measurement uncertainties associated with pressure, temperature, mass flow rate, and thrust. These measurement uncertainties are then used to estimate the uncertainties of the specific impulse and characteristic velocity for both ground and altitude testing using uncertainty analysis techniques. Initially, 1% uncertainty estimates are assumed for each variable. Then, more specific uncertainty estimate variation cases are run to illustrate the usefulness of the uncertainty analysis techniques. This study includes the data reduction methods with the description for the selected performance parameters. A general uncertainty analysis is performed for each of the data reduction methods. The relative contributions of the different variables' uncertainties to the overall uncertainties of the selected performance parameters are also included. This process can help to identify the critical measurements from an uncertainty standpoint and can be a significant guide in the cost effective use of resources to reduce the test uncertainty.

This study is limited to evaluating the data reduction equations for the performance parameters of interest relative to the uncertainties of the equation input variables. Uncertainties associated with the assumptions made to derive the data

reduction equations are not included. Therefore, caution is advised when comparing the results of different methods. Full comparisons can only be made once the assumptions have been considered. The current work will be extended in this sense in the future.

1.1 Background

The dream of being able to take off from a U.S. airport and travel to space at a price comparable to flying abroad with the Concorde will come true one day with the advance of NASA's launch technology program. With the dream in mind, multiple air-breathing engine configurations are being developed and tested. Rocket-Based Combined Cycle (RBCC) is one of the air-breathing engine concepts being tested [1].

Rocket Based Combined Cycle (RBCC) propulsion combines elements of rocket and air breathing propulsion into a single, integrated engine. RBCC engines are capable of operating in several modes such as ducted rocket, ramjet, scramjet, and pure rocket. Vehicles employing RBCC engines will have a higher trajectory-averaged specific impulse than conventional rockets by utilizing atmospheric oxygen over a portion of the ascent trajectory. Therefore, RBCC vehicle will be capable of carrying heavier payloads. In coming decades, air-breathing technologies will dramatically reduce the cost to orbit, reduce trip time between destinations, and increase vehicle reliability as well as crew safety.

RBCC propulsion systems consist of four modes of operation. Initially, an air-augmented rocket provides high specific impulse at speeds, such as Mach 0 to 3.5

conditions. The ramjet mode, for example Mach 3.5 to 7, uses an air-breathing jet engine without a mechanical compressor or turbine. Compression is accomplished entirely by ram; thus, ramjet mode is sensitive to vehicle forward speed and non-existent at rest. The scramjet mode (~Mach 7) features supersonic air-flow throughout the engine as the altitude increases. Both ramjet and scramjet are mechanically simpler, but aerodynamically more complex, than conventional jet engines; therefore, ramjet and scramjet provide much greater efficiency, permitting long-duration hypersonic flight [2]. The last mode is pure rocket only where the air inlet is closed, usually from Mach 8 and above. The on-board rocket will provide the final boost to low earth orbit. (Note that the Mach number of the four modes of operation is only an example and the Mach number for the modes may vary slightly.)

Recently, design and testing of RBCC propulsion systems have successfully been completed at a sub-scale level, with the results warranting further engine development. This further development is known as ISTAR, Integrated System Test of an Air-breathing Rocket. Under ISTAR, a flight-weight RBCC propulsion system having a thrust on the order of 50K pounds force will be developed to serve as a test bed. Extensive ground testing and altitude testing of RBCC components, subsystems, and engine systems across all propulsion operational modes, except the final rocket mode, will be initiated under ISTAR.

The RBCC concept for ISTAR uses the Strutjet air-breathing engine with six rockets thrusters in each strut. There are a total of four flow paths and each has three struts. Therefore, 18 rocket thrusters can be found in one flow path for a total of 72 rocket

thrusters for the four flow paths (full system). Figure 1-1 shows the Strutjet RBCC with the full system and rocket thrusters. A detailed discussion can be found in reference 3.

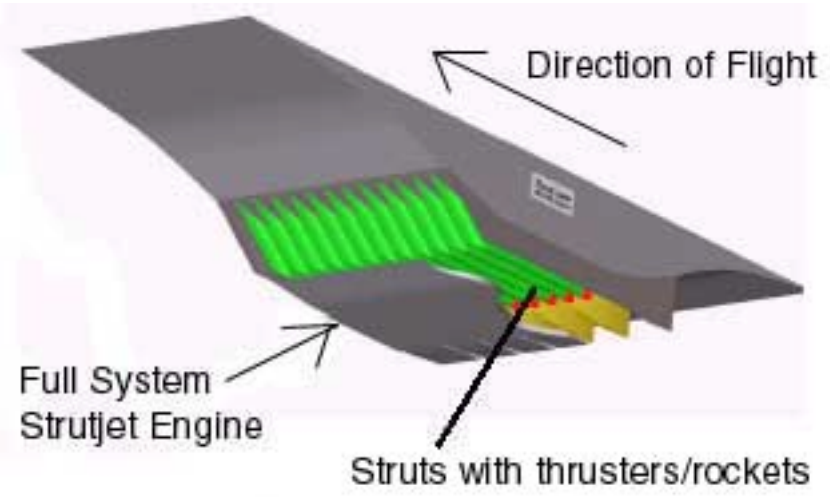

Figure 1-1: Strutjet Engine with Integrated Strutrockets used in RBCC Engine

Ground and altitude testing at 50% of the full-scale level for only one flow path is planned for the ISTAR program. However a variety of RBCC engine testing will occur at various test centers based on each center's expertise.

1.2 Project Objective

The purpose of this study was to realize the greatest benefit of Rocket Based Combined Cycle (RBCC) engine testing by using uncertainty analysis techniques with the focus to determine the specific impulse and characteristic velocity of the engine.

Specific impulse, Isp, is the thrust force per unit weight of propellant and it is an important figure of merit of the performance of a rocket propulsion system, which is similar to the concept of miles per galloon parameter used with automobiles. A higher specific impulse means better performance of the engines. Five methods to obtain specific impulse will be evaluated in this study to determine the uncertainty associated with each method. Characteristic velocity, C* (ft/sec), is independent of nozzle characteristics and can be determined by experimental data of chamber pressure, throat diameter, and propellant mass flow rate. C* efficiency is also an important performance parameter as it is used to express the degree of completion of the energy release and the creation of high temperature and pressure gas in the chamber.

Uncertainty is defined as the interval around a result from an experiment or a design calculation where the true result is expected to lie with a certain degree of confidence. A 95% degree of confidence is frequently used in engineering applications. Five data reduction methods of determining the specific impulse were explored in this study to determine the uncertainty associated with each method. Characteristic velocity was also evaluated. With the use of uncertainty analysis techniques, critical measurement uncertainties can be identified and these will provide guidance for the design of the RBCC engine system in the future.

1.3 Test Facility Review

Based on each Center's expertise, various test facilities have been considered for RBCC engine ground testing and altitude testing. This study includes examples of test facilities and run conditions that may be used. Uncertainty analysis techniques are used to evaluate the specific impulse and characteristic velocity uncertainties based on the run conditions that may be achieved during testing.

RBCC engine testing initiated by the ISTAR program is the flight-weight ground test bed of an RBCC engine. The primary ISTAR industry development team includes Rocketdyne Propulsion & Power (The Boeing Co.) of Canoga Park, California; Pratt & Whitney Space Propulsion (United Technologies Corp.) of West Palm Beach, Florida; and Aerojet Missile and Space Propulsion (GenCorp, Inc.) of Sacremento, California. This team is known as the Rocket Based Combined Cycle Consortium or RBC^3. Testing may be carried out by any of the consortium members. Other possible test facilities are located at NASA Langley Research Center, NASA Dryden Flight Research Center, Arnold Engineering Development Center (AEDC), GASL Test Complex, and NASA Glenn Research Center [1]. Brief overviews of some of these facilities are given in the following paragraphs.

The Aerodynamic and Propulsion Test Unit (APTU) at Arnold Engineering Development Center (AEDC) is a blow-down, freejet test facility designed for true temperature aerodynamic, propulsion, and material/structures freejet testing. A vitiated air heater (VAH) provides the required temperature. Liquid oxygen (LOX) is added

upstream of the VAH to provide the correct oxygen mole fraction at the freejet nozzle exit plane for use by the test article. Multiple nozzles are available to cover a range of APTU test conditions from Mach numbers 2.2 to 4.1 and exit diameters from 32 inches to 38 inches. The test capability upgrade for APTU was designed to provide a flow total temperature of 4700 ^{o}R at a total pressure as high as 2800 psia and a mass flow rate up to 180 lb_m/sec. Two nozzles are available with area ratios of 16.63 and 296.3. Both nozzles have an exit diameter of 42 inches. The throat diameter for each nozzle is 2.53 inches and 0.14 inches. Further discussion can be found in reference [4].

Glenn Research Center, Plum Brook Station is the primary NASA site for altitude testing of medium/large test articles in the 1K to 400K pounds thrust range, including all liquid oxygen and liquid hydrogen testing. The Hypersonic Tunnel Facility (HTF) is a blow-down, freejet wind tunnel that is capable of simulating true enthalpy flight conditions at Mach 5, 6, and 7. The facility uses non-vitiated flow. The high stagnation temperatures required for simulating true enthalpy are produced by flowing clean nitrogen gas through a 3 MW graphite core storage heater. Clean gaseous oxygen is mixed with the heated gaseous nitrogen to yield the test medium of simulated air. Stagnation temperature, stagnation pressure, and altitude are controlled during tunnel operation to generate the desired test conditions. Three discrete hypersonic nozzles, each with an exit diameter of 42 inches, are used to set the facility Mach number conditions 5, 6, or 7. The facility spans from 20.7 to 36.6 km (68,000 to 120,000 ft) altitude, 0.48 to 8.27 MPa (70 to 1200 psia) nozzle inlet stagnation pressure, and 1220 to 2170 K (2200 to 3900 R) nozzle inlet stagnation temperature. Table 1-1 outlines the operating ranges and

maximum run times for each Mach number condition. The facility's size and long run duration allow for component and full systems testing of flight-rated structures and air breathing propulsion systems. The facility is capable of supporting both hydrogen and hydrocarbon-fueled propulsion systems. The use of non-vitiated flow for propulsion testing most closely represents actual flight conditions and minimizes potential discrepancies between ground testing and flight performance. The use of the HTF to support direct-connect testing is currently being developed to allow testing of large-scale combustors in a non-vitiated flow [5].

The Langley 8-Foot High Temperature Tunnel (8-Ft HTT) at NASA Langley Research Center is a combustion-heated, hypersonic, blow-down-to-atmosphere wind tunnel that provides simulation of flight enthalpy for Mach numbers of 4, 5, and 7 through altitude range from 50,000 to 120,000 ft. The open-jet test section is 8 ft in diameter and 12-ft long. The test section will accommodate very large models, air-breathing hypersonic propulsion systems, and structural and thermal protection system (TPS) components. Stable wind tunnel test conditions can be provided up to 60 sec. The facility uses standard strain gauges, pressure transducers, electronically-scanned pressure (ESP), and thermocouple instrumentation mounted inside or outside the model. The range of the run conditions is presented in Table 1-2. Hypersonic air breathing propulsion system tests are performed with the propulsion test article (e.g., Hyper-X flight vehicle) attached to a model support pedestal mounted on an external force measurement balance. Propellant fuel (e.g., gaseous hydrogen, liquid hydrocarbon) and purge gases are supplied to the test article by the facility [6].

Mach No.	Nozzle					Test Section		
	Stagnation Pressure, MPa (psia)	Stagnation Temperature, K (^{o}R)	Mass Flow, kg/sec (lb_m/sec)	D_t, in	D_e, in	Altitude, km (kft)	Run Time, sec	
5	2.83 (410)	1222 (2200)	86 (189)	7.2	42.0	20.7 (68)	103	a
	0.48 (70)	1344 (2420)	14 (31)	7.2	42.0	32.9 (108)	294	b
6	8.27 (1200)	1647 (2965)	101 (222)	4.9	42.0	21.9 (72)	42	a
	1.00 (144)	1839 (3310)	12 (25)	4.9	42.0	36.6 (120)	294	b
7	8.27 (1200)	2128 (3830)	47 (104)	3.2	42.0	28.3 (93)	90	a
	2.96 (430)	2167 (3900)	16 (36)	3.2	42.0	36.6 (120)	180	c

Table 1-1: Hypersonic Tunnel Facility Upper and Lower Operating Limits

a – Limited by maximum stagnation temperature change of 111 ^{o}C (200 ^{o}F)
b – Limited by steam availability
c – Limited by diffuser and mixer temperature limits

Mach No.	Stagnation Pressure, psia	Stagnation Temperature, ^{o}R	Dynamic Pressure, psf	Altitude Simulation, kft
4	50 - 310	1640	525 - 3100	47 – 85
5	90 - 530	2350	350 - 2000	65 – 100
7	600 - 3500	2500 - 3650	320 - 1900	80 - 120

Table 1-2: Langley 8-Foot High-Temperature Tunnel Run Conditions

The Combustion-Heated Scramjet Test Facility (CHSTF) at NASA Langley Research Center offers the capability to test subscale propulsive flow-paths (inlet, combustor, partial nozzle, etc.) of hypersonic vehicles at conditions simulating Mach numbers from 3.5 to 6.0. The facility normally operates at heater stagnation pressures

between 50 and 500 psia and stagnation temperatures between 1300 ^{o}R and 3000 ^{o}R. Test gas mass flow rates range from 15 to 60 lb_m/sec [7].

Flight-testing is offered at NASA's Dryden Flight Research Center. Full-flight envelope direct-thrust measurements using strain gages on a supersonic aircraft offers advantages over analytical-based thrust calculation methods. The direct thrust measurement method uses a simpler sensor arrangement and minimal data processing compared to analytical techniques, which normally require costly engine modeling and multi-sensor arrangements throughout the engine. However, direct thrust measurement produces less accuracy due to the difficulty in mounting and calibrating the strain gages as well as their ability to account for the secondary forces that influence the thrust reading at the engine mount. Therefore, the strain-gage technique has been used primarily in the subsonic speed range. NASA Dryden Flight Research Center successfully applied the strain gage-based direct thrust-measurement technique on a supersonic aircraft to a maximum speed of Mach 2.0 [8].

Boeing Rocketdyne's Rocket Nozzle Test Facility (RNTF) provides the capability to cold-flow test, reduced-scale propulsion system models to evaluate the relative performance effects of configuration and operating condition changes. The RNTF facility operates in a blow-down mode providing high-pressure nitrogen flow through a model propulsion system while the effects of operation with different model back pressures or configurations are investigated. The third flow stream has been used to simulate inlet flows for air-breathing engines with the capability of 20 lb_m/sec flow rate at 1015 psia total pressure. Any desired pressure between 1015 to 5015 psia can be set. A

single-component balance is available to measure model thrust with a replaceable load cell whose range can be selected for the expected thrust. A six-component balance assembly is also available for tests requiring determination of secondary forces and moments, but requires detailed calibration and has not been used extensively. To simulate air-augmented operation of an RBCC engine, a full-scale engine is tested at low-pressure ratios, average 10. The testing is done with model inlet flow, and another at low-pressure ratios with flow only through the simulated rocket motors. For air-augmented tests, flow temperatures can be obtained up to 500 ^{o}F. Reference [9] provides more details.

GASL's Blow-down Test Complex consists of five active test facilities all capable of accelerating enthalpies to free-stream Mach 8 conditions. A new combustion-heated test facility, called Leg VI, has been incorporated into the GASL Aerospace Test Complex. Leg VI resides in a newly constructed wing at GASL's Long Island operation though this facility is an integral part of the Blow-down Laboratory. Facility features include the capability of operating from free-stream Mach 2 to 8. Future plans for the Leg VI facility include upgrades enabling (1) trajectory simulations, (2) runtimes to several minutes, (3) measurement of multi-component forces and moments on the engine models, (4) testing of model sizes to 20 ft in length and inlet capture areas representative of 10,000 pound thrust-class engines. Legs I and II utilize fully-integrated thrust stands and combustion-fired air heaters. The direct-connect facilities are capable of flowing at a maximum 80 lb_m/sec of test gas with equivalent flight dynamic pressures of 4000 psf. Leg III is a smaller scale facility, similar to the direct-connect legs used to create high

heating rates in an environment for the evaluation of high temperature materials and actively-cooled structures. The complex also contains two freejet test facilities, Leg IV and V, capable of generating dynamic pressures to 1000 psf at Mach 8. The Leg V test facility, known as the Flight Acceleration Simulation Test (FAST) facility, has the ability to "fly" a trajectory on the ground with real-time variation of Mach number, enthalpy, and dynamic pressure. Another unique feature of this facility is the ability to rapidly open the test cabin, allowing an engineer to inspect the engine at the completion of each test with little time delay. The current type of testing performed at GASL with its rapid model access is extremely beneficial to the Rocket Based Combined Cycle (RBCC) engines with imbedded rockets, in which routine inspections are required. More details can be found in reference [10].

The Propulsion Systems Laboratory (PSL) at NASA Glenn Research Center is a ground-based test facility that can provide true flight simulation for experimental research on air-breathing propulsion systems. Two engine test cells, PSL-3 and PSL-4, with the Mach number capabilities up to 3 and 6, respectively, can simulate altitude up to 70,000 ft. Engine airflow of 480 lb_m/sec is available at an inlet pressure of 55 psia or 380 lb_m/sec at 165 psia. This facility can support mass flow rate up to 750 lb_m/sec, and can measure horizontal-axis thrust measurement up to 50,000 lb_f and vertical and lateral axes force measurements up to 15,000 lb_f [11].

The 8x6-Foot Supersonic Wind Tunnel at NASA's Glenn Research Center is an atmospheric tunnel with a flexible wall nozzle located upstream of the test section. The facility is constructed entirely of stainless steel used to create an authentic free-stream

airflow when flexed in and out. It is a transonic propulsion wind tunnel able to reach speeds up to Mach 2.0, when a seven-stage motor-driven compressor located inside the tunnel is used. The facility is capable of testing large-scale aero-propulsion hardware in a continuous air stream at Mach numbers from 0 to 0.1 and 0.25 to 2.0 with the relative altitude from 1,000 to 35,000 ft. The stagnation pressure ranges from 15.3 to 25 psia, and the temperature ranges from 60 ^{o}F to 250 ^{o}F. The facility operates either in an aerodynamic closed-loop cycle for testing aerodynamic performance or in a propulsion open-loop cycle that tests live-fuel burning engines and models. In the propulsion cycle, the tunnel operates by continuously drawing outside air through an air dryer and exhausting it back into the outside environment [12].

The Abe Silverstein 10x10 Supersonic Wind Tunnel at NASA Glenn was designed to test supersonic propulsion components such as inlets, nozzles, propulsion system integration, and full-scale jet and rocket engines. The facility is also suited for launch vehicle tests. It can operate either in closed-loop system (aerodynamic cycle) or open-loop system (propulsion cycle) and can reach test section speeds ranging from Mach 2.0 to 3.5 and very low speeds from 0 to Mach 0.4. Gust and Mach plates are sometimes installed to expand local Mach number conditions between 1.5 and 4.1. There is also continuous operation across the entire speed and altitude regime. In the propulsive cycle, the tunnel operates by drawing outside air through a very large air dryer and exhausting it back into the outside environment. This mode is used for models that introduce contaminants into the air stream or use potentially explosive gas mixtures or when the tunnel air-heater is used to simulate flight temperatures. During the

aerodynamic cycle, the tunnel runs as a closed-system as a variable-density facility that can simulate pressure altitude conditions ranging from 50,000 to 150,000 ft. Dry air is added to maintain test conditions [13].

1.4 Project Overview

A test facility review was carried out initially to study the different possible test facilities for RBCC engine testing. The purpose of the survey was to obtain background information and example run conditions that might be helpful in the evaluation of the performance parameters using uncertainty analyses. Chapter 2 provides a discussion of the uncertainty analysis methodology that was used to evaluate the uncertainty in the test results. In Chapter 3, the basic measurement uncertainties were evaluated for use in the test results studies. The results of interest presented in Chapter 4 include specific impulse and characteristic velocity. Five data reduction methods for determining specific impulse were studied. Theoretical and actual characteristic velocity were evaluated to obtain C* efficiency. The example run conditions with the uncertainty estimates used in the general uncertainty analyses are presented in Chapter 5. This study also provides guidance in estimating the uncertainties of the input variables and in reducing the uncertainties in the test results.

CHAPTER II

UNCERTAINTY ANALYSIS METHODOLOGY

2.1 Overview

The basic measurements of the variables such as temperature, pressure, mass flow rate, and thrust have uncertainties associated with them. These basic measurements are often used in a data reduction equation (DRE) to calculate some desired test result. The basic measurement uncertainties will propagate through the data reduction equations into the calculated results. The calculated results presented in this study are specific impulse and characteristic velocity. This propagation process is known as uncertainty analysis. A brief overview of uncertainty analysis techniques and the propagation of uncertainty estimates through the data reduction equations will be discussed in this chapter. However, detailed discussion of the uncertainty analysis techniques can be obtained from reference 14.

"Accuracy" is generally used to indicate the relative closeness of agreement between an experimentally-determined value of a quantity and its true value. Error is the difference between the experimentally-determined value and the truth; therefore, as error decreases, accuracy is said to increase. Only in rare instances is the true value of a quantity known. Thus, it is necessary to estimate error, and that estimate is called an uncertainty, U. Uncertainty estimates are made at some confidence level. A 95%

confidence estimate, for instance, means that the true value of the quantity is expected to be within the $\pm$U interval about the experimentally-determined value 95 times out of 100 [14].

In the planning phase of a program, the approach used considers only the general or overall uncertainties. This approach is called general uncertainty analysis (GUA). A detailed uncertainty analysis (DUA) then considers the systematic (bias) and random (precision) components of uncertainty separately and combines them for the overall uncertainty. Often, more than one measurement method can be used to obtain the values needed in a data reduction equation (DRE) [16]. Also, more than one DRE can be used to calculate the needed result. A general analysis allows one to evaluate different methods available and determine the relative importance of each measured quantity. The analysis results can then be used to choose the best DRE or measurement method and to improve critical measurements, thereby, reducing the uncertainty of the result. This chapter will focus on showing all of the equations necessary to calculate the needed quantities for both general uncertainty analysis and detailed uncertainty analysis so that the process is understood.

2.2 General Uncertainty Analysis

A general uncertainty analysis performed in the planning phase of an experimental program allows the determination of the best approach for meeting the test

objectives. Consider a general case in which an experimental result, r, is a function of J measured variables X_i:

$$r = r(X_1, X_2, ..., X_J) \tag{2-1}$$

Equation (2-1) is the data reduction equation used for determining the result, r from J measured variables X_i. Then the uncertainty in the result is given by

$$U_r^2 = \left(\frac{\partial r}{\partial X_1}\right)^2 U_{X_1}^2 + \left(\frac{\partial r}{\partial X_2}\right)^2 U_{X_2}^2 + ... + \left(\frac{\partial r}{\partial X_J}\right)^2 U_{X_J}^2 \tag{2-2}$$

where the U_{Xi} are the uncertainties in the measured variables X_i. The test results of interest in this study are the specific impulse and characteristic velocity. Specific impulse, for example, is a function of thrust and mass flow rate measurements. Therefore, to obtain the uncertainty of the specific impulse, the uncertainties of the thrust and mass flow rate measurements are needed. Further discussion of different measured variables such as pressure, temperature, thrust, and mass flow rate are presented in Chapter 3. The uncertainties of the measured variables from Chapter 3 are then used in the specific impulse, Isp, and characteristic velocity, C* uncertainty analyses.

If the partial derivatives are defined as absolute sensitivity coefficients,

$$\theta_i = \frac{\partial r}{\partial X_i} \tag{2-3}$$

equation (2-2) can be written as

$$U_r^2 = \sum_{i=1}^{J} \theta_i^2 U_{X_i}^2 \tag{2-4}$$

In equations (2-2) and (2-4), a 95% confidence level is assumed for the uncertainty estimate for most engineering applications. In this study, the non-dimensionalized form of equation (2-2) is used because it is extremely useful in the planning phase of a program. First, divide each term in the equation (2-2) by r^2. Then, in each term on the right-hand side, multiply by $(X_i/X_i)^2$, which is equal to 1. Equation (2-2) is rewritten as

$$\frac{U_r^2}{r^2} = \left(\frac{X_1}{r}\frac{\partial r}{\partial X_1}\right)^2\left(\frac{U_{X_1}}{X_1}\right)^2 + \left(\frac{X_2}{r}\frac{\partial r}{\partial X_2}\right)^2\left(\frac{U_{X_2}}{X_2}\right)^2 + \ldots + \left(\frac{X_J}{r}\frac{\partial r}{\partial X_J}\right)^2\left(\frac{U_{X_J}}{X_J}\right)^2 \qquad (2\text{-}5)$$

where U_r/r is the relative uncertainty of the result. The factors U_{Xi}/X_i are the relative uncertainties for each variable and are presented as percentages in this study.

Two approaches can be used to evaluate the contributions of the various terms to the uncertainty of the result, namely, Uncertainty Magnification Factor (UMF) and Uncertainty Percentage Contribution (UPC).

The UMF values are defined as

$$UMF_i = \frac{X_i}{r}\frac{\partial r}{\partial X_i} \qquad (2\text{-}6)$$

The UMF for a given measured variable indicates the influence of the uncertainty in that variable on the uncertainty in the result, and it is purely a function of the DRE without taking into consideration any uncertainty of the measured variable. A UMF greater than one indicates that the uncertainty of the certain variable is magnified as it propagates through the data reduction equation. A UMF less than one indicates that the uncertainty in that variable is diminished as it propagates through the data reduction equation. (Note that UMF is taken as the absolute value since the term is squared in the uncertainty

equation.) In the design phase, the UMF values help in choosing the appropriate DRE's, measurement methods, etc.

The second approach takes the analysis a step further to include uncertainty in each variable to calculate the Uncertainty Percentage Contribution (UPC). UPC is defined as

$$UPC_i = \frac{\left(\frac{X_i}{r}\frac{\partial r}{\partial X_i}\right)^2\left(\frac{U_{X_i}}{X_i}\right)^2}{\left(\frac{U_r}{r}\right)^2} \tag{2-7}$$

UPC is a function of UMF and uncertainties of each variable as well as the total uncertainty. The sum of the UPC values total 100% of the uncertainty in the result.

$$UPC_{X_1} + UPC_{X_2} + ... + UPC_{X_J} = 100\% \tag{2-8}$$

This approach shows the sensitivity of the squared uncertainty of the result to the squared uncertainty effect of each of the variables for a particular situation where values for the variables are known and the uncertainties for each variable have been estimated [16]. UPC calculations are extremely useful from the later planning phase throughout the execution of the experiment. UPC's are useful as a guide in reducing the total uncertainty of the test result. If a measured variable has a very high UPC, then this implies that a significant reduction in the uncertainty of that particular measurement will significantly reduce the uncertainty in the test result. UPC's can also identify when it is not worth expending resources to improve a particular measurement.

2.3 Detailed Uncertainty Analysis

Total error can be considered to be composed of two components, a precision (random) component, ε, and a bias (systematic) component, β. An error is classified as random if it contributes to the scatter of the data; otherwise, it is a systematic error. A systematic error is a fixed error that can be reduced by calibration; a random error is a variable error that can be reduced by running multiple experiments. As an estimate of β, a systematic uncertainty or bias limit, B, is defined. A 95% confidence estimate for the systematic uncertainty can be interpreted as the range that contains 95% of possible systematic errors. As an estimate of the magnitude of the random errors, a precision uncertainty as precision limit, P, for a single reading is defined. A 95% confidence estimate of P is interpreted to mean that the $\pm$ P interval about the single reading of X_i should cover the (biased) parent population mean, μ, 95 times out of 100.

As stated in the previous section, in nearly all experiments, the measured values of different variables are combined using a data reduction equation (DRE) to form some desired result. A general representation of a data reduction equation is as presented in equation (2-1).

$$r = r(X_1, X_2, ..., X_J) \tag{2-1}$$

Here r is the experimental result determined from J measured variables X_J. Each of the measured variables contains systematic errors and random errors. These errors in the measured values then propagate through the data reduction equation, thereby, generating the systematic and random errors in the experimental result, r. Uncertainty analysis is

used to estimate the random and systematic uncertainties of the result, P_r and B_r respectively, and the corresponding total uncertainty of the result, U_r. The 95% confidence expression for U_r is

$$U_r^2 = B_r^2 + P_r^2 \tag{2-9}$$

where B_r is the systematic uncertainty of the result and P_r is the random uncertainty of the result [14].

Detailed uncertainty analysis is used in this study to determine the uncertainty of the pressure measurements, temperature measurements, and the direct thrust measurement. For direct measurements, elemental sources are evaluated to obtain an overall systematic uncertainty estimate for each measurement type. The main difference between GUA and DUA is that systematic uncertainties must be considered separately from random uncertainties. A detailed discussion of determining the uncertainties of the temperature, pressure, and thrust measurements using DUA is presented in Chapter 3.

2.3.1 Systematic Uncertainty

The first step in estimating systematic uncertainty is to evaluate the elemental error sources that affect each of the measurements. The systematic uncertainty estimates for each X_i variable are the root sum square combination of the elemental systematic uncertainties.

$$B_i = \left[\sum_{j=1}^{M} (B_i)_j^2 \right]^{1/2} \tag{2-10}$$

The systematic uncertainty of the result is defined as

$$B_r^2 = \sum_{i=1}^{J} \theta_i^2 B_i^2 + 2\sum_{i=1}^{J-1} \sum_{k=i+1}^{J} \theta_i \theta_k B_{ik} \tag{2-11}$$

The second term of equation (2-11) accounts for systematic errors that are common between variables and are, therefore, correlated. The partial derivatives of each measured variable, θ_i are defined as

$$\theta_i = \frac{\partial r}{\partial X_i} \tag{2-12}$$

The factor B_{ik} is the 95% confidence estimates of the covariance appropriate for the systematic errors in X_i and X_k that are common and is determined from

$$B_{ik} = \sum_{\alpha=1}^{L} (B_i)_\alpha (B_k)_\alpha \tag{2-13}$$

where variables X_i and X_k share L identical systematic error sources.

2.3.2 Random Uncertainty

The random uncertainty (precision limit) of the result is defined as

$$P_r = \sum_{i=1}^{J} \theta_i^2 P_i^2 + 2\sum_{i=1}^{J-1} \sum_{k=i+1}^{J} \theta_i \theta_k P_{ik} \tag{2-14}$$

where P_{ik} is the 95% confidence estimate of the covariance appropriate for the precision errors in X_i and X_k, and the 95% confidence large sample ($N \geq 10$) random uncertainty for each variable X_i is estimated as

$$P_i = 2S_{X_i} \tag{2-15}$$

Here, S_{Xi} is the sample standard deviation

$$S_{X_i} = \left[\frac{1}{N-1} \sum_{k=1}^{N} \left[(X_i)_k - \overline{X} \right]^2 \right]^{1/2} \tag{2-16}$$

and the mean value for variable X_i is defined as

$$\overline{X_i} = \frac{1}{N} \left[\sum_{k=1}^{N} (X_i)_k \right] \tag{2-17}$$

where N is the number of individual readings X_i. The sample standard deviation for the mean is defined as

$$S_{\overline{X_i}} = \frac{S_{X_i}}{\sqrt{N}} \tag{2-18}$$

and the 95% confidence large sample random uncertainty limit for the mean value is approximated as

$$P_{\overline{X_i}} = 2S_{\overline{X_i}} \tag{2-19}$$

Typically, correlated precision uncertainties have been neglected so that the P_{ik}'s in equation (2-14) are taken as zero. These covariance terms account for correlation between errors in different measurements. The precision errors have been considered to be random; therefore, the correlation between them has been taken to be zero. That assumption is generally true; however, in some case, the random (precision) errors are correlated and the covariance terms are important [16].

The uncertainty analysis techniques discussed above are used to obtain uncertainty estimates for all of the basic measurements such as temperature, pressure, mass flow rate, and thrust. These basic measurements will be discussed in Chapter 3.

Chapter 4 will use the uncertainty estimates from Chapter 3 and determine the uncertainty of the specific impulse and characteristic velocity using uncertainty analysis techniques.

CHAPTER III

BASIC MEASUREMENTS

3.1 Background

Often, more than one measurement method can be used to obtain the basic measurements such as temperature, pressure, mass flow rate, and thrust. Since these basic measurements are needed in determining the specific impulse and characteristic velocity, or the test results, the uncertainty associated with these basic measurements will contribute to the uncertainty in the test results.

As will be discussed next, temperature measurements can be done with measurement devices such as type E or K thermocouples, Resistance Temperature Detectors (RTDs), or temperature transmitters. Pressure transducers or pressure transmitters can be used to obtain pressure measurements. Mass flow rate can be measured by a venturi, cavitating venturi, orifice, V-cone, turbine, or coriolis flow meter. Direct thrust measurements can be obtained using load cells in various way. The exact techniques used to make a measurement must be evaluated to estimate the uncertainty of the measurement. The uncertainties associated with the basic measurements will be discussed in the next sections.

3.2 Measurement Types

3.2.1 Temperature

Temperatures are often measured with thermocouples for rocket engine testing. Thermocouple consists of two dissimilar metals joined together and an emf will exist between the two metals. This emf generated will be dependant on the temperature of the connection [15]. Typically, Type E thermocouples are used for cryogenics, and Type K thermocouples are used for ambient and higher temperatures. Resistance temperature detectors (RTDs) are also occasionally used. They consist of some type of resistive element, which is exposed to the temperature to be measured. The temperature is indicated through a measurement of the change in resistance of the element. Detailed discussion of RTDs can be found in [15]. Thermocouples lack accuracy relative to RTDs although the response is faster than RTDs. For steady-state temperature, RTDs are useful since the thermal time constant can reach 500 milliseconds or greater depending on the manufacturer and model. Additionally, aerospace testing requires temperature instrumentation to be robust to survive the extreme environments of rocket engine testing. In most cases, temperature instrumentation must withstand pressures measured in thousands of PSI and cryogenic flow rates of hundreds of lb_m/sec [16].

3.2.2 Pressure

Transducers with signal conditioning for bridge excitation, gain, and signal filtering can be used to measure pressure, including differential pressure. These devices have a mV output, for example, 0-30 mV. End-to-end data check capabilities of transducers using resistance calibration (R_{Cal}) are extremely beneficial in guaranteeing data quality and determining the instrument's health prior to test.

Pressure can also be measured by another device called a transmitter. It combines a pressure transducer with a mA output signal, for example 4-20 mA, but does not require the same level of signal conditioning as the transducer. Response time of pressure transducers and transmitters is similar provided that the transmitters are not incorporating an internal processor for linearization and conversion. "Dumb" transmitters have passive electronics that lack the time delay created by the processor thus giving them a much faster time response [16].

3.2.3 Mass Flow rate

Accurately measuring flow rates has been a challenge, especially in the case of cryogenics. Numerous methods exist to accommodate the diverse flow conditions and medium found in rocket testing. Issues such as materials compatibility, high pressure with high flow rates, two-phase flow, low flow rates, etc., play a major role in how the specific flow parameter is obtained [16]. Venturi, cavitating venturi, orifice, V-cone,

turbine, and coriolis flow meters were evaluated in this study to obtain the uncertainty of the mass flow rate.

3.2.3.1 Venturi

Venturi flow meters are often used to measure fluid flow due to their low permanent pressure loss, durability, and lack of moving parts. A venturi meter is a device to measure flow rate of a fluid in a pipe. As shown in Figure 3-1, they are part of a class of flow meters known as differential pressure measurement device since a pressure drop across a region in the meter is produced, and this pressure differential is used to determine the flow rate through the meter. At the throat, the area is reduced and the velocity is increased. The venturi volumetric flow rate is given by equation (3-1).

$$Q = C_d A \sqrt{\frac{2gh}{1-\beta^4}} \tag{3-1}$$

Here C_d is the dimensionless discharge coefficient, A is the area of the pipe (or inlet), g is the acceleration due to gravity, h is the effective differential head, and β is the ratio of throat diameter, d_2 to pipe diameter, d_1. Therefore, the actual rate of flow through a venturi, w, is given by equation (3-2).

$$w = C_d \frac{\pi}{4} d_2^{\,2} \sqrt{\frac{2\rho(P_1 - P_2)}{\left(1-\beta^4\right)}} \tag{3-2}$$

where ρ is the fluid density, P_1 is the pipe or inlet pressure, and P_2 is the throat pressure.

A thermal expansion factor, F_a is needed to account for the expansion and contraction of most materials as their temperature increases or decreases. Equation (3-3) represents incompressible flow with the expansion factor, Y, is unity.

$$w = 0.52502 C_d \, {d_2}^2 \, F_a \sqrt{\frac{\rho(P_1 - P_2)}{1 - \left(\frac{d_2}{d_1}\right)^4}} \tag{3-3}$$

When measuring a compressible fluid, the expansion factor, Y, is used. For a venturi and cavitating venturi, this factor is given by equation (3-4) as in reference [17].

$$Y = \left[\left(\frac{P_2}{P_1}\right)^{2/\gamma} \frac{\gamma}{\gamma - 1} \frac{1 - (P_2/P_1)^{(\gamma-1)/\gamma}}{1 - (P_2/P_1)} \frac{1 - (A_2/A_1)^2}{1 - (A_2/A_1)^2 (P_2/P_1)^{2/\gamma}} \right]^{1/2} \tag{3-4}$$

As derived in reference [17], the data reduction equation for compressible flow is determined with P_1 and P_2 in psia, T in ^oR, d_1 and d_2 in inches, and ρ in lb_m/ft^3.

$$w = 0.52502 C_d \, {d_2}^2 \, F_a \sqrt{\frac{\frac{\gamma}{\gamma - 1} P_1 \rho \left(\frac{P_2}{P_1}\right)^{2/\gamma} \left[1 - \left(\frac{P_2}{P_1}\right)^{\gamma - 1/\gamma}\right]}{1 - \left(\frac{d_2}{d_1}\right)^4 \left(\frac{P_2}{P_1}\right)^{2/\gamma}}} \tag{3-5}$$

The data reduction equation used for a cavitating venturi is identical to a venturi flow meter. As shown in Figure 3-1 and 3-2, the difference between these two devices is the shape of the venturi section. A nozzle exists in the cavitating venturi that causes a sudden formation and collapse of low-pressure bubbles or cavitation [17]. For the cavitating venturi, $d_1 >> d_2$ making the $(d_2/d_1)^4$ term in equation (3-3) and (3-5) very small.

This term is often considered negligible and not included in the equation for the cavitating venturi.

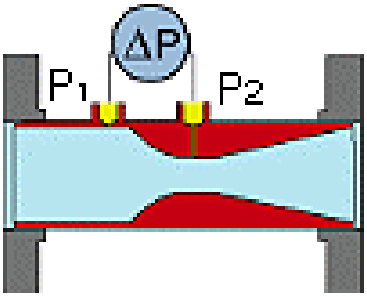

Figure 3-1: Schematic of Venturi Flow Meter

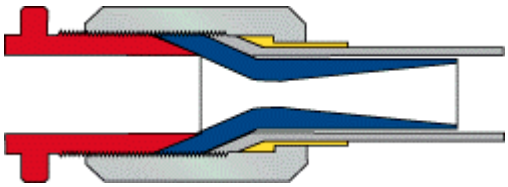

Figure 3-2: Schematic of Cavitating Venturi

3.2.3.2 Orifice

The orifice plate is used to measure fluid flow through the differences in pressure from upstream to the downstream side of a partially obstructed pipe. The plate offers a precisely-measured obstruction that narrows the pipe and forces the flowing substance to constrict. The greater the flow rate, the greater the difference in pressure as the substance

maintains its constricted state for a longer distance passing the downstream element. Different kinds of orifice plates include concentric, eccentric, and segmental, each of which has different shapes and placements for measuring different processes [15, 18]. Orifice plates are in common use in many installations due to low installation cost, ease of installation, and the flexibility of adjusting the desired flow rate [17]. However, orifice meters have larger permanent pressure loss due to the presence of eddies downstream of the meter as shown in Figure 3-3.

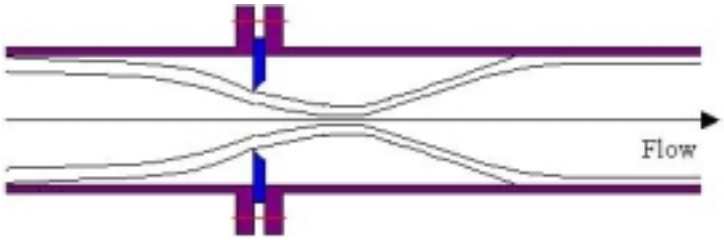

Figure 3-3: Schematic of Orifice Plate

The calibration equation for orifice meters in terms of mass flow rate, w, and pressure drop is usually written as

$$w = KAYF_a\sqrt{\frac{2\rho(\Delta P)}{\left[1-\beta^4\right]}} \tag{3-6}$$

Here, K is the flow coefficient, A is the pipe cross-sectional area, Y is the expansion factor as in equation (3-4), F_a is the thermal expansion factor, ρ is the fluid density, β is the ratio of throat diameter, d_2, to pipe diameter, d_1, and ΔP is the change of pressure between upstream and downstream of the flow meter. This is the same principal as used

for the venturi as in equation (3.2) except the discharge coefficient, C_d, is replaced by the flow coefficient, K. The resulting data reduction equation used for the orifice flow meter is

$$w = K\frac{\pi}{4}d_2{}^2 Y F_a \sqrt{\frac{2\rho(\Delta P)}{\left[1-\left(\frac{d_2}{d_1}\right)^4\right]}} \qquad (3\text{-}7)$$

Expansion factor, Y, is at unity for incompressible flow; equation (3-4) must be used for compressible flow. F_a is the thermal expansion factor. ΔP is the change in pressure between the inlet and throat (P_1- P_2). β is the ratio of throat diameter to the inlet diameter, d_2/d_1.

3.2.3.3 V-cone

The venturi-cone (V-cone) element is a proprietary design that promises consistent performance at low Reynolds numbers and is insensitive to velocity profile distortion or swirl effects. However, it is relatively expensive.

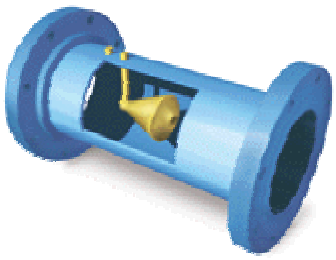

Figure 3-4: Schematic of V-cone Flow Meter

The V-cone restriction has a unique geometry that minimizes accuracy degradation due to wear, making it a good choice for high velocity flows and erosive/corrosive applications. The V-cone flow meter is similar to orifice and venturi flow meters. The only difference between them is the beta ratio, β. The beta ratio of a V-cone is given by

$$\beta = \frac{\sqrt{D^2 - d^2}}{D} \tag{3-8}$$

Here, D is the inside diameter of the pipe, and d is the cone diameter. The mass flow rate is given by equation (3-9).

$$w = C_d A \sqrt{\frac{2\rho\Delta P}{(1-\beta^4)}} \tag{3-9}$$

Here C_d is the discharge coefficient, A is the pipe cross-sectional area, ρ is the fluid density, and ΔP is the pressure difference. For incompressible flow, the data reduction equation is

$$w = \frac{\pi}{4} D^2 C_d Y F_a \sqrt{2 g_c \rho \Delta P} \frac{\left(\sqrt{1-\frac{d^2}{D^2}}\right)^2}{\sqrt{1-\left(\sqrt{1-\frac{d^2}{D^2}}\right)^4}} \tag{3-10}$$

Where Y is the expansion factor and F_a is thermal expansion factor. The expansion factor, Y, is at unity for the incompressible case. The expansion factor, Y, is not unity for

the compressible case [17]. It can be obtained using the expression in equation (3-11), which is identical to equation (3-4).

$$Y = \sqrt{\frac{1-\beta^4 \frac{\gamma}{\gamma-1}\left(1-\frac{\Delta P}{P_1}\right)^{2/\gamma}\left[1-\left(1-\frac{\Delta P}{P_1}\right)^{\gamma-1/\gamma}\right]}{\left\{1-\left[\beta^4\left(1-\frac{\Delta P}{P_1}\right)^{2/\gamma}\right]\right\}\left[1-\left(1-\frac{\Delta P}{P_1}\right)\right]}} \qquad (3\text{-}11)$$

Therefore, the data reduction equation for compressible flow can be obtained by substituting the expansion factor, Y, into the data reduction equation for the incompressible case [19, 20].

3.2.3.4 Turbine Meter

The turbine meter is a popular type of flow-measurement device. Figure 3-5 shows that as the fluid moves through the meter, it causes a rotation of the small turbine wheel. A permanent magnet is enclosed in the turbine-wheel body so that it rotates with the wheel. A reluctance pickup attached to the top of the meter detects a pulse for each revolution of the turbine wheel. Since the mass flow is proportional to the number of wheel revolutions, the total pulse output may be taken as an indication of total flow. The pulse rate is proportional to mass flow rate, w, and the transient response of the meter is very good. A flow coefficient, K, for the turbine meter is defined to derive the equation of the mass flow rate.

$$w = \left(\frac{f}{K}\right) \qquad (3\text{-}12)$$

Here, f is the pulse frequency (cycles/s). The flow coefficient, K, (cycles/kg) is dependant on flow rate and the kinematic viscosity of the fluid, ν. A calibration curve for a typical meter is needed from the manufacturer. The flow coefficient, K, will be provided by the manufacturer [15].

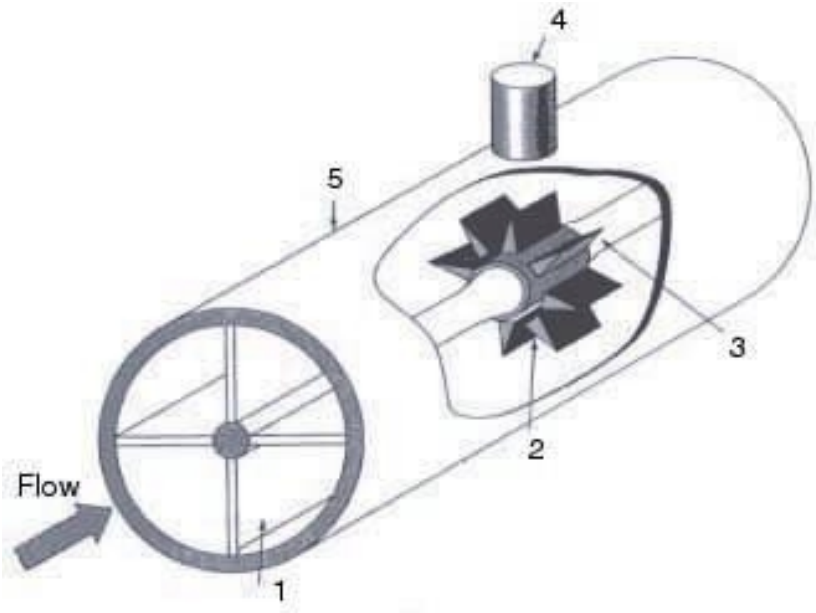

Figure 3-5: Schematic of turbine meter. (1) Inlet straightening vanes, (2) rotating turbine blades with embedded magnet, (3) smooth after-body to reduce pressure drop, (4) reluctance pickup, (5) meter body for insert in pipe or flow channel

3.2.3.5 Coriolis

The coriolis flow meter is a type of insertion meter that is used to measure the mass flow rate by using the Coriolis acceleration on the flowing fluid and determining the

resulting developed force. The developed force is directly related to the mass flow rate independent of the fluid properties.

Commercially available units for the metering of liquids are based on a scheme in which the pipe flow is diverted from the main pipe and divided between two bent, parallel, adjacent tubes of equal diameter, as shown in Figure 3-6. In general, a fluid particle passing through the meter tube that is rotating (due to the oscillating tube) relative to the fixed pipe experiences the acceleration. The Coriolis acceleration acts in a plane perpendicular to the tube axes and develops a force gradient that creates a twisting motion or oscillating rotation about the tube plane [21].

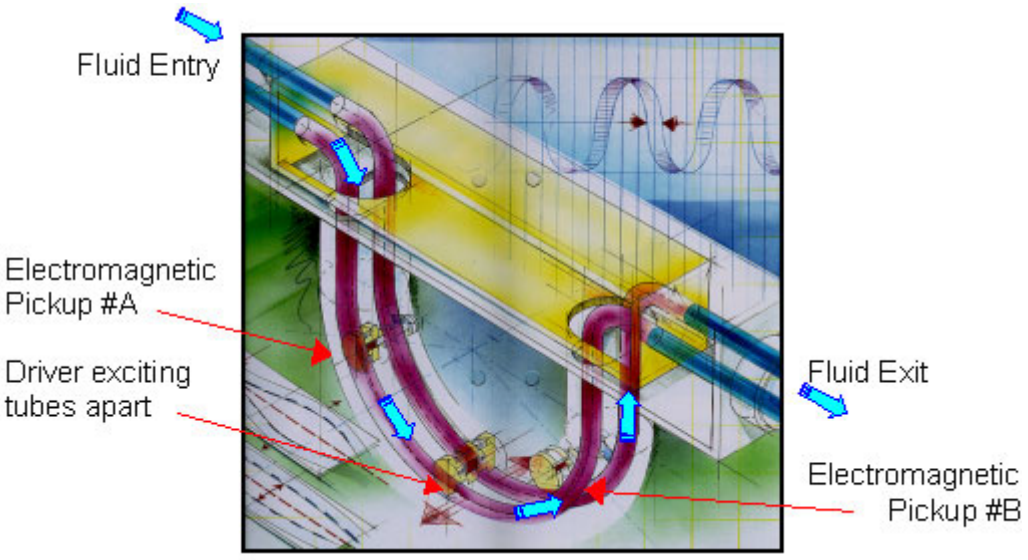

Figure 3-6: Example Interior of the Coriolis Meter

The tube walls guide the process fluid as it flows through the U-Tube pathway. With no fluid inside the tubes, the driver excites the tubes apart causing a parallel deflection as shown in Figure 3-7(a). As the fluid flows down the first half of the U-Tubes, it will tend to deflect the tubes in towards each other as shown in Figure 3-7(b). Conversely, when the fluid flows up the second half of the U-Tubes, it will tend to deflect the tubes out away from each other as shown in Figure 3-7(c).

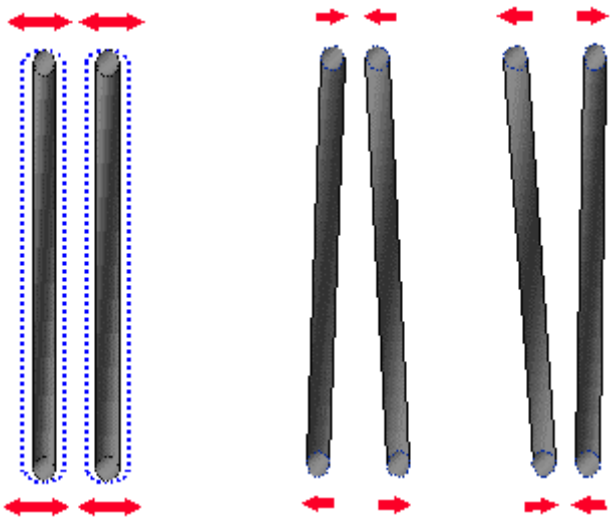

(a) (b) (c)

Figure 3-7: Schematic of Tube with and without Flow

Figure 3-8 shows the baseline deflection of the tubes from the driver as shown by sine wave (a) and the Coriolis twist from the pickup coil is designated by sine wave (b) [22].

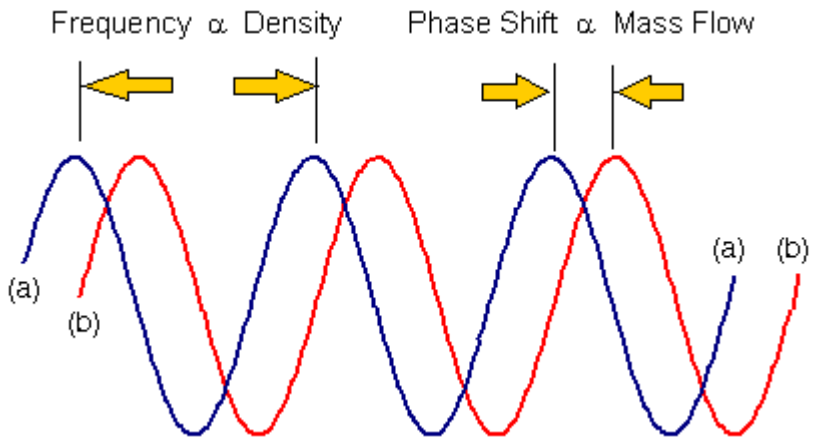

Figure 3-8: Schematic of the Baseline Deflection

The meter principle is unaffected by changing fluid properties, but temperature changes will affect the overall meter stiffness. This effect can be compensated for electronically. A very desirable feature is an apparent insensitivity to installation position [22].

3.2.4 Thrust

Thrust is the force produced by a rocket propulsion system acting upon a vehicle. It is the reaction experienced by its structure due to the ejection of propellant at high velocity. Readers are referred to reference [23] for more details on thrust. The Thrust Measurement System (TMS) consists of two functional systems: a measurement system and a calibration system. For a single- axis measurement system, the system will react to one force and one moment produced by the thrust of the engine under test. A six-axis

measurement system reacts to three forces and three moments produced by the thrust. The calibration system provides the capability of applying accurately known loads or dead weights to the measurement system, which is useful in removing uncertainties from the thrust measurement. During the testing, forces and moments from the Thrust Measurement System (TMS) will be recorded by a data acquisition system (DAS) [24].

A one-axis measurement system only is presented in this research. Load cells are used for direct thrust measurement. Uncertainty of the load cells measurement is presented in this study.

3.3 Measurement Uncertainty Examples

Since various measurement methods are available for evaluation, these will introduce different elemental error sources depending on the calibration and test procedures. Therefore, the uncertainties associated with the different calibration and test procedures will vary. Several example methods will be given in this chapter to demonstrate how the uncertainties are calculated for specific situations. The uncertainties of each measurement method are presented with the detail of how the uncertainty values were determined from the elemental sources. The uncertainties of the measurements discussed include temperature, pressure, mass flow rate, and thrust measurements. These measurement uncertainties were then used to evaluate the uncertainty of the specific impulse and characteristic velocity. Five methods of determining specific impulse are

presented Chapter 4. Characteristic velocity analyses are also presented in Chapter 4. Detail calculations of the uncertainty analyses are included in this study.

3.3.1. Temperature

In this research, temperature measurements were evaluated with type E and type K thermocouples as well as RTD's. The type E thermocouples are typically used for room temperature and below (down to 36 ^{o}R), whereas the type K thermocouples are used for room temperature and above (up to 3460 ^{o}R). The thermocouples can be used with a Uniform Temperature Reference (UTR) or temperature transmitter. RTD's can also be used with the temperature transmitters.

As an example, consider a thermocouple used along with a UTR in the test facility to obtain a temperature measurement (Figure 3-9). Standard temperature versus milivolt curves are used to obtain temperature based on the facility voltage measurement. (The thermocouple is not calibrated in the calibration laboratory to provide these curves.) The test facility calibration involves a voltage input downstream of the UTR with a voltage tolerance for the data acquisition system (V_{cal}). An RTD is used to measure the UTR temperature.

For the sample procedure described above, the uncertainty in the test temperature measurement must consider elemental error sources from the test procedure. Elemental error sources to consider include the manufacturer's specifications on the accuracy of the thermocouple, the UTR, and the facility voltage calibration. Sources related to the UTR

include the uniformity of the block temperature and the uncertainty of the RTD used to measure the block temperature. Sources related to the voltage calibration include the voltage input device, the tolerance of the voltage calibration, and the possible system drift. These uncertainty sources are combined using the uncertainty analysis techniques described previously to give the overall uncertainty of the test temperature measurement [16]. The uncertainty analysis to get the overall uncertainty of a test temperature for this sample procedure will be briefly discussed here.

Consider the example of a Type E thermocouple with UTR as shown in Figure 3-9 and a temperature reading of -200 ^{o}C with the input gain of 100 and post-test drift tolerance of 10 mV. According to Omega manufacturer's specification, the uncertainty of the reading is 1.7 ^{o}C if T > -170 ^{o}C; U = 1% of reading if T < -170 ^{o}C.

$$U_1 = 1\%(-200\ ^oC) = -2\ ^oC$$

According to Kaye Instruments UTR application notes, the error associated with the UTR and RTD is 0.15 ^{o}C.

$$U_2 = 0.15\ ^oC$$

The uncertainty of the UTR temperature uniformity is 0.03 ^{o}C according to Kaye Instruments UTR application notes with the assumption of 2.5 ^{o}F/hr change in temperature.

$$U_3 = 0.03\ ^oC$$

The voltage calibration input device uncertainty depends on the temperature due to thermocouple sensitivity. For the error associated with this input device, the uncertainty is 0.2 ^{o}C if the temperature reading is greater than –200 ^{o}C; U = 0.5 ^{o}C if -200 ^{o}C > T > -240 ^{o}C; U = 0.75 ^{o}C if –240 ^{o}C > T > -250 ^{o}C; U = 2.00 ^{o}C if –250 ^{o}C> T > -270 ^{o}C.

$$U_4 = 0.5\,^{o}C$$

Assume the type E thermocouple has the sensitivity of 30 ^{o}C/mV, the input gain of 100, and the post-test drift tolerance of 10 mV. Then the uncertainty associated with the possible system drift after voltage calibration is considered as follow.

$$U_5 = 30\frac{^{o}C}{mV}\left(\frac{10mV}{100}\right) = 3\,^{o}C$$

Since no actual experiment is carried out in this research, additional installation effects and the random uncertainty are neglected. The overall temperature uncertainty is the root-sum square of the elemental error sources.

$$U_T = \sqrt{(U_1)^2 + (U_2)^2 + (U_3)^2 + (U_4)^2 + (U_5)^2}$$

$$U_T = 3.64\,^{o}C$$

The uncertainties of the elemental errors U_2, U_3, and U_5 stays constant when the above process is repeated to take more temperature readings. However, U_1 and U_4 depend on the temperature value. The system drift, U_5, is the dominant error source in this example. This term can be reduced by changing the tolerance or allowable drift for the posttest check.

This is an example of determining uncertainty in a temperature measurement. Uncertainty of temperature will vary depending on the test facility and procedures. Microsoft Excel worksheets are attached in Appendix A as a reference.

As another example, now consider the same temperature measurement made with a temperature transmitter rather than a UTR (Figure 3-10). Again, standard temperature versus millivolt curves are used to obtain temperature based on the facility voltage measurement. When used in the test facility, a resistor is placed in the circuit to convert the current output of the transmitter to a voltage for the data acquisition system. The test facility calibration involves a voltage input downstream of the resistor with a voltage tolerance for the data acquisition system (V_{cal}), as in the previous example.

For the sample procedure described above, the uncertainty in the test temperature measurement must again consider elemental error sources from the test procedure. Elemental error sources to consider include the manufacturer's specifications on the accuracy of the thermocouple, sources related to the transmitter, the circuit resistor, and sources related to the facility voltage calibration. Sources for the manufacturer's specifications on the thermocouple and the V_{cal} are the same as in the previous example. Sources related to the transmitter can be obtained from the manufacturer's specifications. Sources related to the circuit resistor must be determined from the resistor specification. These uncertainty sources are combined using the uncertainty analysis techniques described previously to give the overall uncertainty of the test temperature measurement [16]. Complete calculation of the overall temperature uncertainty can be obtained from the Excel worksheets provided in Appendix A.

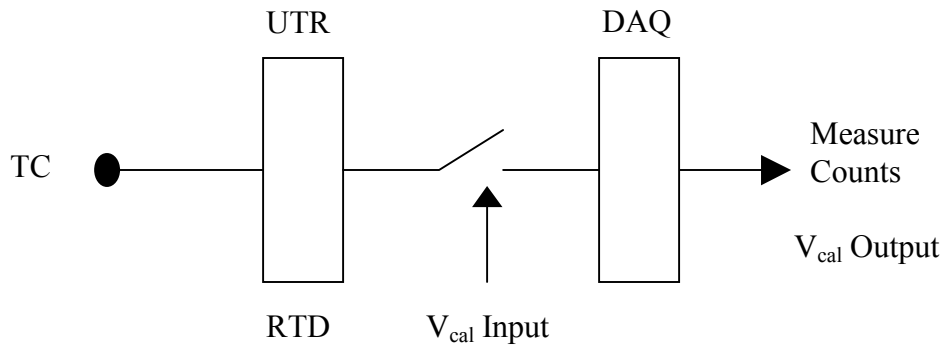

Figure 3-9: Thermocouple Measurement with UTR

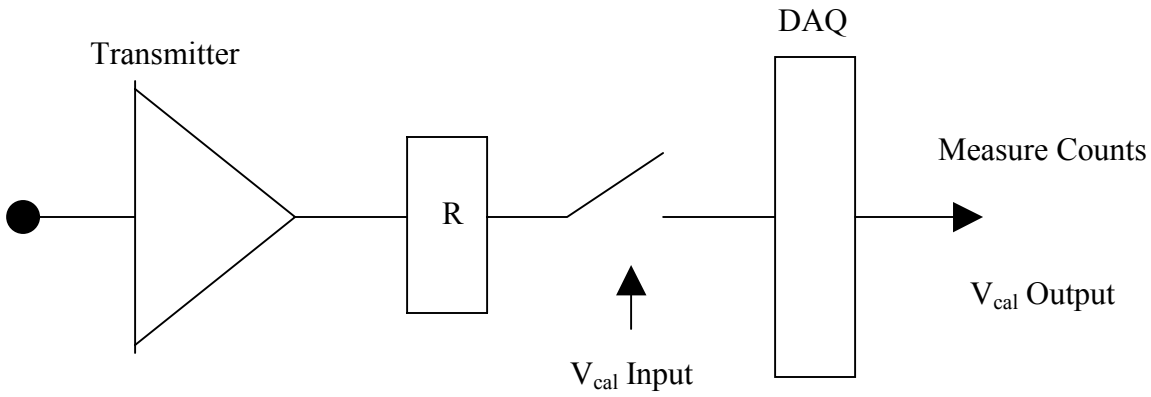

Figure 3-10: Thermocouple Measurement with Transmitter

3.3.2 Pressure

Pressure measurements can be made with a broad range of pressure transducers and pressure transmitters. Again, examples will be given to show how uncertainties are estimated for particular situations.

As an example, consider a 2000-psi pressure transducer. The transducer has an internal shunt resistor. The transducer is calibrated at the calibration laboratory over the 2000-psi range. A pressure standard is used to set and measure equal increments of pressure between 0 and 2000-psi. The mV output of the pressure transducer is recorded. A curve-fit of the pressure versus mV data is then produced. The calibration also provides the output resistance for 0% and 80% for the internal shunt resistor. The transducer is then used in the test stand for engine testing. An end-to-end calibration of the transducer is done prior to testing using the internal shunt resistor (R_{cal}). This end-to-end calibration is used to match the output of the test data acquisition system to the data from the calibration laboratory (Figure 3-11).

For the sample procedure described above, the uncertainty in the test pressure measurement must consider elemental error sources from the calibration laboratory procedure and the test facility procedures. Sources of error for the calibration include the pressure standard, the voltage measurement, the resistance measurement, and the curve-fit of the data. These sources must be combined using the uncertainty analysis technique described in Chapter 2 to give the overall uncertainty of the calibration. For the test facility calibration procedure, the uncertainties associated with the shunt resistance, the tolerances allowed in matching the calibration laboratory data, and the possible system drift with time must be considered. These uncertainty estimates are combined with the calibration laboratory uncertainty using the uncertainty analysis techniques described previously to give the overall uncertainty of the test pressure measurement [16].

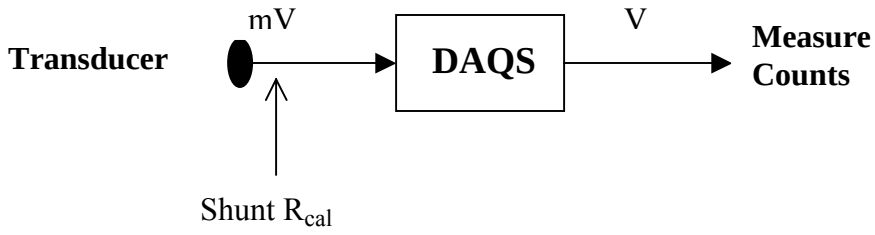

Figure 3-11: Pressure Measurement with Transducer

For this example, consider that the 2000-psi pressure transducer was used to make a differential pressure measurement. The transducer was calibrated in the calibration lab with a systematic uncertainty of 0.25% full-scale or 5 psi. The shunt resistor accounts for an uncertainty of 2 psi. Uncertainty due to system drift after calibration is about 6.94 psi.

$$U_{cal\_lab} = 5\ psi$$

$$U_{shunt} = 2\ psi$$

$$U_{drift} = 6.94\ psi$$

Uncertainty of the pressure measurement, U_p, is the root-sum-square of all elemental sources.

$$U_p = \sqrt{(U_{cal\_lab})^2 + (U_{shunt})^2 + (U_{drift})^2 + (U_{atm})^2}.$$

$$U_p = 9.01\ psi$$

In contrast, now consider the same 2000-psi pressure measurement made with a pressure transmitter. For example, the transmitter is calibrated in the calibration laboratory over the 2000-psi range. A pressure standard is used to set and measure equal

increments of pressure between 0 and 2000-psi. The mA output of the pressure transmitter is recorded. A curve-fit of the pressure versus mA data is then produced. When the transmitter is used in the test stand, a resistor is used to convert the mA output signal to voltage. The data acquisition system is then calibrated to a certain voltage tolerance to match the calibration laboratory data.

For the sample procedure described above, the uncertainty in the test pressure measurement must again consider elemental error sources from the calibration laboratory procedure and the test facility procedures. Sources of error for the calibration include the pressure standard, the current measurement and tolerance, and the curve-fit of the data. These sources must be combined using the uncertainty analysis techniques described previously to give the overall uncertainty of the calibration. For the test facility calibration procedure, the uncertainty associated with the input resistance, the tolerance allowed in matching the calibration laboratory data voltage, and the possible system drift with time must be considered. These uncertainty estimates are combined with the calibration laboratory uncertainty using the uncertainty analysis techniques described previously to give the overall uncertainty of the test pressure measurement.

Any changes in the procedures described above for the pressure measurements will change the elemental error sources that need to be considered. This, in turn, will change the uncertainty estimate for the measurement. Therefore, it is vital that the correct procedure be evaluated to determine the uncertainty value [16]. Detailed calculations are presented in the attached Excel worksheets in Appendix A.

3.3.3 Mass Flow Rate

As discussed previously, mass flow rate can be measured with a variety of devices. These devices include a venturi, cavitating venturi, orifice, v-cone, turbine meter, or coriolis meter. Since mass flow rate is not a direct measurement like temperature and pressure, the correct data reduction equation must be used to evaluate the uncertainty of the mass flow rate depending on the device, measurement procedures, and calculation procedure. As presented previously, the data reduction equation for each device is written in terms of the measured variables. Changes in the measured variables, calculation method, etc., will change the DRE and thus affect the uncertainty calculation for the mass flow rate measurement.

With the DREs presented in section 3.2.3 for various flow measurement devices, uncertainty analyses were performed based on the uncertainty techniques discussed in Chapter 2. A brief discussion on the uncertainty analysis techniques carried out to determine the uncertainty of the mass flow rate will be presented next. The detailed procedures for calculating the uncertainty of the mass flow rate can be found in the attached MathCAD calculation worksheets in Appendix B. These uncertainties of the mass flow rate will then be used to evaluate the uncertainty of the specific impulse and characteristic velocity as presented in Chapter 4.

3.3.3.1 Venturi

The DRE used to perform the uncertainty analysis for incompressible flow of a venturi meter and a cavitating venturi is obtained from equation (3-3). An example of the general uncertainty analysis based on Equation (3-3) will be evaluated.

$$w = 0.52502 C_d \, {d_2}^2 \, F_a \sqrt{\frac{\rho(\Delta P)}{1 - \left(\frac{d_2}{d_1}\right)^4}} \tag{3-3}$$

Based on the DRE above, GUA from Chapter 2 was applied to determine the UMF and UPC values for each measured variable. The uncertainty of the mass flow rate and its UMF and UPC values, based on 1% uncertainty estimates for each variable, are presented in Table 3-1. The venturi mass flow rate uncertainty is about 2.56%. (Note that this analysis is strictly an example. Actual test conditions will vary.) Based on the UPC values in Table 3-1, throat diameter contributes the most uncertainty to the test result. (The uncertainty of the test result is magnified when the UMF is greater than one.) Therefore, a more precise measurement device or multiple measurements can be used to reduce the test uncertainty. On the contrary, it is not worth expanding resources to improve the density and inlet diameter measurements due to their low UPC values. Refer to Appendix B for more details.

Measured Variables	Nominal Values	UMF	UPC (%)
C_d	0.98	1.0	15.29
d_2 (in)	0.25	2.0	61.78
F_a	0.99	1.0	15.29
ρ_1 (lbm/ft^3)	41.33	0.5	3.82
ΔP(psia)	700	1.1	3.82
d_1 (in)	0.95	0.0	0.00
w (lbm/sec)	5.43		
U_w (lbm/sec)	0.139		
U_w (%)	2.56		

Table 3-1: Example GUA for Venturi Flow Meter

3.3.3.2 Orifice

The data reduction equation used to calculate the uncertainty of the mass flow rate associated with the orifice meter is derived from equation (3-7).

$$w = K\frac{\pi}{4}d_2{}^2 Y F_a \sqrt{\frac{2\rho(\Delta P)}{\left[1-\left(\frac{d_2}{d_1}\right)^4\right]}} \qquad (3\text{-}7)$$

Based on the uncertainty analysis techniques presented in Chapter 2 and the example given in section 3.3.3.1, uncertainty of the orifice mass flow rate and its UMF and UPC values can be obtained.

3.3.3.3 V-cone

The data reduction equation of a V-cone for incompressible flow is derived from equation (3-10).

$$w = \frac{\pi}{4} D^2 C_d Y F_a \sqrt{2 g_c \rho \Delta P} \frac{\left(\sqrt{1-\frac{d^2}{D^2}}\right)^2}{\sqrt{1-\left(\sqrt{1-\frac{d^2}{D^2}}\right)^4}} \qquad (3\text{-}10)$$

As an example, the above DRE was analyzed based on 1% uncertainty estimates for each variable by using the GUA in Chapter 2. The results of the uncertainty analysis are presented in Table 3-2. The V-cone mass flow rate uncertainty is found to be approximately 3.94%. (Note that this analysis is strictly an example to illustrate the GUA used in this study. Actual test conditions may vary.) Based on the UPC values in Table 3-2, pipe inside diameter contributes the most uncertainty to the test result. (The uncertainty of the test result is magnified when UMF is greater than one.) Therefore, a more precise measurement device or multiple measurements can be used to reduce the test uncertainty. On the contrary, it is not worth expanding resources to improve the density measurement due to its low UPC value. Refer to Appendix B for more details.

Measured Variables	Nominal Values	UMF	UPC
D (in)	0.90	3.2	67.57
d (in)	0.33	1.2	9.88
C_d	0.82	1.0	6.44
Y	1.00	1.0	6.44
F_a	1.00	1.0	6.44
ρ (lbm/ft^3)	41.33	0.5	1.611
ΔP (psia)	2.15	1.1	14.79
w (lbm/sec)	5.68		
U_w (lbm/sec)	0.22		
U_w (%)	3.94		

Table 3-2: Example GUA for V-cone Flow Meter

3.3.3.4 Turbine Meter

The data reduction equation used to calculate the uncertainty of the mass flow rate associated with a turbine meter is derived as

$$w = \left(\frac{f}{K} \right) \tag{3-12}$$

where f is the pulse frequency, (*cycles/*sec). The flow coefficient, K, (*cycles/kg*) is dependant on flow rate and the kinematic viscosity of the fluid, ν. The pulse frequency can be measured with approximately 0.5% uncertainty. For example, the flow coefficient is provided by the manufacturer with the uncertainty of about 0.5% [15].

In order to perform an uncertainty analysis, the derivatives of the mass flow rate with respect to pulse frequency and flow coefficient must be obtained. With the nominal values of the measured variables and their realistic uncertainty estimates, the mass flow rate uncertainty, the uncertainty magnification factors (UMF), and uncertainty percentage contributions (UPC) can be obtained using the methodology presented in Chapter 2.

3.3.3.5 Coriolis

Uncertainties of commercially available Coriolis flow meters depend on the manufacturer and turndown ratio of the meter. For example, a systematic uncertainty as low as $\pm$ 0.25% of mass flow rate, with turndown of about 20 to 1 can be achieved. Also, uncertainties as low as $\pm$ 0.10% with 100 to 1 turndown ratio can be obtained. Since the uncertainty estimate must be obtained from the manufacturer and combined with specific test procedures, no DRE will be provided to perform the uncertainty analysis for a Coriolis meter.

3.3.4 Thrust

Load cells can be used to measure thrust. Manufacturer's specifications were used to estimate the uncertainty of a thrust measurement as an example. Elemental sources such as non-linearity, hysteresis, zero balance, thermal zero coefficient, and thermal sensitivity coefficient must be considered in order to evaluate the uncertainty of the thrust. For example, Ormond load cells have non-linearity of $\pm$ 0.07% FS, hysteresis

of $\pm$ 0.02% FS, zero balance of $\pm$ 1% FS, thermal zero coefficient of $\pm$ 0.0014% FS/^{o}F, thermal sensitivity coefficient of $\pm$ 0.0007% load/^{o}F. The measurement uncertainty associated with the load cells is the root-sum-square of all elemental sources as presented in Chapter 2. According to the manufacturer, a reasonable uncertainty due to calibration for a single component thrust measurement system should be taken as 1.027% [24]. Detailed calculations can be found in Appendix C. Therefore, the uncertainty of the thrust is the root-sum-square of the uncertainty due to the calibration process and the measurement system.

$$U_{Thrust} = \sqrt{(B_{cal})^2 + (B_{mea})^2}$$

where B_{cal} is the systematic uncertainty due to calibration, and B_{mea} is the systematic uncertainty due to measurement system.

CHAPTER IV

PERFORMANCE PARAMETERS

4.1 Background

Specific impulse and characteristic velocity (C*actual, C*theoretical, C* efficiency) will be discussed in this chapter. These parameters help to determine the performance of the RBCC engine system. Specific impulse, Isp, is the thrust force per unit weight of propellant. Specific impulse is an important figure of merit of the performance of a rocket propulsion system, which is similar to the concept of miles per gallon parameter used with automobiles [23]. A higher specific impulse means better performance. Five methods to obtain specific impulse will be evaluated in this study to determine the uncertainty associated with each method.

Characteristic velocity, C* (ft/sec), is independent of nozzle characteristics and can be determined by experimental data of chamber pressure, throat diameter, and propellant mass flow rate. C* efficiency is also an important performance parameter as it is used to express the degree of completion of the energy release and the creation of high temperature and pressure gas in the chamber [23]. In this study, characteristic velocity will be evaluated for a single thruster, not the full engine system.

Basic measurement uncertainty estimates obtained from Chapter 3 will be used to evaluate the overall uncertainty for specific impulse and characteristic velocity. The five

methods of determining specific impulse will be presented first, followed by the expressions for characteristic velocity, which includes C* theoretical, C* actual, and C* efficiency. Uncertainty analysis methodology from Chapter 2 will be used to perform general uncertainty analyses of the performance parameters. The results will be presented in Chapter 5.

4.2 Calculated Performance Parameters

4.2.1 Specific Impulse

4.2.1.1 Method 1

Method 1 is the direct measurement of engine thrust and propellant mass flow rate. The specific impulse (sec) is defined as thrust force, F, divided by the sum of oxidizer mass flow rate, w_o, and fuel mass flow rate, w_f.

$$Isp_1 = \frac{F}{(w_o + w_f)} \frac{g_c}{g_o} \tag{4-1}$$

Here g_o is the gravitational acceleration at sea level, and g_c is the dimensional conversion constant 32.174 $(lb_m\text{-ft})/(lb_f\text{-sec}^2)$ in the English system and 1.0 (dimensionless) in the SI system [23, 25].

4.2.1.2 Method 2

Method 2 involves the chamber pressure and area to determine thrust along with propellant mass flow rate. The specific impulse (sec) is a function of thrust coefficient, C_F, stagnation chamber pressure, P_c, throat diameter, D_t, oxidizer mass flow rate, w_o, and fuel mass flow rate, w_f. The constants, g_o and g_c, are the same for method 1.

$$Isp_2 = \frac{C_F P_c \pi D_t^2}{4 (w_o + w_f)} \frac{g_c}{g_o} \tag{4-2}$$

The thrust coefficient can be thought of as representing the amplification of thrust due to the gas expanding in the supersonic nozzle as compared to the thrust that would be exerted if the chamber pressure acted over the throat diameter only. It is a convenient parameter for seeing the effects of chamber pressure or altitude variations in a given nozzle configuration, or to correct sea-level results for flight altitude conditions. Thrust coefficient is a function of pressure ratio, P_c/P_e, nozzle area ratio, A_e/A_t, and specific heat ratio [23, 25].

4.2.1.3 Method 3

Method 3 involves the use of ideal rocket relationships. The method evaluates specific impulse (sec) of an engine in terms of a chamber temperature, T_c, chamber pressure, P_c, exit pressure, P_e, ambient pressure, P_3, oxidizer mass flow rate, w_o, fuel mass flow rate, w_f, and throat diameter, D_t. The relation is based on the assumption that

there is no change in the composition of the exhaust gas as it progresses through the nozzle. Again, the constants, g_o and g_c, are the same as previous methods.

$$Isp_3 = \sqrt{\frac{2R_c g_c}{g_o^{\,2}}\left(\frac{\gamma}{\gamma-1}\right)\left(\frac{T_c}{M}\right)\left[1-\left(\frac{P_e}{P_c}\right)^{\left(\frac{\gamma-1}{\gamma}\right)}\right]} + \frac{(P_e - P_3)\pi D_e^{\,2} g_c}{4(w_o + w_f) g_o} \qquad (4\text{-}3)$$

For a liquid propellant rocket, the idealized theory postulates an injection system in which the fuel and oxidizer are mixed perfectly resulting in a homogeneous working substance. A good rocket injector can approach this condition closely. Isentropic expansion relations in the rocket nozzle are assumed, where the maximum heat is converted to kinetic energy of the jet. The energy lost to the wall is also neglected because the losses are difficult to measure and usually very small in nozzles. The ideal rocket relationships assume well-designed supersonic nozzles where the conversion of thermal energy into directed kinetic energy of the exhausted gases proceeds smoothly without normal shocks or discontinuities [23]. Any increase in the chamber temperature (usually caused by increase in energy release) or any decrease of molecular mass of the propellant (usually achieved by using light molecular mass gases rich in hydrogen content) will help improve the performance of the rocket; thus, increase the engine specific impulse [23, 25].

4.2.1.4 Method 4

Method 3 uses one-dimensional model equations with the assumption that the exhaust gases exiting the nozzle are axially directed. In reality, the gases exiting are directed at an angle to the motor centerline depending upon the nozzle geometry curvature. This results in a loss of propulsive efficiency due to nozzle divergence effects. In order to compensate for the non-axial behavior of the exhaust gas velocity profile, a theoretical correction factor can be applied to the momentum term of the thrust equation. Method 4 considers nozzle divergence angle effects on performance [23, 25]. The nozzle divergence factor, λ_N, is defined as

$$\lambda_N = \frac{1}{2}(1+\cos(\theta)) \tag{4-4}$$

where θ represents the nozzle divergence half angle. Small nozzle divergence half angles cause most of the momentum to be axial, and thus give a high specific impulse. However, the long nozzle has a penalty in rocket propulsion system mass, vehicle mass, and also design complexity, and vice versa. Modifying the method 3 specific impulse expression to account for the nozzle divergence effect yields

$$Isp_4 = \left[\frac{1}{2}(1+\cos(\theta))\right]\sqrt{\frac{2R_c g_c}{{g_o}^2}\left(\frac{\gamma}{\gamma-1}\right)\left(\frac{T_c}{M}\right)\left[1-\left(\frac{P_e}{P_c}\right)^{\left(\frac{\gamma-1}{\gamma}\right)}\right]} + \frac{(P_e - P_3)\pi {D_e}^2 g_c}{4(w_o + w_f)g_o} \tag{4-5}$$

4.2.1.5 Method 5

Method 5 evaluates specific impulse assuming chemical equilibrium is maintained during the nozzle expansion process. In this case, reactions due to high temperature dissociation and recombination of the single fluid are considered. The specific impulse is based on the exit velocity assuming a negligible nozzle gas flow inlet velocity [25].

The specific impulse can be related in terms of chamber temperature, nozzle exit temperature and pressure, and ambient conditions:

$$Isp_5 = \sqrt{\frac{2C_{p,eff}\, g_c}{{g_o}^2}\left(\frac{T_c - T_e}{M}\right)} + \frac{(P_e - P_3)\pi {D_e}^2 g_c}{4(w_o + w_f) g_o} \qquad (4\text{-}6)$$

Typically, iterative calculations are performed in determining the level of dissociation at several points in the nozzle to obtain the temperature of the exhaust gas. The method used assumes both a chamber and exit temperature can be measured in order to assess the performance [25].

4.2.2 Characteristic Velocity

4.2.2.1 C* Theoretical

For the ideal case, the maximum value of C* is a function of gas properties such as specific heat ratio, γ, chamber temperature, T_1, universal gas constant, Rc, and molecular mass, M.

$$C^*_{theo} = \frac{\sqrt{\gamma \frac{Rc}{M} T_1 g_c}}{\gamma \sqrt{[2/(\gamma+1)]^{(\gamma+1)/(\gamma-1)}}} \tag{4-7}$$

4.2.2.2 C* Actual

Characteristic velocity, C* actual (ft/sec), is independent of nozzle characteristic and can be determined by chamber pressure, P_c, throat area, A_t, throat diameter, D_t, and total propellant flow rate, m. The variables at the right in equation (4-8) are the same as defined previously.

$$C^*_{act} = \frac{P_c A_t g_c}{m} = \frac{P_c \pi D_t^{\,2} g_c}{4(w_f + w_o)} \tag{4-8}$$

4.2.2.3 C* Efficiency

*C** efficiency can be determined by the ratio of the actual value, as determined from equation (4-8), and the theoretical value, as obtained from equation (4-7).

$$\eta_{C^*} = \frac{C^*_{act}}{C^*_{theo}} \tag{4-9}$$

C* efficiency is an important performance parameter that is used to express the degree of completion of the energy release and the creation of high temperature and pressure gas in the chamber.

CHAPTER V

PERFORMANCE PARAMETER UNCERTAINTY ANALYSES

5.1 Background

Figure 5-1 shows an example of the RBCC vehicle with the full system design as well as the single thruster design. For instance, the flow path of an RBCC vehicle may have several identical sections. Each section may consist of multiple struts with multiple imbedded rockets or thrusters. The entire system (cowl to tail) may be evaluated for performance or a single thruster may be evaluated. Representative values for a conceptual RBCC engine were used in this study. The values were derived considering values that would be needed for a scaled version of one flow path, which could be a typical test scenario.

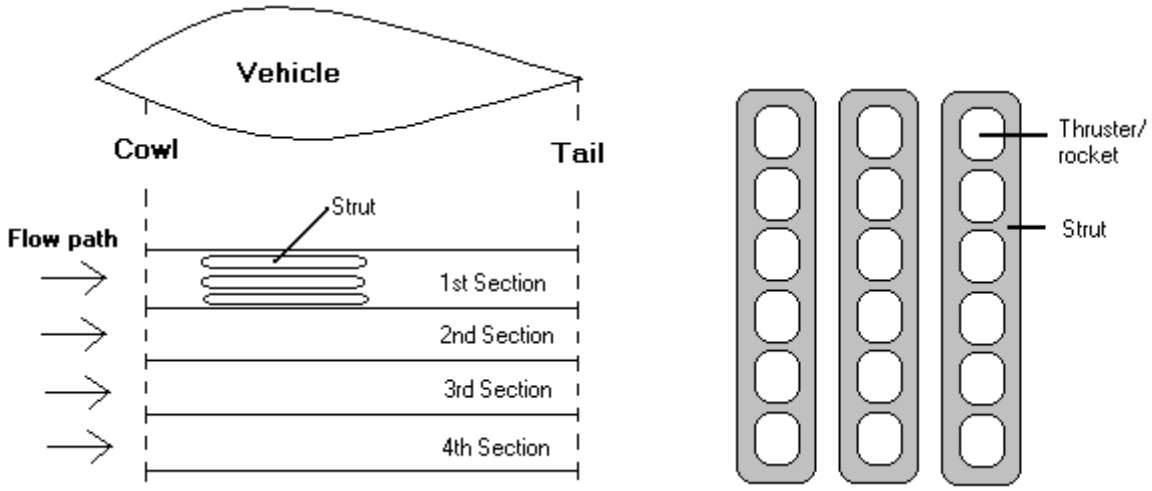

(a) (b)

Figure 5-1: (a) Full Engine System from Cowl to Tail, (b) Single Thruster/Rocket

Uncertainty analyses for specific impulse focused on both the full engine system from cowl to tail, as well as a single thruster. Uncertainty analyses of characteristic velocity were based on the single thruster only.

5.2 Specific Impulse

As discussed in Chapter 4, five methods of determining specific impulse were evaluated in this study. Method 1 involved direct thrust and mass flow rate measurements. A total of five cases were run for method 1. Cases 1 through 4 were run for the full engine system from cowl to tail for one out of four flow-paths at 50% scale. Case 1 was run to simulate the air augmented rocket mode where the fuel and oxidizer

are supplied by the system; therefore, higher thrust is generated in this mode compared to the ramjet and scramjet modes. Case 2 was the ramjet mode, operated at about Mach 3.5, where the rocket mode is switched off. A decrease in oxidizer and fuel flow rate can be observed from case 1 to case 2. Case 3 simulated the ramjet mode at Mach 5.0 without rocket propulsion. Since the Mach number was increased from Mach 3.5 to 5.0, the thrust and flow rates generated also increased. While the rockets were still switched off, scramjet mode was activated at about Mach 7 (case 4). Case 5 used the thrust value obtained from method 2 for a single thruster. The run conditions for method 1 are shown in Table 5-1.

Method 2 involved the determination of thrust coefficient, throat diameter, chamber pressure, oxidizer flow rate, and fuel flow rate for a single thruster to achieve specific impulse. Thrust coefficient is a function of specific heat ratio, nozzle expansion ratio, and the pressure ratio across the nozzle, but it is independent of the chamber temperature [23]. Example run conditions for method 2 are presented in Table 5-1.

	Method 1					Method 2
Variables	Case 1	Case 2	Case 3	Case 4	Case 5	Case 1
F (lbf)	4500	2200	2400	1600	125	-
C_F	-	-	-	-	-	1.7
P_c (psia)	-	-	-	-	-	1500
D_t (in)	-	-	-	-	-	0.250
w_o (lbm/sec)	8.000	0.120	0.140	0.110	0.464	0.464
w_f (lbm/sec)	2.500	1.500	1.800	1.500	0.066	0.066
Isp (sec)	428.6	1358.0	1237.0	993.8	235.9	236.2

Table 5-1: Example Run Conditions of Specific Impulse for Methods 1 and 2

Methods 3, 4, and 5 also account for a single thruster. Direct comparisons cannot be made between the full system and single thruster evaluations. Both ground testing and altitude testing at 55,000 ft (Mach 3.5) were evaluated using Methods 3, 4, and 5. Method 3 assumes isentropic expansion relations in the rocket nozzle where the maximum heat is converted to kinetic energy of the vehicle. Method 3, case 1 was run at optimum condition where the nozzle exit pressure equaled the atmospheric pressure. Method 3, case 2 was carried out at the altitude of 55,000 ft. This creates a lower atmospheric pressure, thus increasing the specific impulse of the rocket. Method 4 is identical to method 3 except method 4 considers the effects of nozzle divergence angle on the performance of the rocket. The same cases were run for method 4 as for method 3. A decrease in specific impulse can be observed in method 4 compared to method 3.

Method 5 assumes chemical equilibrium is maintained during the nozzle expansion process. Case 1 was based on ground testing at the optimum condition. Case

2 was run at the altitude of 55,000 ft. Case 3 was identical to case 1 except the nozzle exit temperature was increased. Case 4 was identical to case 2 except the nozzle exit pressure was decreased. Example run conditions for all the cases for methods 3, 4, and 5 are summarized in Table 5-2.

	Method 3		Method 4		Method 5			
Variables	Case 1	Case 2	Case 1	Case 2	Case 1	Case 2	Case 3	Case 4
R_c (BTU/ lbmol-R)	1.986	1.986	1.986	1.986	-	-	-	-
Cp_{eff} (BTU/ lbmol-R)	-	-	-	-	11.916	11.916	11.916	11.916
γ	1.2	1.2	1.2	1.2	-	-	-	-
θ (deg)			23.5	23.5	-	-	-	-
T_c (^oR)	5450	5450	5450	5450	5450	5450	5450	5450
T_e (^oR)	-	-	-	-	2500	2500	2800	2500
M (lb/lbmol)	21.5	21.5	21.5	21.5	21.5	21.5	21.5	21.5
P_e (psia)	14.0	14.0	14.0	14.0	14.0	14.0	14.0	12.5
P_c (psia)	1500	1500	1500	1500	-	-	-	-
P_3 (psia)	14.0	2.277	14.0	2.277	14.0	2.277	14.0	2.277
D_e (in)	0.87	0.87	0.87	0.87	0.87	0.87	0.87	0.87
w_o (lbm/sec)	0.464	0.464	0.464	0.464	0.464	0.464	0.464	0.464
w_f (lbm/sec)	0.066	0.066	0.066	0.066	0.066	0.066	0.066	0.066
Isp (sec)	281.1	294.2	269.4	282.6	281.1	294.3	266.4	282.8

Table 5-2: Example Run Conditions of Specific Impulse for Methods 3, 4 and 5

5.2.1 1% Uncertainty Estimates

For the initial uncertainty analyses of the specific impulse, a 1% uncertainty was assumed for each variable. The results will be given and discussed in Section 5.4.

5.2.2 Uncertainty Estimate Variation Cases

After the initial 1% uncertainty cases, more realistic uncertainty estimates were run for the various methods. A discussion of possible uncertainty sources for the various measurements and how the more realistic uncertainty estimates were obtained follows. This discussion provides guidance of uncertainty estimates for future evaluations.

The uncertainty of the temperature measurement can reach as high as 10% [25]. This uncertainty estimate sounds large, but several factors that come into play when measuring the temperature must be considered Firstly, in most cases, the temperature distribution is not constant over the chamber and nozzle exit. Conceptual bias is the bias that arises when a cross-sectional average value required in the data reduction equation is replaced by an average of multiple point measurements. The cross-sectional average is the integral; therefore, a summation of the values must be made to estimate the integral. If enough measurements are made, then the summation is approximately equal to the integral, and conceptual bias can be neglected. Otherwise, conceptual bias needs to be considered for temperature measurement [26]. Temperature at the chamber and nozzle exit represents the average temperature. Assuming only one point measurement is made at each of these locations, the temperature measurement represents the condition at one

spatial point, thus creating a conceptual bias uncertainty associated with the temperature measurement. The type of measurement devices used can also affect the uncertainty of the temperature measurement as discussed in Chapter 3. Finally, measuring the extremely high temperatures for RBCC engine testing is a difficult task and will cause the uncertainty of the temperature measurements to be higher. All these error sources may contribute to the uncertainty of the temperature measurement.

For the RBCC full system design, which is simulated by specific impulse GUA method 1 (cases 1 through 4), a pressure variation of 10% is used as a check on combustion stability. If the uncertainty of the pressure stays within 10%, the RBCC full engine system is considered stable. However, less pressure variation is expected for a single thruster analysis. A 10% uncertainty estimate for pressure measurement at the nozzle exit, chamber pressure, and ambient air, is possible if several factors are taken into consideration when measuring the pressure during the test. As with temperature, the conceptual bias must be considered [26]. The steadiness of the test facility can also be one of the uncertainty sources. Engine vibration during the testing may cause variation of the pressure measurement over time. The type of measurement device, measurement methods, etc., will affect the uncertainty of the pressure measurement as discussed in Chapter 3. Therefore, the uncertainties of the pressure measurements must consider all possible error sources.

The diameter measurement can be off by as much as 0.015 inches full-scale. Again, several factors must be considered when evaluating the diameter uncertainty. If the throat is not measured after manufacture, the uncertainty estimate should be based on

manufacturing tolerances. If the throat is measured after manufacture, the uncertainty should be less, but this is not guaranteed. The uncertainty of the diameter measurement depends on the accuracy of the measurement device as well as the ease of access to a small throat diameter. Also, the diameter measurement occurs in an ambient environment, whereas the throat diameter will go through expansion and contraction due to high temperature and pressure during the actual engine testing. This depends on the thermal conductivity of the material used. These possible error sources should be considered when evaluating the uncertainty of the diameter.

The uncertainty of the density may vary from 1% to 10% depending on the type of propellant used. To properly estimate the uncertainty in this property value, the data scatter associated with the original property data should be analyzed [25]. Since density is a function of temperature and pressure, the initial density data points can be obtained with various conditions of temperature and pressure. To obtain the density percentage error, pressure input should be kept constant while varying the temperature and vice versa. This will help in determining more accurate density uncertainty at certain temperature and pressure conditions.

A 1% uncertainty of the thrust measurement may be achieved if extreme care is taken with the calibration and test procedures. Load cells specification can be obtained from the manufacturer with its calibration data curve for different types of load cells desired. For example, Ormond 69 series load cells can be calibrated within $\pm$ 1.027%. Load cells specification such as non-linearity, hysteresis, zero balance, and thermal coefficient need to be considered in thrust measurement analysis. The uncertainty

associated with thrust measurement will also vary depending on the test set-up and procedures at different test facilities.

Thrust coefficient changes with the change of altitude, and it is a function of specific heat ratio, chamber pressure, ambient pressure, and nozzle expansion ratio. The uncertainty of the thrust coefficient can be as high as 5% for the full system and 3% for a single thruster. The actual or more logical value of thrust coefficient can only be achieved by actual test results because the gas properties and specific heat ratio, which change along the chamber axis, will affect the true value of thrust coefficient [27].

Mass flow rate uncertainty can be estimated at 2% or less depending on the type of flow meter used. As discussed in Chapter 3, mass flow rate data reduction equations are functions of discharge coefficient, thermal expansion factor, inlet and throat diameters, and the inlet density in many cases (except for turbine meters and coriolis flow meters). MathCAD worksheets are attached in Appendix B for the detailed calculation of determining the uncertainty of the mass flow rate with data reduction equations.

The universal gas constant, R_c, and molecular mass, M, were estimated as $\pm$ 0.5% as they are not measured variables and have no significant effect on the uncertainty of the results. Uncertainty of the specific heat ratio, γ, and effective specific heat at constant pressure, Cp_{eff}, were set to $\pm$ 1% in this study. These properties change along the chamber axis during the actual testing. To properly estimate the uncertainties in these property values, the data scatter associated with the original property data should be analyzed. Nozzle divergence half angle, θ, was estimated as $\pm$ 1% in this study.

However, it depends on the manufacturer specifications, and the uncertainty may vary during the actual system testing.

Estimates of the variable measurement uncertainties used for full system testing and single thruster testing are summarized in Table 5-3. These estimates were made based on knowledge of instrumentation measurement limits and uncertainty factors discussed above. The results using these uncertainty estimates will be given and discussed in Section 5.4.

	Uncertainty Estimate Variations (%)	
Measured Variables	Full System	Single Thruster
Temperature (chamber, nozzle exit)	± 8.0 %	± 3.0 %
Pressure (chamber, nozzle exit, ambient)	± 8.0 %	± 3.0 %
Diameter (throat)	± 3.0 %	± 3.0 %
Diameter (nozzle exit)	± 1.0 %	± 1.0 %
Fluid Density	± 5.0 %	± 5.0 %
Universal Gas Constant	± 0.5 %	± 0.5 %
Molecular Mass	± 0.5 %	± 0.5 %
Specific Heat Ratio	± 1.0 %	± 1.0 %
Effective Specific Heat at Constant Pressure	± 1.0 %	± 1.0 %
Nozzle Divergence Half Angle	± 1.0 %	± 1.0 %
Thrust	± 1.0 %	± 1.0 %
Thrust Coefficient	± 5.0 %	± 3.0 %
Mass Flow Rate	± 2.0 %	± 1.0 %

Table 5-3: Uncertainty Estimate Variation Cases

5.3 Characteristic Velocity

The uncertainty analyses for characteristic velocity focused on the single thruster only, not the full engine system from cowl to tail. The example nominal values to determine characteristic velocity are shown in Table 5-4.

	C* Theoretical (ft/sec)		C* Actual (ft/sec)			C* Efficiency (%)		
Variables	Case 1	Case 2	Case 1	Case 2	Case 3	Case 1	Case 2	Case 3
γ	1.2	1.2	-	-	-	1.2	1.2	1.2
R_c (BTU/ lbmol-R)	1.986	1.986	-	-	-	1.986	1.986	1.986
M (lb/lbmol)	21.5	21.5	-	-	-	21.5	21.5	21.5
T_c (^{o}R)	5300	5600	-	-	-	5600	5600	5600
P_c (psia)	-	-	1400	1500	1600	1400	1500	1600
D_t (in)	-	-	0.25	0.25	0.25	0.25	0.25	0.25
w_o (lbm/sec)	-	-	0.464	0.464	0.464	0.464	0.464	0.464
w_f (lbm/sec)	-	-	0.066	0.066	0.066	0.066	0.066	0.066
C*	5398	5549	4172	4470	4768	0.752	0.806	0.859

Table 5-4: Example Run Conditions for Characteristic Velocity

5.3.1 1% Uncertainty Estimates

For the initial uncertainty analyses of the characteristic velocity, a 1% uncertainty was assumed for each variable, as with the specific impulse analyses. The results will be given and presented in Section 5.4.

5.3.2 Uncertainty Estimate Variation Cases

The more realistic uncertainty estimates required for the characteristic velocity analyses can be obtained from Table 5-3, where only the uncertainty estimates for the single thruster will be used. The results using these uncertainty estimates will be given and discussed in the next section.

5.4 Discussion of Results

Tables 5-5, 5-6, 5-8, and 5-9 show the result uncertainties and UPC values for the specific impulse analyses. The result uncertainties and the UPC values presented in Tables 5-5 and 5-6 are based on 1% uncertainties for the input variables. The analyses based on 1% uncertainty for each input variable shows the possible influence of the variables similar to a UMF analysis. Since all of the uncertainties are equal, the results are analogous to UMF results. Direct thrust measurement contributes the most uncertainty to the test result in method 1. Oxidizer flow rate and fuel flow rate also contribute significant uncertainty to the test result depending on the RBCC mode of

operation. Fuel flow rate tends to dominate the test uncertainty during ramjet and scramjet mode. The oxidizer flow rate is very small since these are air-breathing modes. The thrust contributes significantly to the test uncertainty in air- augmented rocket mode (method 1, case 1). Single thruster analysis using method 2 shows a large uncertainty contribution from the throat diameter measurement. Specific heat ratio tends to dominate the test uncertainty in methods 3 and 4 for the single thruster analyses. Moreover, the chamber temperature measurement drives the test uncertainty of method 5.

Tables 5-8 and 5-9 show the UPC values of specific impulse based on the uncertainty estimate variation cases provided in Table 5-3. With reference to these uncertainty estimates, oxidizer flow rate and fuel flow rate in the full engine system contribute the most to the uncertainty of the test result. The single thruster design in method 1, case 5, and method 2 tends to be affected mostly by the thrust measurement and nozzle throat diameter measurement uncertainties, respectively. The 1% uncertainty estimate for thrust is reasonable but difficult to obtain. Any effort to lower the thrust uncertainty would not likely be worthwhile. The throat diameter was shown to be a variable to watch from the 1% uncertainty cases, and it had high uncertainty for the single thruster here. Method 2 single thruster design evaluation is not recommended because it contributes more uncertainty to the test result than the thrust performance determination method (method 1, case 5). However, method 1 cannot be used for the single thruster unless the testing is done individually. Single thruster system testing must use another method instead of using method 1. Direct comparisons cannot be made between the full engine system and the single thruster design.

Specific impulse single thruster evaluation methods provided in Table 5-9 show that the chamber temperature uncertainty dominates the uncertainty in the test result. A more accurate temperature value is needed. More data points should be taken to reduce the uncertainty due to the conceptual bias. Methods 3 and 4 show a low uncertainty in the test results, but remember that isentropic relationships and pure axial thrust were assumed. If these assumptions are not valid, the uncertainty due to the assumptions has not been accounted for. Remember that this work was limited to the uncertainties of the measured variables in the data reduction equations only. The effect of the assumptions used to derive the data reduction equations on the uncertainty is the subject of the future work. In this study, the uncertainty in the test result was lower when the analyses were run above sea level at the altitude of 55,000 ft. Refer to Appendix D for more details.

The UPC values for the characteristic velocity uncertainty analyses are presented in Tables 5-7 and 5-10. The uncertainty contributions of each measured variable based on 1% uncertainty presented in Table 5-7 shows the possible influence of the variables similar to a UMF analysis. Table 5-7 predicts major uncertainty contributions from chamber temperature and throat diameter. Uncertainty estimate variation cases provided in Tables 5-10 show more realistic uncertainty contributions of each input variable in the test result. The chamber temperature and throat diameter were shown to be the variables to watch from the 1% uncertainty cases (Table 5-7), and they had high uncertainties in the uncertainty estimate variation cases. Uncertainty of the chamber pressure measurement does contribute to the uncertainty in the test result, but not as great as the chamber temperature.

In general, oxidizer flow rate and fuel flow rate in the specific impulse analyses contribute the most uncertainty in the test result for the full system design, whereas, thrust and throat diameter measurement uncertainties are critical in the single thruster evaluation of method 1, case 5, and method 2. Furthermore, chamber temperature measurement uncertainty is critical for methods 3, 4, and 5. Based on the characteristic velocity uncertainty analyses, the chamber temperature and throat diameter measurement uncertainties dominate the uncertainty in the final result.

When one measurement uncertainty is found to affect the uncertainty in the test result, improvements should be made to lower the uncertainty of the particular measurement. However, when this is done, the percentage contribution to the total uncertainty of the other variables will increase. For example, consider the specific impulse evaluation in method 2. When the uncertainty of the throat diameter is reduced from 3% to 1%, the percentage contribution to the uncertainties of the thrust coefficient and chamber pressure will increase. However, the overall uncertainty is lower; therefore, the percentage value is a percentage of a lower number. This idea should be kept in mind when interpreting UPC results.

	UPC (%)					
	Method 1					Method 2
Variables	Case 1	Case 2	Case 3	Case 4	Case 5	Case 1
F	61.08	53.68	53.59	53.40	56.12	-
C_F	-	-	-	-	-	14.75
P_c	-	-	-	-	-	14.75
D_t	-	-	-	-	-	58.98
w_o	35.46	0.30	0.28	0.25	43.01	11.30
w_f	3.46	46.02	46.13	46.35	0.87	0.23
Isp (sec)	428.6	1358.0	1237.0	993.8	235.9	236.2
U_{Isp} (sec)	5.48	18.54	16.90	13.60	3.15	6.15
U_{Isp} (%)	1.28	1.37	1.37	1.37	1.34	2.60
Total UPC (%)	100	100	100	100	100	100

Table 5-5: Specific Impulse Analyses of Methods 1 and 2 based on 1% Uncertainty Estimates for all Variables

	UPC (%)							
	Method 3		Method 4		Method 5			
Variables	Case 1	Case 2	Case 1	Case 2	Case 1	Case 2	Case 3	Case 4
R_c	16.91	16.83	16.82	16.73	-	-	-	-
Cp_{eff}	-	-	-	-	16.24	16.17	13.56	16.25
γ	48.71	48.47	48.46	48.20	-	-	-	-
θ	-	-	0.49	0.49	-	-	-	-
T_c	16.91	16.83	16.82	16.73	55.44	55.18	57.36	55.46
T_e	-	-	-	-	11.67	11.61	15.14	11.67
M	16.91	16.83	16.82	16.73	16.24	16.17	13.56	16.25
P_e	0.02	0.02	0.01	0.01	0.20	0.20	0.19	0.20
P_c	0.34	0.34	0.34	0.33	-	-	-	-
P_3	0.21	0.01	0.23	0.01	0.20	0.01	0.19	0.16
D_e	0.00	0.59	0.00	0.64	0.00	0.57	0.00	0.01
w_o	0.00	0.11	0.00	0.12	0.00	0.11	0.00	0.00
w_f	0.00	0.00	0.00	0.00	0.00	0.00	0.00	0.00
Isp	281.1	294.2	269.4	282.6	281.1	294.3	266.4	282.8
U_{Isp} (sec)	3.42	3.43	3.28	3.29	3.49	3.50	3.62	3.49
U_{Isp} (%)	1.22	1.17	1.22	1.17	1.24	1.36	1.36	1.23
Total UPC (%)	100	100	100	100	100	100	100	100

Table 5-6: Specific Impulse Analyses of Methods 3, 4 and 5 based on 1% Uncertainty Estimates for all Variables

	UPC (%)							
	C* Theoretical (ft/sec)		C* Actual (ft/sec)			C* Efficiency (%)		
Variables	Case 1	Case 2	Case 1	Case 2	Case 3	Case 1	Case 2	Case 3
γ	14.69	14.69	-	-	-	1.94	1.94	1.94
R_c	28.44	28.44	-	-	-	3.75	3.75	3.75
M	28.44	28.44	-	-	-	3.75	3.75	3.75
T_c	28.44	28.44	-	-	-	3.75	3.75	3.75
P_c	-	-	17.30	17.30	17.30	15.01	15.01	15.01
D_t	-	-	69.18	69.18	69.18	60.05	60.05	60.05
w_o	-	-	13.26	13.26	13.26	11.51	11.51	11.51
w_f	-	-	0.27	0.27	0.27	0.23	0.23	0.23
C*	5398	5549	4172	4470	4768	0.752	0.806	0.859
U_{C^*}	50.62	52.03	100.32	107.48	114.65	0.02	0.02	0.02
U_{C^*} (%)	0.94	0.94	2.41	2.41	2.41	2.58	2.58	2.58
Total UPC (%)	100	100	100	100	100	100	100	100

Table 5-7: Characteristic Velocity Analyses based on 1% Uncertainty Estimates for all Variables

	UPC (%)					
	Method 1					Method 2
Variables	Case 1	Case 2	Case 3	Case 4	Case 5	Case 1
F	28.18	22.47	22.40	22.27	56.12	-
C_F	-	-	-	-	-	16.43
P_c	-	-	-	-	-	16.43
D_t	-	-	-	-	-	65.72
w_o	65.43	0.49	0.47	0.42	43.01	1.40
w_f	6.39	77.04	77.13	77.32	0.87	0.03
Isp (sec)	428.6	1358.0	1237.0	993.8	235.9	236.2
U_{Isp} (sec)	8.07	28.65	26.14	21.06	3.15	17.48
U_{Isp} (%)	1.88	2.11	2.11	2.12	1.34	7.40
Total UPC (%)	100	100	100	100	100	100

Table 5-8: Uncertainty Estimate Variation Cases for Specific Impulse Analyses of Methods 1 and 2

	UPC (%)							
	Method 3		Method 4		Method 5			
Variables	Case 1	Case 2	Case 1	Case 2	Case 1	Case 2	Case 3	Case 4
R_c	1.97	1.98	1.97	1.98	-	-	-	-
Cp_{eff}	-	-	-	-	2.59	2.59	2.02	2.59
γ	22.72	22.84	22.65	22.78	-	-	-	-
θ	-	-	0.23	0.23	-	-	-	-
T_c	70.98	71.36	70.77	71.18	79.47	79.60	76.73	79.51
T_e	-	-	-	-	16.72	16.75	20.25	16.73
M	1.97	1.98	1.97	1.98	0.65	0.65	0.50	0.65
P_e	0.06	0.06	0.04	0.04	0.29	0.29	0.25	0.29
P_c	1.42	1.43	1.41	1.42	-	-	-	-
P_3	0.89	0.02	0.96	0.03	0.29	0.01	0.25	0.23
D_e	0.00	0.28	0.00	0.30	0.00	0.09	0.00	0.00
w_o	0.00	0.05	0.00	0.06	0.00	0.02	0.00	0.00
w_f	0.00	0.00	0.00	0.00	0.00	0.00	0.00	0.00
Isp	281.1	294.2	269.4	282.6	281.1	294.3	266.4	282.8
U_{Isp} (sec)	5.01	5.00	4.80	4.79	8.74	8.73	9.38	8.74
U_{Isp} (%)	1.78	1.70	1.78	1.70	3.11	2.97	3.52	3.09
Total UPC (%)	100	100	100	100	100	100	100	100

Table 5-9: Uncertainty Estimate Variation Cases for Specific Impulse Analyses of Methods 3, 4, and 5

	UPC (%)							
	C* Theoretical (ft/sec)		C* Actual (ft/sec)			C* Efficiency (%)		
Variables	Case 1	Case 2	Case 1	Case 2	Case 3	Case 1	Case 2	Case 3
γ	5.16	5.16	-	-	-	0.27	0.27	0.27
R_c	2.50	2.50	-	-	-	0.13	0.13	0.13
M	2.50	2.50	-	-	-	0.13	0.13	0.13
T_c	89.85	89.85	-	-	-	4.66	4.66	4.66
P_c	-	-	19.66	19.66	19.66	18.64	18.64	18.64
D_t	-	-	78.63	78.63	78.63	74.56	74.56	74.56
w_o	-	-	1.67	1.67	1.67	1.59	1.59	1.59
w_f	-	-	0.03	0.03	0.03	0.03	0.03	0.03
C*	5398	5549	4172	4470	4768	0.752	0.806	0.859
U_{C*}	85.25	87.81	282.28	302.44	322.60	0.052	0.056	0.06
U_{C*} (%)	1.58	1.58	6.77	6.77	6.77	6.95	6.95	6.95
Total UPC (%)	100	100	100	100	100	100	100	100

Table 5-10: Uncertainty Estimate Variation Cases for Characteristic Velocity Analyses

CHAPTER VI

SUMMARY AND CONCLUSIONS

Many data reduction methods are available to evaluate the performance parameters from an RBCC engine system. This study included the performance parameter evaluations based on five methods of determining specific impulse. Theoretical and actual characteristic velocities were also analyzed to determine the C* efficiency. Additionally, the study included the basic measurement uncertainties, such as temperatures, pressures, mass flow rates, and thrust, which contribute to the uncertainties in the performance parameter results.

General uncertainty analyses were completed for all of the parameter results of interest. Cases for the full system and single thruster design were run. The initial uncertainty analyses were based on 1% uncertainty contribution in each variable. Then, uncertainty estimate variation cases were simulated to study the more realistic examples. The result uncertainties and uncertainty percentage contribution (UPC) values were calculated for all cases. The UPC values showed the influence of each measured variable on the uncertainty of the test result of interest. Through the UPC analyses, the uncertainties of particular measurements that contributed significantly to the uncertainty in the test result could be identified. Therefore, this can be a significant guide in the cost effective use of resources to reduce the test uncertainty.

Based on UPC values, oxidizer flow rate and fuel flow rate in the specific impulse analyses contributed the most uncertainty in the test result for the full system design, whereas, thrust and throat diameter measurement uncertainties were critical in the single thruster evaluation of method 1, case 5, and method 2, respectively. Single thruster design evaluation using method 2 is not recommended because it contributes more uncertainty in the test result than the thrust performance determination method (method 1, case 5). However, method 1 cannot be used for the single thruster unless the testing is done individually rather than integrated with the full system.

Furthermore, chamber temperature was critical in methods 3, 4, and 5. A more accurate temperature measurement is needed. More data points should be taken to reduce the uncertainty due to the conceptual bias. Methods 3 and 4 for specific impulse analyses hold only if the axial thrust and isentropic relationships are valid. Otherwise, the uncertainty that might be present is not accounted for in this analysis. Therefore, one must remember the limitations of the current work in comparing the different methods. Also, no direct comparison of data reduction methods should be attempted between the RBCC full system design and single thruster design.

Based on the characteristic velocity uncertainty analyses, the chamber temperature and throat diameter measurement uncertainties dominated the uncertainty in the final result. Uncertainty of the chamber pressure measurement did contribute to the uncertainty in the test result, but not as great as the chamber temperature.

In conclusion, this study has well predicted the possible uncertainty contributions of the basic measurements, such as temperature, pressure, mass flow rate, and thrust that

propagate through the data reduction equations into the uncertainty of the test results of interest. Uncertainty analysis procedures were developed to aid in evaluating the best data reduction equations to use based on the expected uncertainties of the measured variables. Applying the procedures developed in this work can improve test results obtained during RBCC systems testing.

REFERENCES CITED

[1] NASA Facts, “Hypersonics Research and Development,” Marshall Space Flight Center, FS-2003-01-01-MSFC, 2003.

[2] NASA Facts, “Integrated System Test of an Air-breathing Rocket (ISTAR),” Marshall Space Flight Center, FS-2003-01-02-MSFC, 2003.

[3] Neill, T. M., and Gladstone, J. D., “Durability Demonstration of Small High Performance Rocket Thrusters for RLV Applications,” AIAA 99-2357.

[4] Garrard, D., and Rigney, S., “New Test Capability at AEDC’s Aerodynamic and Propulsion Test Unit (APTU),” Jacob Sverdrup AEDC Group, TN 2002.

[5] NASA Glenn Research Center Plum Brook Station, “Hypersonic Tunnel Facility,” <http://facilities.grc.nasa.gov/htf/index.html>, February 2003.

[6] NASA Langley Research Center, “8-Foot High Temperature Tunnel,” <http://wte.larc.nasa.gov/facilities/hypersonic/8ft.cfm?field=10&id=2&fac=1>, February 2003.

[7] NASA Langley Research Center, “Combustion-Heated Scramjet Test Facility (CHSTF),” <http://wte.larc.nasa.gov/facilities/hypersonic/combustion.cfm?field=12&id=2&fac=1>, February 2003.

[8] Cornners, Timothy R., Sims, Robert L., “Full Flight Envelope Direct Thrust Measurement on a Supersonic Aircraft,” Dryden Flight Research Center, NASA/TM-1998-206650, 1998.

[9] McCullough, G., H., and Ostermier, B. J., “The Rocket Nozzle Test Facility - Its Capabilities and Role in Developing Propulsion Systems,” Rocketdyne Propulsion and Power.

[10] Modroukas, D., Rubin, D., Engers, R., and Swartwout, W., “Design and Construction of a New Aeropropulsion Test Leg at GASL,” AIAA-2000-2689, 2000.

[11] NASA Glenn Research Center, "Propulsion Systems Laboratory," <http://facilities.grc.nasa.gov/psl/psl_desc.html>, February 2003.

[12] NASA Glenn Research Center, "Aerospace Facilities: 8x6 Supersonic Wind Tunnel," <http://facilities.grc.nasa.gov/8x6/8x6_quick.html>, February 2003.

[13] NASA Glenn Research Center, "Aerospace Facilities: Abe Silverstein Supersonic Wind Tunnel," <http://facilities.grc.nasa.gov/10x10/10x10_quick.html>, February 2003.

[14] Coleman, H. W., and Steele, W. G., *Experimentation and Uncertainty Analysis for Engineers*, 2nd Edition, Wiley, New York 1999.

[15] Holman, J. P., *Experimental Methods for Engineers*, 7th Edition, McGraw Hill, New York, 2001.

[16] Hudson, S. T., Ryan, H. M, Hughes, M. S., and Hammond, J. M., "Test Facility Uncertainty Analyses for RBCC Systems Testing," AIAA 2002-3607, 2002.

[17] *Fluid Meters, Their Theory and Application*, 6th Edition, ASME, New York, 1971.

[18] Flow Meter Directory: "Orifice Plate Flow Meter", <http://www.flowmeterdirectory.com/flowmeter_orifice_plate.html>, MAY 15, 2003.

[19] Advanced Differential Pressure Flow Meter Technology, "V-cone Installation Operation & Maintenance Manual," McCrometer Inc., California, 1992.

[20] Flow Calculation for the V-cone Flow Meter, McCrometer Inc., California, 1992. Literature Part # 24509-54.

[21] Figliola, R. S., Beasley, D. E., Theory and Design for Mechanical Measurements, 2nd Edition, Wiley, New York, 1995.

[22] Flow Meter Directory: "Coriolis Mass Flow Meter" <http://www.flowmeterdirectory.com/flowmeter_coriolis.html>, MAY 15, 2003.

[23] Sutton, G. P., Biblarz, Oscar, *Rocket Propulsion Elements*, 7th Edition, Wiley, New York, 2001.

[24] Single Component Thrust Measuring System, Statement of Work, SCT-98-036-200K-C, Ormond Inc., 1998.

[25] P.Markopoulos and Hugh W. Coleman and Clark W. Hawk, “An Uncertainty Assessment of Performance Evaluation Methods for Solar Thermal Absorber/Thruster Testing,” AIAA 96-3012, 1996.

[26] Heng, Boon Liang, “Evaluating Data Averaging Techniques for High Gradient Flow Fields through Uncertainty Analysis,” Master Thesis, Dept. of Mechanical Engineering, Mississippi State University, Starkville, MS, August, 2001.

[27] Huzel, Dieter K., Huang, David H., *Modern Engineering for Design of Liquid-Propellant Rocket Engines*, Volume 147, Progress in Astronautics and Aeronautics, Washington, DC, 1992.

APPENDIX A

EXCEL WORKSHEETS

Table A-1: Type E Thermocouple with UTR

Type E Thermocouple with UTR

SSC :Temperature range 36 °R to 660 °R (-424 °F to 200 °F) (-253 °C to 93 °C)
NIST :Temperature range 6 °R to 2292 °R (-454 °F to 1832 °F) (-270 °C to 1000 °C)
Omega :Temperature range 132 °R to 2112 °R (-328 °F to 1652 °F) (-200 °C to 900 °C)

Indicator	Color
Input required from user	Yellow
MSU uncertainty input values	Bright Green
Results	**Red Bold**

Input Gain (100,200,300, 500 or 1000)	100

Post-test Drift Tolerance (mV)
10

Temperature Readings	°R	°F	°C
1	132.00	-328.00	-200.00
2	2112.00	1652.00	900.00
3	60.00	-400.00	-240.00
4	100.00	-360.00	-217.78
5	200.00	-260.00	-162.22
6	300.00	-160.00	-106.67
7	350.00	-110.00	-78.89
8	400.00	-60.00	-51.11
9	660.00	200.00	93.33
10	640.00	180.00	82.22

Uncertainty Calculations

Systematic

Elemental Source	B (^{o}C)	B (^{o}F)	B (^{o}R)	Comments
Thermocouple Readings				
1	2.00	3.60	3.60	Omega manufacturer's spec. (Valid down to -200^{o}C.)
2	1.70	3.06	3.06	
3	2.40	4.32	4.32	
4	2.18	3.92	3.92	
5	1.70	3.06	3.06	
6	1.70	3.06	3.06	
7	1.70	3.06	3.06	
8	1.70	3.06	3.06	
9	1.70	3.06	3.06	
10	1.70	3.06	3.06	
UTR RTD	0.15	0.27	0.27	Kaye Instruments UTR application notes.
UTR Uniformity	0.03	0.05	0.05	Kaye Instruments UTR application notes- Fig.3. Assume 2.5^{o}F/hr change in T.
Vcal Input Device				
1	0.50	0.90	0.90	Depends on temperature due to TC sensitivity (^{o}C/mV).
2	0.20	0.36	0.36	Model 501J specs.
3	0.75	1.35	1.35	
4	0.50	0.90	0.90	
5	0.20	0.36	0.36	
6	0.20	0.36	0.36	
7	0.20	0.36	0.36	
8	0.20	0.36	0.36	
9	0.20	0.36	0.36	

10	0.20	0.36	0.36	
System Drift after Vcal	3.00	5.40	5.40	Assume a sensitivity of 30°C/mV (only valid T>-170°C).
DAQS Linearity	0.00	0.00	0.00	Assume negligible.
Additional Source ?	0.00	0.00	0.00	Add as needed.
Additional Source ?	0.00	0.00	0.00	Add as needed.
Installation Effects				Must be evaluated for each test.
1	0.00	0.00	0.00	Examples: 1. Interactions of the transducer with the system. 2. System disturbances due to the transducer.
2	0.00	0.00	0.00	
3	0.00	0.00	0.00	
4	0.00	0.00	0.00	
5	0.00	0.00	0.00	
6	0.00	0.00	0.00	
7	0.00	0.00	0.00	
8	0.00	0.00	0.00	
9	0.00	0.00	0.00	
10	0.00	0.00	0.00	

Total Systematic	T (°C)	B (°C)	T (°F)	B (°F)	T (°R)	B (°R)
1	-200.00	3.64	-328.00	6.56	132.00	6.56
2	900.00	3.46	1652.00	6.22	2112.00	6.22
3	-240.00	3.92	-400.00	7.05	60.00	7.05
4	-217.78	3.74	-360.00	6.74	100.00	6.74
5	-162.22	3.46	-260.00	6.22	200.00	6.22
6	-106.67	3.46	-160.00	6.22	300.00	6.22
7	-78.89	3.46	-110.00	6.22	350.00	6.22
8	-51.11	3.46	-60.00	6.22	400.00	6.22
9	93.33	3.46	200.00	6.22	660.00	6.22
10	82.22	3.46	180.00	6.22	640.00	6.22

Random		Comments
1 2 3		Must be evaluated for each test.

Summary	°C		°F		°R	
	Temp.	Unc.	Temp.	Unc.	Temp.	Unc.
Systematic	-200.00	3.64	-328.00	6.56	132.00	6.56
Random		0.00		0.00		0.00
Total Uncertainty		3.64		6.56		6.56
Systematic	900.00	3.46	1652.00	6.22	2112.00	6.22
Random		0.00		0.00		0.00
Total Uncertainty		3.46		6.22		6.22
Systematic	-240.00	3.92	-400.00	7.05	60.00	7.05
Random		0.00		0.00		0.00
Total Uncertainty		3.92		7.05		7.05
Systematic	-217.78	3.74	-360.00	6.74	100.00	6.74
Random		0.00		0.00		0.00
Total Uncertainty		3.74		6.74		6.74
Systematic	-162.22	3.46	-260.00	6.22	200.00	6.22
Random		0.00		0.00		0.00
Total Uncertainty		3.46		6.22		6.22

Systematic	-106.67	3.46	-160.00	6.22	300.00	6.22
Random		0.00		0.00		0.00
Total Uncertainty		3.46		6.22		6.22
Systematic	-78.89	3.46	-110.00	6.22	350.00	6.22
Random		0.00		0.00		0.00
Total Uncertainty		3.46		6.22		6.22
Systematic	-51.11	3.46	-60.00	6.22	400.00	6.22
Random		0.00		0.00		0.00
Total Uncertainty		3.46		6.22		6.22
Systematic	93.33	3.46	200.00	6.22	660.00	6.22
Random		0.00		0.00		0.00
Total Uncertainty		3.46		6.22		6.22
Systematic	82.22	3.46	180.00	6.22	640.00	6.22
Random		0.00		0.00		0.00
Total Uncertainty		3.46		6.22		6.22

Table A-2: Pressure Transducer

Indicator	Color
Input required from user	Yellow
MSU uncertainty input values	Bright Green
Results	**Red Bold**

Is this an absolute pressure calculated from a differential pressure measurement?	YES

Input Gain (200 or 300)	300

Input Class (A, B or C)	A

Input Uncertainty From Key # Calculation	2

Input Full Scale Range (psi)	2000

Input Posttest Check Tolerance	mV	V	counts
(mV, V, or counts, otherwise, set to 0)	0.00	0.00	100.00

mV	V	counts
0.1042	0.0313	100.0000

Sensitivity	psi / mV	psi / V	psi / count
	66.667	222.222	0.069

Uncertainty Calculations

Systematic

Elemental Source	B (psi)	Comments
Cal. Lab Transducer Calibrations	5	Transducers after calibration according to uncertainty classification.
Shunt Resistor	2.00	From key # uncertainty.
Facility Calibrations	0.00	Assume negligible.
Drift After Calibration	6.94	Calculated based on sensitivity and post-test check tolerance.
P_{atm} Correction	2.00	Only applies if calculate absolute pressure from differential measurement.
Additional Source?	0.00	Add as needed.
Additional Source?	0.00	Add as needed.
Installation Effects	0.00	Add as needed.

Random	P (psi)	Comments
1	0.00	Must be evaluated for each test.

Summary	psi	
	Pressure	Uncertainty
Systematic	2000	9.01
Random		0.00
Total Uncertainty		9.01

APPENDIX B

MATHCAD WORKSHEETS FOR MASS FLOW RATE

SAMPLE VENTURI METER UNCERTAINTY ANALYSIS

Incompressible mass flow rate over venturi, *w*:

$$w\left(C_d, d_2, F_a, \rho_1, \Delta P, d_1\right) := 0.52502 C_d \cdot \left(d_2\right)^2 \cdot F_a \cdot \sqrt{\frac{\rho_1 \cdot \Delta P}{\left[1 - \left(\frac{d_2}{d_1}\right)^4\right]}}$$

Yellow boxes indicate input required from the user.

Light blue boxes indicate the results obtained.

User needs to update variable input values.

$C_d := 0.98$		discharge coefficient
$d_2 := 0.25$	in	throat diameter
$F_a := 0.99$		thermal expansion factor
$\rho_1 := 41.33$	$\frac{lbm}{ft^3}$	fluid density
$\Delta P := 700$	psi	change in pressure
$d_1 := 0.95$	in	inlet diameter

Current input assumes 1% uncertainty for each variable. User needs to update. Input uncertainty values as a percent of the variable's value.

$\%U_{Cd} := 0.01$	uncertainty of discharge coefficient
$\%U_{d2} := 0.01$	uncertainty of throat diameter
$\%U_{Fa} := 0.01$	uncertainty of thermal contraction factor
$\%U_{\rho 1} := 0.01$	uncertainty of fluid density (Myprops)
$\%U_{\Delta P} := 0.01$	uncertainty of change in pressure
$\%U_{d1} := 0.01$	uncertainty of inlet diameter

$$UMF = \frac{X_i}{r} \cdot \frac{dr}{dX_i}$$ Uncertainty Magnification Factor (UMF)

$$UMF_{Cd} := \frac{C_d}{w(C_d, d_2, F_a, \rho_1, \Delta P, d_1)} \cdot \frac{d}{dC_d} w(C_d, d_2, F_a, \rho_1, \Delta P, d_1)$$ $UMF_{Cd} = 1$

$$UMF_{d2} := \frac{d_2}{w(C_d, d_2, F_a, \rho_1, \Delta P, d_1)} \cdot \frac{d}{dd_2} w(C_d, d_2, F_a, \rho_1, \Delta P, d_1)$$ $UMF_{d2} = 2.01$

$$UMF_{Fa} := \frac{F_a}{w(C_d, d_2, F_a, \rho_1, \Delta P, d_1)} \cdot \frac{d}{dF_a} w(C_d, d_2, F_a, \rho_1, \Delta P, d_1)$$ $UMF_{Fa} = 1$

$$UMF_{\rho 1} := \frac{\rho_1}{w(C_d, d_2, F_a, \rho_1, \Delta P, d_1)} \cdot \frac{d}{d\rho_1} w(C_d, d_2, F_a, \rho_1, \Delta P, d_1)$$ $UMF_{\rho 1} = 0.5$

$$UMF_{\Delta P} := \frac{\Delta P}{w(C_d, d_2, F_a, \rho_1, \Delta P, d_1)} \cdot \frac{d}{d\Delta P} w(C_d, d_2, F_a, \rho_1, \Delta P, d_1)$$ $UMF_{\Delta P} = 0.5$

$$UMF_{d1} := \frac{d_1}{w(C_d, d_2, F_a, \rho_1, \Delta P, d_1)} \cdot \frac{d}{dd_1} w(C_d, d_2, F_a, \rho_1, \Delta P, d_1)$$ $UMF_{d1} = -9.638 \times 10^{-3}$

At this stage, the uncertainty of the incompressible mass flow rate of the venturi can be calculated.

Let $\frac{U_w}{w} = \%U$ $\frac{U_{Cd}}{Cd} = \%U_{Cd}$ $\frac{U_{d2}}{d_2} = \%U_{d2}$ $\frac{U_{Fa}}{F_a} = \%U_{Fa}$

$\frac{U_{\rho 1}}{\rho_1} = \%U_{\rho 1}$ $\frac{U_{\Delta P}}{\Delta P} = \%U_{\Delta P}$ $\frac{U_{d1}}{d1} = \%U_{d1}$

$$\%U := \sqrt{\left[\left(UMF_{Cd}\right)^2\cdot\left(\%U_{Cd}\right)^2 + \left(UMF_{d2}\right)^2\cdot\left(\%U_{d2}\right)^2 + \left(UMF_{Fa}\right)^2\cdot\left(\%U_{Fa}\right)^2\right] ... + \left(UMF_{\rho 1}\right)^2\cdot\left(\%U_{\rho 1}\right)^2 + \left(UMF_{\Delta P}\right)^2\cdot\left(\%U_{\Delta P}\right)^2 + \left(UMF_{d1}\right)^2\cdot\left(\%U_{d1}\right)^2}$$

$\%U = 2.557\%$ Uncertainty of the mass flow rate as a %

$$w := 0.52502 C_d\cdot\left(d_2\right)^2\cdot F_a\cdot\sqrt{\frac{\rho_1\cdot\Delta P}{\left[1-\left(\frac{d_2}{d_1}\right)^4\right]}}$$

$w = 5.428$ $\frac{lbm}{sec}$ Mass flow rate of venturi meter

Since $\frac{U_w}{w} = \%U$ $U_w := w\cdot\%U$ $U_w = 0.139$ $\frac{lbm}{sec}$ Uncertainty of the mass flow rate

$$UPC_X = \frac{(UMF_X \cdot U_X)^2}{U^2}$$ Uncertainty Percentage Contribution (UPC)

$$UPC_{Cd} := \frac{(UMF_{Cd} \cdot \%U_{Cd})^2}{\%U^2}$$ $UPC_{Cd} = 15.293\%$

$$UPC_{d2} := \frac{(UMF_{d2} \cdot \%U_{d2})^2}{\%U^2}$$ $UPC_{d2} = 61.765\%$

$$UPC_{Fa} := \frac{(UMF_{Fa} \cdot \%U_{Fa})^2}{\%U^2}$$ $UPC_{Fa} = 15.293\%$

$$UPC_{\rho 1} := \frac{(UMF_{\rho 1} \cdot \%U_{\rho 1})^2}{\%U^2}$$ $UPC_{\rho 1} = 3.823\%$

$$UPC_{\Delta P} := \frac{(UMF_{\Delta P} \cdot \%U_{\Delta P})^2}{\%U^2}$$ $UPC_{\Delta P} = 3.823\%$

$$UPC_{d1} := \frac{(UMF_{d1} \cdot \%U_{d1})^2}{\%U^2}$$ $UPC_{d1} = 1.421 \times 10^{-3}\%$

$$UPC_{Cd} + UPC_{d2} + UPC_{Fa} + UPC_{\rho 1} + UPC_{\Delta P} + UPC_{d1} = 1$$

$$UMF := \begin{pmatrix} |UMF_{Cd}| \\ |UMF_{d2}| \\ |UMF_{Fa}| \\ |UMF_{\rho 1}| \\ |UMF_{\Delta P}| \\ |UMF_{d1}| \end{pmatrix} \qquad UPC := \begin{pmatrix} UPC_{Cd} \\ UPC_{d2} \\ UPC_{Fa} \\ UPC_{\rho 1} \\ UPC_{\Delta P} \\ UPC_{d1} \end{pmatrix} \qquad xdata := \begin{pmatrix} 1 \\ 2 \\ 3 \\ 4 \\ 5 \\ 6 \end{pmatrix}$$

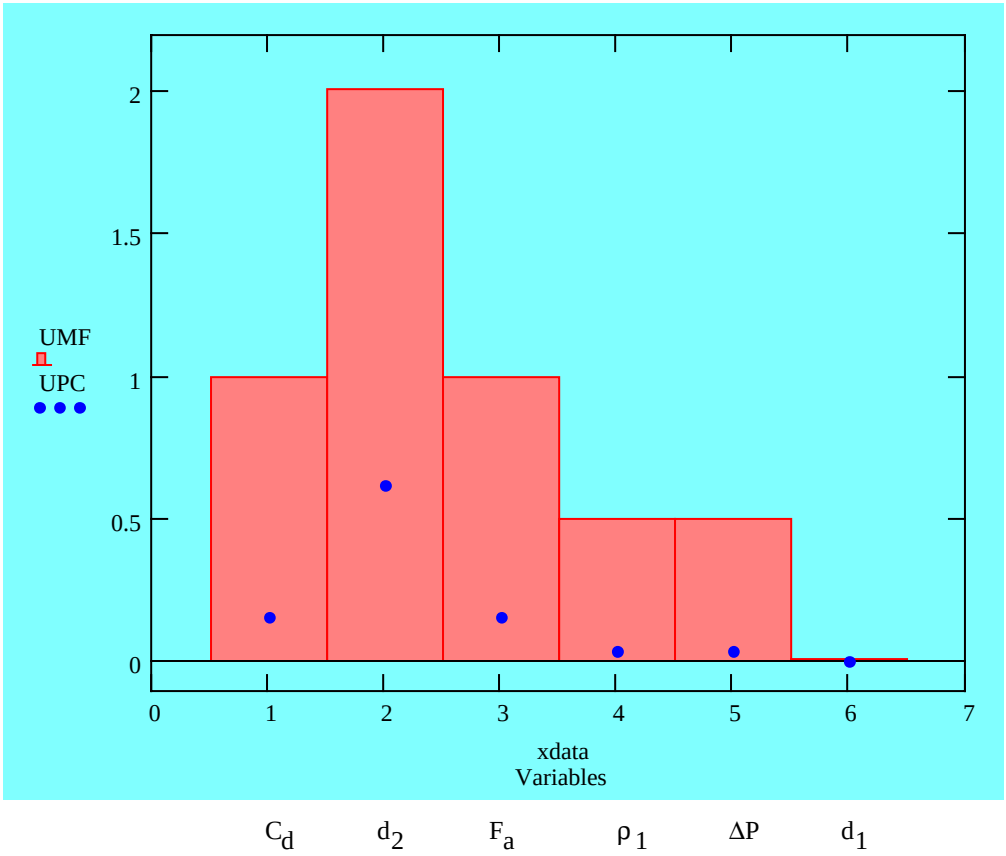

Figure B-1: UMF and UPC Values for Incompressible Venturi Flow Meter

SAMPLE V-CONE METER UNCERTAINTY ANALYSIS

Incompressible mass flow rate over V-cone, *w*:

$$w\left(C_d, Y, F_a, \rho, g_c, D, d, \Delta P\right) := \frac{\pi}{4}\cdot D^2 \cdot C_d \cdot Y \cdot F_a \cdot \sqrt{2 \cdot g_c \cdot \rho \cdot \Delta P} \cdot \frac{\left(\sqrt{1 - \frac{d^2}{D^2}}\right)^2}{\sqrt{1 - \left(\sqrt{1 - \frac{d^2}{D^2}}\right)^4}}$$

Yellow boxes indicate input required from the user.

Light blue boxes indicate the results obtained.

User needs to update variable input values.

$C_d := 0.82$	discharge coefficient
$Y := 1$	expansion factor
$F_a := 1$	thermal expansion factor
$\rho := 41.33\frac{lb}{ft^3}$	fluid density
$g_c := 32.2\frac{lb \cdot ft}{lbf \cdot s^2}$	proportionality constant
$D := 0.9in$	meter inside diameter
$d := 0.33in$	cone diameter
$\Delta P := 2.15psi$	pressure difference

Current input assumes 1% uncertainty for each variable. User needs to update.
Input uncertainty values as a percent of the variable's value.

$\%U_{Cd} := 0.01$ uncertainty of discharge coefficient

$\%U_{Y} := 0.01$ uncertainty of expansion factor

$\%U_{Fa} := 0.01$ uncertainty of thermal expansion factor

$\%U_{\rho} := 0.01$ uncertainty of fluid density

$\%U_{D} := 0.01$ uncertainty of meter inside diameter

$\%U_{d} := 0.01$ uncertainty of cone diameter

$\%U_{\Delta P} := 0.01$ uncertainty of change in pressure

$UMF = \frac{X_i}{r} \cdot \frac{dr}{dX_i}$ Uncertainty Magnification Factor (UMF)

$UMF_{Cd} := \frac{C_d}{w(C_d, Y, F_a, \rho, g_c, D, d, \Delta P)} \cdot \frac{d}{dC_d} w(C_d, Y, F_a, \rho, g_c, D, d, \Delta P)$ $UMF_{Cd} = 1$

$UMF_{Y} := \frac{Y}{w(C_d, Y, F_a, \rho, g_c, D, d, \Delta P)} \cdot \frac{d}{dY} w(C_d, Y, F_a, \rho, g_c, D, d, \Delta P)$ $UMF_{Y} = 1$

$UMF_{Fa} := \frac{F_a}{w(C_d, Y, F_a, \rho, g_c, D, d, \Delta P)} \cdot \frac{d}{dF_a} w(C_d, Y, F_a, \rho, g_c, D, d, \Delta P)$ $UMF_{Fa} = 1$

$UMF_{\rho} := \frac{\rho}{w(C_d, Y, F_a, \rho, g_c, D, d, \Delta P)} \cdot \frac{d}{d\rho} w(C_d, Y, F_a, \rho, g_c, D, d, \Delta P)$ $UMF_{\rho} = 0.5$

$UMF_{D} := \frac{D}{w(C_d, Y, F_a, \rho, g_c, D, d, \Delta P)} \cdot \frac{d}{dD} w(C_d, Y, F_a, \rho, g_c, D, d, \Delta P)$ $UMF_{D} = 3.239$

$UMF_{d} := \frac{d}{w(C_d, Y, F_a, \rho, g_c, D, d, \Delta P)} \cdot \frac{d}{dd} w(C_d, Y, F_a, \rho, g_c, D, d, \Delta P)$ $UMF_{d} = -1.239$

$UMF_{\Delta P} := \frac{\Delta P}{w(C_d, Y, F_a, \rho, g_c, D, d, \Delta P)} \cdot \frac{d}{d\Delta P} w(C_d, Y, F_a, \rho, g_c, D, d, \Delta P)$ $UMF_{\Delta P} = 0.5$

At this stage, the uncertainty of the incompressible mass flow rate of the v-cone can be calculated.

Let $\frac{U_w}{w} = \%U$ $\frac{U_{Cd}}{Cd} = \%U_{Cd}$ $\frac{U_Y}{Y} = \%U_Y$ $\frac{U_{Fa}}{F_a} = \%U_{Fa}$ $\frac{U_\rho}{\rho} = \%U_\rho$

$\frac{U_{gc}}{g_c} = \%U_{gc}$ $\frac{U_D}{D} = \%U_D$ $\frac{U_d}{d} = \%U_d$ $\frac{U_{\Delta P}}{\Delta P} = \%U_{\Delta P}$

$$\%U := \sqrt{\left(UMF_{Cd}\right)^2\cdot\left(\%U_{Cd}\right)^2 + \left(UMF_Y\right)^2\cdot\left(\%U_Y\right)^2 + \left(UMF_{Fa}\right)^2\cdot\left(\%U_{Fa}\right)^2 + \left(UMF_\rho\right)^2\cdot\left(\%U_\rho\right)^2 \ldots + \left(UMF_D\right)^2\cdot\left(\%U_D\right)^2 + \left(UMF_d\right)^2\cdot\left(\%U_d\right)^2 + \left(UMF_{\Delta P}\right)^2\cdot\left(\%U_{\Delta P}\right)^2}$$

$\%U = 3.94\%$ Uncertainty of the mass flow rate as a %

$$w := \frac{\pi}{4}\cdot\sqrt{2\cdot g_c\cdot\rho}\cdot\frac{D^2\cdot\left(\sqrt{1-\frac{d^2}{D^2}}\right)^2}{\sqrt{1-\left(\sqrt{1-\frac{d^2}{D^2}}\right)^4}}\cdot\sqrt{\Delta P}\cdot C_d\cdot Y\cdot F_a$$

$w = 5.684\frac{lb}{sec}$ Mass flow rate of V-cone

Since $\frac{U_w}{w} = \%U$ $U_w := w\cdot\%U$ $U_w = 0.224\frac{lb}{sec}$ Uncertainty of the mass flow rate

$$UPC_X = \frac{(UMF_X \cdot U_X)^2}{U^2}$$ Uncertainty Percentage Contribution (UPC)

$$UPC_{Cd} := \frac{(UMF_{Cd} \cdot \%U_{Cd})^2}{\%U^2}$$ $UPC_{Cd} = 6.442\%$

$$UPC_Y := \frac{(UMF_Y \cdot \%U_Y)^2}{\%U^2}$$ $UPC_Y = 6.442\%$

$$UPC_{Fa} := \frac{(UMF_{Fa} \cdot \%U_{Fa})^2}{\%U^2}$$ $UPC_{Fa} = 6.442\%$

$$UPC_\rho := \frac{(UMF_\rho \cdot \%U_\rho)^2}{\%U^2}$$ $UPC_\rho = 1.611\%$

$$UPC_D := \frac{(UMF_D \cdot \%U_D)^2}{\%U^2}$$ $UPC_D = 67.569\%$

$$UPC_d := \frac{(UMF_d \cdot \%U_d)^2}{\%U^2}$$ $UPC_d = 9.883\%$

$$UPC_{\Delta P} := \frac{(UMF_{\Delta P} \cdot \%U_{\Delta P})^2}{\%U^2}$$ $UPC_{\Delta P} = 1.611\%$

$$UPC_{Cd} + UPC_Y + UPC_{Fa} + UPC_\rho + UPC_D + UPC_d + UPC_{\Delta P} = 100\%$$

$$UMF := \begin{pmatrix} |UMF_{Cd}| \\ |UMF_{Y}| \\ |UMF_{Fa}| \\ |UMF_{\rho}| \\ |UMF_{D}| \\ |UMF_{d}| \\ |UMF_{\Delta P}| \end{pmatrix} \quad UPC := \begin{pmatrix} UPC_{Cd} \\ UPC_{Y} \\ UPC_{Fa} \\ UPC_{\rho} \\ UPC_{D} \\ UPC_{d} \\ UPC_{\Delta P} \end{pmatrix} \quad xdata := \begin{pmatrix} 1 \\ 2 \\ 3 \\ 4 \\ 5 \\ 6 \\ 7 \end{pmatrix}$$

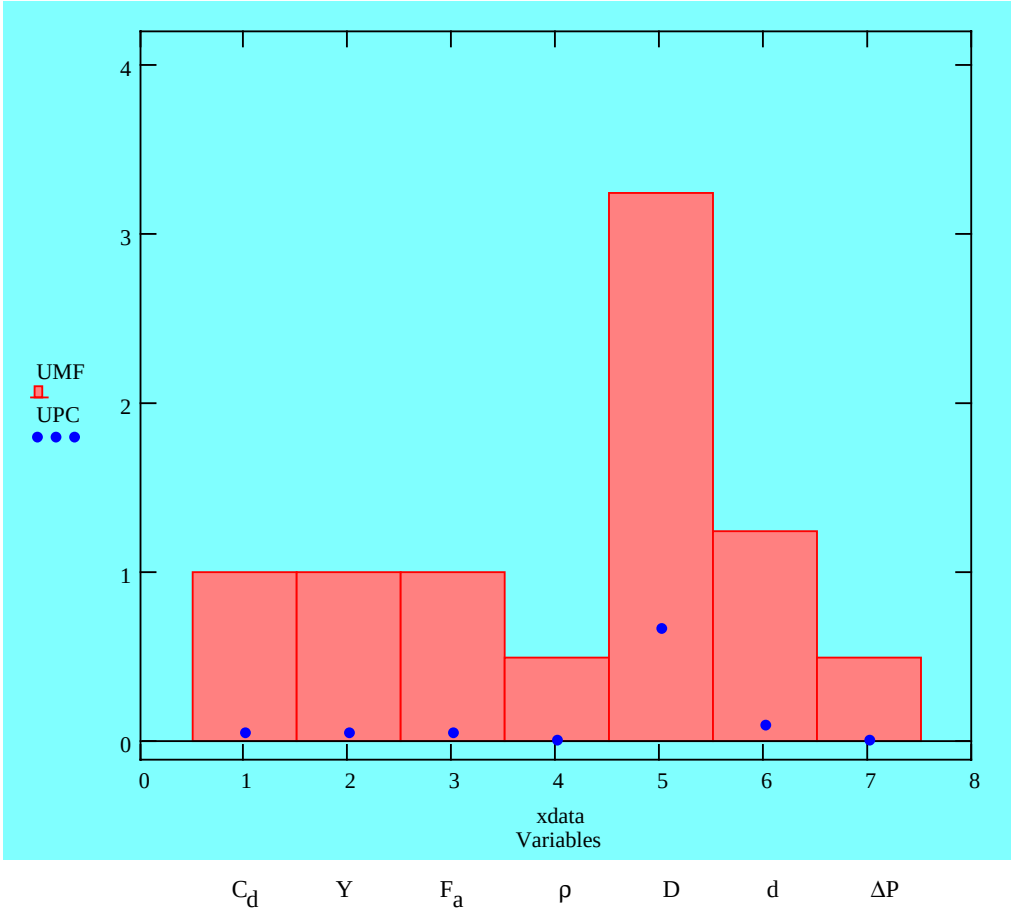

Figure B-2: UMF and UPC Values for Incompressible V-cone Flow Meter

APPENDIX C

MATHCAD WORKSHEETS FOR THRUST

SINGLE THRUST MEASUREMENT SYSTEM

Load Cells : Ormond Series 69
Measurement range : 10,000 - 100,000 lbf
Temperature : 15 - 135 degF

Load cells series 69 specifications:

Yellow boxes indicate input required from the user.

Light blue boxes indicate the results obtained.

User needs to update variable input values.

Non-linearity	$U_{NL} := 0.07\%$	FS
Hysteresis	$U_{HY} := 0.02\%$	FS
Zero balance	$U_{ZB} := 1.00\%$	FS
Thermal zero coefficient	$U_{TZ} := 0.0014\%$	$\frac{FS}{degF}$
Thermal sensitivity coefficient	$U_{TS} := 0.0007\%$	$\frac{load}{degF}$

Full scale load:	$FS := 100000$	lbf
Applied load	$F := 50000$	lbf
Initial Temperature	$T_1 := 15$	degF
Final Temperature	$T_2 := 125$	degF
Change in Temperature	$\Delta T := T_2 - T_1$	$\Delta T = 110$ degF

Change in Temperature $\Delta T := T_2 - T_1$ $\Delta T = 110$ degF

According to the calibration curve provided by Ormond Inc., the uncertainty of the calibrator load cells is 0.335% of load. When hysteresis exists in the calibration, the uncertainty is determined to be 0.439% of load. Therefore, the uncertainty of calibration will be taken as 0.439% of load in this study.

$U_{CAL} := 0.439\%$ load

With the load cells specifications provided, the uncertainty of the thrust measurement system can be determined.

$$U_{MEAS} := \sqrt{(U_{NL} \cdot FS)^2 + (U_{HY} \cdot FS)^2 + (U_{ZB} \cdot FS)^2 + (U_{TZ} \cdot FS \cdot T_1)^2 + (U_{TS} \cdot F \cdot \Delta T)^2}$$

$U_{MEAS} = 1003.605$ Uncertainty of the measurement

Total uncertainty of the load cells / thrust is the root-sum-square of the uncertainty of the calibration and the uncertainty of the measurement.

$$U_{thrust} := \sqrt{(U_{CAL} \cdot F)^2 + (U_{MEAS})^2}$$ $U_{thrust} = 1027.328$ Uncertainty of the thrust

$$\%U := \frac{U_{thrust}}{FS}$$ $\%U = 1.027\%$ Percentage uncertainty of the thrust

APPENDIX D

MATHCAD WORKSHEETS FOR SPECIFIC IMPULSE

SPECIFIC IMPULSE METHOD I

$$Isp_1(F, w_o, w_f, g_o, g_c) := \frac{F}{(w_o + w_f)} \cdot \frac{g_c}{g_o}$$

Yellow boxes indicate input required from the user.

Light blue boxes indicate the results obtained.

User needs to update variable input values.

case 1

$kN := 1000N$ ORIGIN:= 1 $i := 1..40$

$F := 4500lbf$ Measured thrust

$w_o := 8\frac{lb}{sec}$ Oxidizer flow rate

$w_f := 2.5\frac{lb}{sec}$ Fuel flow rate

$g_c := 32.2\frac{lb \cdot ft}{lbf \cdot s^2}$ Dimensionless conversion constant

$g_o := 32.2\frac{ft}{s^2}$ gravitational acceleration at sea level

User needs to update uncertainty for each variable.

$\%U_F := 0.01$ Uncertainty of measured thrust (%)

$\%U_{wo} := 0.02$ Uncertainty of oxidizer flow rate (%)

$\%U_{wf} := 0.02$ Uncertainty of fuel flow rate (%)

$$UMF = \frac{X_i}{r} \cdot \frac{dr}{dX_i}$$ Uncertainty Magnification Factors

$$UMF_F := \frac{F}{Isp_1(F, w_o, w_f, g_o, g_c)} \cdot \frac{d}{dF} Isp_1(F, w_o, w_f, g_o, g_c)$$ $UMF_F = 1$

$$UMF_{wo} := \frac{w_o}{Isp_1(F, w_o, w_f, g_o, g_c)} \cdot \frac{d}{dw_o} Isp_1(F, w_o, w_f, g_o, g_c)$$ $UMF_{wo} = -0.762$

$$UMF_{wf} := \frac{w_f}{Isp_1(F, w_o, w_f, g_o, g_c)} \cdot \frac{d}{dw_f} Isp_1(F, w_o, w_f, g_o, g_c)$$ $UMF_{wf} = -0.238$

At this stage, the uncertainty of the specific impulse is

$Isp_1 := Isp_1(F, w_o, w_f, g_o, g_c)$ $Isp_1 = 428.571s$ Specific Impulse, Isp

Let $\%U = \frac{U_{Isp}}{Isp}$ $\%U_F = \frac{U_F}{F}$ $\%U_{wo} = \frac{U_{wo}}{w_o}$ $\%U_{wf} = \frac{U_{wf}}{w_f}$

$$\%U := \sqrt{(UMF_F)^2 \cdot (\%U_F)^2 + (UMF_{wo})^2 \cdot (\%U_{wo})^2 + (UMF_{wf})^2 \cdot (\%U_{wf})^2}$$

$\%U = 1.884\%$ Uncertainty of the specific impulse as in %

$U_{Isp1} := \%U \cdot Isp_1$ $U_{Isp1} = 8.073s$ Uncertainty of Isp, sec.

$$UPC_X = \frac{(UMF_X \cdot U_X)^2}{U^2}$$ Uncertainty Percentage Contribution (UPC)

$$UPC_F := \frac{(UMF_F \cdot \%U_F)^2}{(\%U)^2} \qquad UPC_F = 28.179\%$$

$$UPC_{wo} := \frac{(UMF_{wo} \cdot \%U_{wo})^2}{(\%U)^2} \qquad UPC_{wo} = 65.431\%$$

$$UPC_{wf} := \frac{(UMF_{wf} \cdot \%U_{wf})^2}{(\%U)^2} \qquad UPC_{wf} = 6.39\%$$

$$UPC_F + UPC_{wo} + UPC_{wf} = 100\%$$

$$UPC := \begin{pmatrix} UPC_F \\ UPC_{wo} \\ UPC_{wf} \end{pmatrix} \qquad UMF := \begin{pmatrix} |UMF_F| \\ |UMF_{wo}| \\ |UMF_{wf}| \end{pmatrix} \qquad xdata := \begin{pmatrix} 1 \\ 2 \\ 3 \end{pmatrix}$$

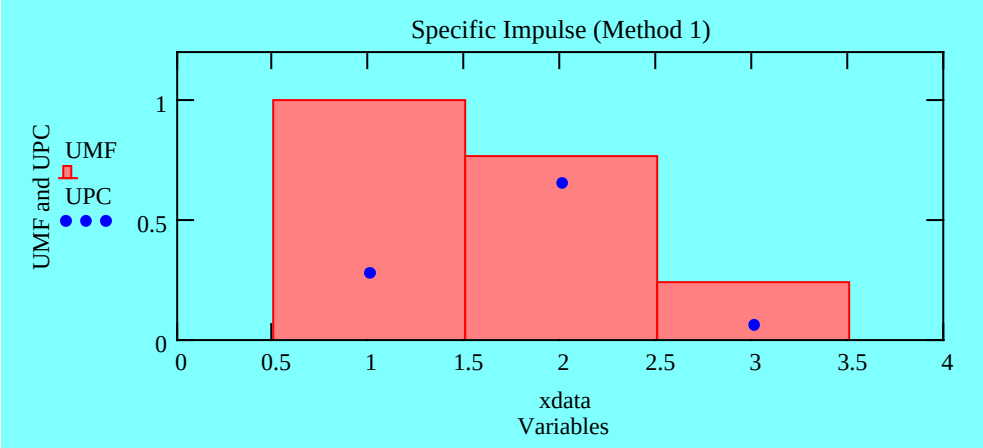

F w_o w_f

Figure D-1: UMF and UPC Values for Specific Impulse Method I

SPECIFIC IMPULSE METHOD II

$$Isp_2(C_F, P_o, D_t, w_o, w_f, g_c, g_o) := \frac{C_F \cdot P_o \cdot \pi \cdot D_t^{\,2}}{4(w_o + w_f)} \cdot \frac{g_c}{g_o}$$

Yellow boxes indicate input required from the user.

Light blue boxes indicate the results obtained.

User needs to update variable input values.

$C_F := 1.7$	Thrust coefficient
$P_o := 1500\,psi$	Nozzle stagnation pressure
$D_t := 0.25\,in$	Throat diameter
$w_o := 0.464\,\frac{lb}{sec}$	Oxidizer flow rate
$w_f := 0.066\,\frac{lb}{sec}$	Fuel flow rate
$g_c := 32.2\,\frac{lb \cdot ft}{lbf \cdot s^2}$	Dimensionless conversion constant
$g_o := 32.2\,\frac{ft}{s^2}$	gravitational acceleration at sea leve

Uncertainty for each variable:

$\%U_{CF} := 0.03$ uncertainty of thrust coefficient

$\%U_{Po} := 0.03$ uncertainty of stagnation pressure at the nozzle

$\%U_{Dt} := 0.03$ uncertainty of throat diameter

$\%U_{wo} := 0.01$ uncertainty of oxidizer flow

$\%U_{wf} := 0.01$ uncertainty of fuel flow

$$UMF = \frac{X_i}{r} \cdot \frac{dr}{dX_i}$$ Uncertainty Magnification Factors

$$UMF_{CF} := \frac{C_F}{Isp_2(C_F, P_o, D_t, w_o, w_f, g_c, g_o)} \cdot \frac{d}{dC_F} Isp_2(C_F, P_o, D_t, w_o, w_f, g_c, g_o)$$ $UMF_{CF} = 1$

$$UMF_{Po} := \frac{P_o}{Isp_2(C_F, P_o, D_t, w_o, w_f, g_c, g_o)} \cdot \frac{d}{dP_o} Isp_2(C_F, P_o, D_t, w_o, w_f, g_c, g_o)$$ $UMF_{Po} = 1$

$$UMF_{Dt} := \frac{D_t}{Isp_2(C_F, P_o, D_t, w_o, w_f, g_c, g_o)} \cdot \frac{d}{dD_t} Isp_2(C_F, P_o, D_t, w_o, w_f, g_c, g_o)$$ $UMF_{Dt} = 2$

$$UMF_{wo} := \frac{w_o}{Isp_2(C_F, P_o, D_t, w_o, w_f, g_c, g_o)} \cdot \frac{d}{dw_o} Isp_2(C_F, P_o, D_t, w_o, w_f, g_c, g_o)$$ $UMF_{wo} = -0.875$

$$UMF_{wf} := \frac{w_f}{Isp_2(C_F, P_o, D_t, w_o, w_f, g_c, g_o)} \cdot \frac{d}{dw_f} Isp_2(C_F, P_o, D_t, w_o, w_f, g_c, g_o)$$ $UMF_{wf} = -0.125$

At this stage, the uncertainty of the specific impulse is

$Isp_2 := Isp_2(C_F, P_o, D_t, w_o, w_f, g_c, g_o)$ $\quad Isp_2 = 236.175s$ Specific Impulse, Isp

Let $\frac{U_{Isp}}{Isp} = \%U$ $\quad \frac{U_{CF}}{C_F} = \%C_F$ $\quad \frac{U_{Po}}{P_o} = \%P_o$

$\frac{U_{Dt}}{D_t} = \%D_t$ $\quad \frac{U_{wo}}{w_o} = \%w_o$ $\quad \frac{U_{wf}}{w_f} = \%w_f$

$$\%U := \sqrt{\left[\left(UMF_{CF}\cdot\%U_{CF}\right)^2 + \left(UMF_{Po}\cdot\%U_{Po}\right)^2 + \left(UMF_{Dt}\cdot\%U_{Dt}\right)^2 + \left(UMF_{wo}\cdot\%U_{wo}\right)^2\right] \ldots + \left(UMF_{wf}\cdot\%U_{wf}\right)^2}$$

$\%U = 7.401\%$ Uncertainty of the specific impulse as in %

$U_{Isp2} := Isp_2\cdot(\%U)$ $\quad U_{Isp2} = 17.48s$ Uncertainty of Isp, sec.

$$UPC_X = \frac{\left(UMF_X \cdot U_X\right)^2}{U^2}$$ Uncertainty Percentage Contribution (UPC)

$$UPC_{CF} := \frac{\left(UMF_{CF} \cdot \%U_{CF}\right)^2}{\%U^2}$$ $UPC_{CF} = 16.429\%$

$$UPC_{Po} := \frac{\left(UMF_{Po} \cdot \%U_{Po}\right)^2}{\%U^2}$$ $UPC_{Po} = 16.429\%$

$$UPC_{Dt} := \frac{\left(UMF_{Dt} \cdot \%U_{Dt}\right)^2}{\%U^2}$$ $UPC_{Dt} = 65.715\%$

$$UPC_{wo} := \frac{\left(UMF_{wo} \cdot \%U_{wo}\right)^2}{\%U^2}$$ $UPC_{wo} = 1.399\%$

$$UPC_{wf} := \frac{\left(UMF_{wf} \cdot \%U_{wf}\right)^2}{\%U^2}$$ $UPC_{wf} = 0.028\%$

$$UPC_{CF} + UPC_{Po} + UPC_{Dt} + UPC_{wo} + UPC_{wf} = 100\%$$

$$UMF := \begin{pmatrix} |UMF_{CF}| \\ |UMF_{Po}| \\ |UMF_{Dt}| \\ |UMF_{wo}| \\ |UMF_{wf}| \end{pmatrix} \qquad UPC := \begin{pmatrix} UPC_{CF} \\ UPC_{Po} \\ UPC_{Dt} \\ UPC_{wo} \\ UPC_{wf} \end{pmatrix} \qquad xdata := \begin{pmatrix} 1 \\ 2 \\ 3 \\ 4 \\ 5 \end{pmatrix}$$

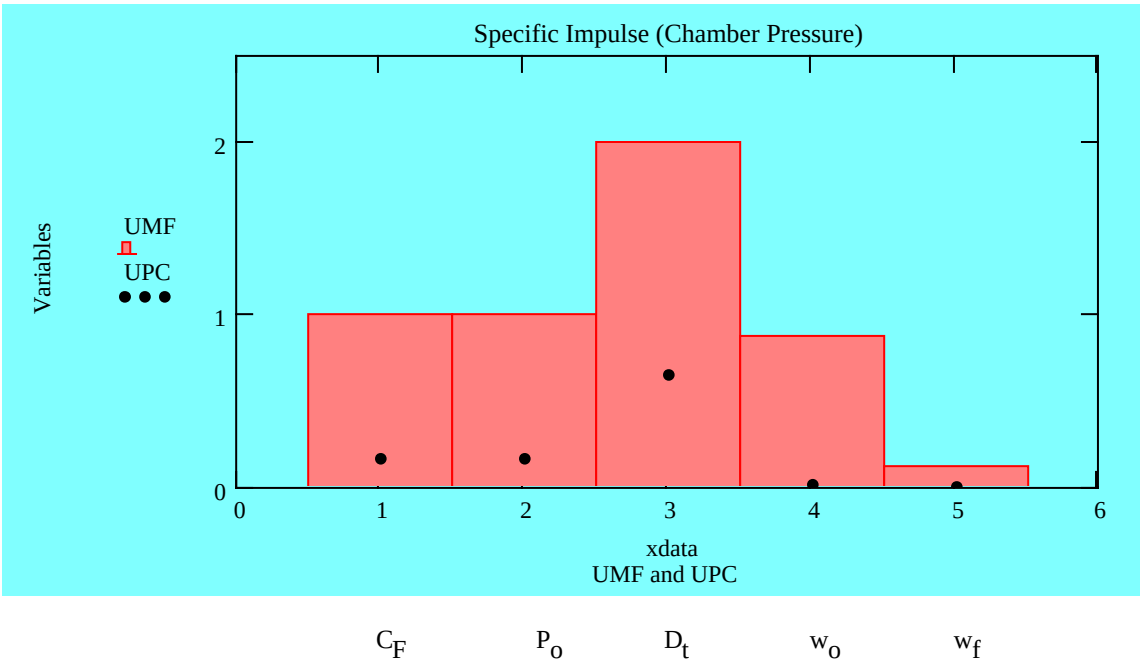

Figure D-2: UMF and UPC Values for Specific Impulse Method 2

SPECIFIC IMPULSE METHOD III

$$Isp_3(Rc,\gamma,T_c,M,P_e,P_c,P_3,D_e,w_o,w_f,g_o,g_c) := \sqrt{\frac{2\cdot Rc\cdot g_c}{g_o^{\,2}}\cdot\left(\frac{\gamma}{\gamma-1}\right)\cdot\left(\frac{T_c}{M}\right)\cdot\left[1-\left(\frac{P_e}{P_c}\right)^{\left(\frac{\gamma-1}{\gamma}\right)}\right]}\ ... + \frac{(P_e-P_3)\cdot\pi\cdot D_e^{\,2}\cdot g_c}{4\cdot(w_o+w_f)\cdot g_o}$$

Yellow boxes indicate input required from the user.

Light blue boxes indicate the results obtained.

User needs to update variable input values.

$lbmol := 1$ $ORIGIN := 1$

$Rc := 1.986\frac{BTU}{lbmol\cdot R}$	Universal gas constant
$\gamma := 1.2$	Specific heat ratio
$T_c := 5450R$	Chamber temperature
$M := 21.5\frac{lb}{lbmol}$	Molar mass/ molecular weight of exit fluid
$P_e := 14psi$	Nozzle exit pressure
$P_c := 1500psi$	Chamber pressure
$P_3 := 14psi$	Ambient pressure
$D_e := 0.87in$	Nozzle exit diameter
$w_o := 0.464\frac{lb}{sec}$	Oxidizer flow rate
$w_f := 0.066\frac{lb}{sec}$	Fuel flow rate

$g_c := 32.2 \frac{lb \cdot ft}{lbf \cdot s^2}$ Dimensionless conversion constant

$g_o := 32.2 \frac{ft}{s^2}$ gravitational acceleration at sea level

Uncertainty for each variable:

$\%U_{Rc} := 0.005$ uncertainty of universal gas constant

$\%U_{\gamma} := 0.01$ uncertainty of specific heat ratio

$\%U_{Tc} := 0.03$ uncertainty of chamber temperature

$\%U_{M} := 0.005$ uncertainty of molar mass/ moleculer weight of exit fluid

$\%U_{Pe} := 0.03$ uncertainty of nozzle exit pressure

$\%U_{Pc} := 0.03$ uncertainty of chamber pressure

$\%U_{P3} := 0.03$ uncertainty of ambient pressure

$\%U_{De} := 0.01$ uncertainty of nozzle exit diameter

$\%U_{wo} := 0.01$ uncertainty of oxidizer flow

$\%U_{wf} := 0.01$ uncertainty of fuel flow

$$UMF = \frac{X_i}{r} \cdot \frac{dr}{dX_i}$$ Uncertainty Magnification Factors

$$UMF_{Rc} := \frac{Rc}{Isp_3\left(Rc, \gamma, T_c, M, P_e, P_c, P_3, D_e, w_o, w_f, g_o, g_c\right)} \cdot \frac{d}{dRc} Isp_3\left(Rc, \gamma, T_c, M, P_e, P_c, P_3, D_e, w_o, w_f, g_o, g_c\right)$$

$$UME_{\gamma} := \frac{\gamma}{Isp_3\left(Rc, \gamma, T_c, M, P_e, P_c, P_3, D_e, w_o, w_f, g_o, g_c\right)} \cdot \frac{d}{d\gamma} Isp_3\left(Rc, \gamma, T_c, M, P_e, P_c, P_3, D_e, w_o, w_f, g_o, g_c\right)$$

$$UMF_{Tc} := \frac{T_c}{Isp_3\left(Rc, \gamma, T_c, M, P_e, P_c, P_3, D_e, w_o, w_f, g_o, g_c\right)} \cdot \frac{d}{dT_c} Isp_3\left(Rc, \gamma, T_c, M, P_e, P_c, P_3, D_e, w_o, w_f, g_o, g_c\right)$$

$$UMF_{M} := \frac{M}{Isp_3\left(Rc, \gamma, T_c, M, P_e, P_c, P_3, D_e, w_o, w_f, g_o, g_c\right)} \cdot \frac{d}{dM} Isp_3\left(Rc, \gamma, T_c, M, P_e, P_c, P_3, D_e, w_o, w_f, g_o, g_c\right)$$

$$UMF_{Pe} := \frac{P_e}{Isp_3\left(Rc, \gamma, T_c, M, P_e, P_c, P_3, D_e, w_o, w_f, g_o, g_c\right)} \cdot \frac{d}{dP_e} Isp_3\left(Rc, \gamma, T_c, M, P_e, P_c, P_3, D_e, w_o, w_f, g_o, g_c\right)$$

$$UMF_{Pc} := \frac{P_c}{Isp_3\left(Rc, \gamma, T_c, M, P_e, P_c, P_3, D_e, w_o, w_f, g_o, g_c\right)} \cdot \frac{d}{dP_c} Isp_3\left(Rc, \gamma, T_c, M, P_e, P_c, P_3, D_e, w_o, w_f, g_o, g_c\right)$$

$$UMF_{P3} := \frac{P_3}{Isp_3\left(Rc, \gamma, T_c, M, P_e, P_c, P_3, D_e, w_o, w_f, g_o, g_c\right)} \cdot \frac{d}{dP_3} Isp_3\left(Rc, \gamma, T_c, M, P_e, P_c, P_3, D_e, w_o, w_f, g_o, g_c\right)$$

$$UMF_{De} := \frac{D_e}{Isp_3\left(Rc, \gamma, T_c, M, P_e, P_c, P_3, D_e, w_o, w_f, g_o, g_c\right)} \cdot \frac{d}{dD_e} Isp_3\left(Rc, \gamma, T_c, M, P_e, P_c, P_3, D_e, w_o, w_f, g_o, g_c\right)$$

$$UMF_{wo} := \frac{w_o}{Isp_3\left(Rc, \gamma, T_c, M, P_e, P_c, P_3, D_e, w_o, w_f, g_o, g_c\right)} \cdot \frac{d}{dw_o} Isp_3\left(Rc, \gamma, T_c, M, P_e, P_c, P_3, D_e, w_o, w_f, g_o, g_c\right)$$

$$UMF_{wf} := \frac{w_f}{Isp_3\left(Rc, \gamma, T_c, M, P_e, P_c, P_3, D_e, w_o, w_f, g_o, g_c\right)} \cdot \frac{d}{dw_f} Isp_3\left(Rc, \gamma, T_c, M, P_e, P_c, P_3, D_e, w_o, w_f, g_o, g_c\right)$$

At this stage, the uncertainty of the specific impulse is

$$Isp_3 := Isp_3(Rc, \gamma, T_c, M, P_e, P_c, P_3, D_e, w_o, w_f, g_o, g_c)$$

$Isp_3 = 281.078s$ Specific Impulse, Isp

Let $\frac{U_{Isp}}{Isp} = \%U$ $\frac{U_{Rc}}{Rc} = \%Rc$ $\frac{U_{\gamma}}{\gamma} = \%\gamma$ $\frac{U_{Tc}}{T_c} = \%T_c$ $\frac{U_M}{M} = \%M$

$\frac{U_{Pe}}{P_e} = \%P_e$ $\frac{U_{Pc}}{P_c} = \%P_c$ $\frac{U_{P3}}{P_3} = \%P_3$ $\frac{U_{De}}{D_e} = \%D_e$ $\frac{U_{wo}}{w_o} = \%w_o$ $\frac{U_{wf}}{w_f}$

$$\%U := \sqrt{\left[\left(UMF_{Rc}\cdot\%U_{Rc}\right)^2 + \left(UMF_{\gamma}\cdot\%U_{\gamma}\right)^2 + \left(UMF_{Tc}\cdot\%U_{Tc}\right)^2 + \left(UMF_{M}\cdot\%U_{M}\right)^2\right] \ldots + \left(UMF_{Pe}\cdot\%U_{Pe}\right)^2 + \left(UMF_{Pc}\cdot\%U_{Pc}\right)^2 + \left(UMF_{P3}\cdot\%U_{P3}\right)^2 + \left(UMF_{De}\cdot\%U_{De}\right)^2 \ldots + \left(UMF_{wo}\cdot\%U_{wo}\right)^2 + \left(UMF_{wf}\cdot\%U_{wf}\right)^2}$$

$\%U = 1.78\%$ Uncertainty of the specific impulse as in %

$U_{Isp3} := Isp_3\cdot(\%U)$ $U_{Isp3} = 5.005s$ Uncertainty of Isp, sec.

$$UPC_X = \frac{(UMF_X \cdot U_X)^2}{U^2}$$ Uncertainty Percentage Contribution (UPC)

$$UPC_{Rc} := \frac{(UMF_{Rc} \cdot \%U_{Rc})^2}{\%U^2}$$ $UPC_{Rc} = 1.972\%$

$$UPC_{\gamma} := \frac{(UMF_{\gamma} \cdot \%U_{\gamma})^2}{\%U^2}$$ $UPC_{\gamma} = 22.717\%$

$$UPC_{Tc} := \frac{(UMF_{Tc} \cdot \%U_{Tc})^2}{\%U^2}$$ $UPC_{Tc} = 70.976\%$

$$UPC_{M} := \frac{(UMF_{M} \cdot \%U_{M})^2}{\%U^2}$$ $UPC_{M} = 1.972\%$

$$UPC_{Pe} := \frac{(UMF_{Pe} \cdot \%U_{Pe})^2}{\%U^2}$$ $UPC_{Pe} = 0.063\%$

$$UPC_{Pc} := \frac{(UMF_{Pc} \cdot \%U_{Pc})^2}{\%U^2}$$ $UPC_{Pc} = 1.417\%$

$$UPC_{P3} := \frac{(UMF_{P3} \cdot \%U_{P3})^2}{\%U^2}$$ $UPC_{P3} = 0.885\%$

$$UPC_{De} := \frac{(UMF_{De} \cdot \%U_{De})^2}{\%U^2}$$ $UPC_{De} = 0.00\%$

$$UPC_{wo} := \frac{(UMF_{wo} \cdot \%U_{wo})^2}{\%U^2}$$ $UPC_{wo} = 0.00\%$

$$UPC_{wf} := \frac{(UMF_{wf} \cdot \%U_{wf})^2}{\%U^2}$$ $UPC_{wf} = 0.00\%$

$UPC_{Rc} + UPC_{\gamma} + UPC_{Tc} + UPC_{M} + UPC_{Pe} + UPC_{Pc} + UPC_{P3} + UPC_{De} \ldots = 100\%$
$+ UPC_{wo} + UPC_{wf}$

$$UMF := \begin{pmatrix} |UMF_{Rc}| \\ |UMF_{\gamma}| \\ |UMF_{Tc}| \\ |UMF_{M}| \\ |UMF_{Pe}| \\ |UMF_{Pc}| \\ |UMF_{P3}| \\ |UMF_{De}| \\ |UMF_{wo}| \\ |UMF_{wf}| \end{pmatrix}$$

$UMF =$

	1
1	
2	
3	
4	
5	
6	
7	
8	
9	
10	

$$UPC := \begin{pmatrix} UPC_{Rc} \\ UPC_{\gamma} \\ UPC_{Tc} \\ UPC_{M} \\ UPC_{Pe} \\ UPC_{Pc} \\ UPC_{P3} \\ UPC_{De} \\ UPC_{wo} \\ UPC_{wf} \end{pmatrix} \qquad xdata := \begin{pmatrix} 1 \\ 2 \\ 3 \\ 4 \\ 5 \\ 6 \\ 7 \\ 8 \\ 9 \\ 10 \end{pmatrix}$$

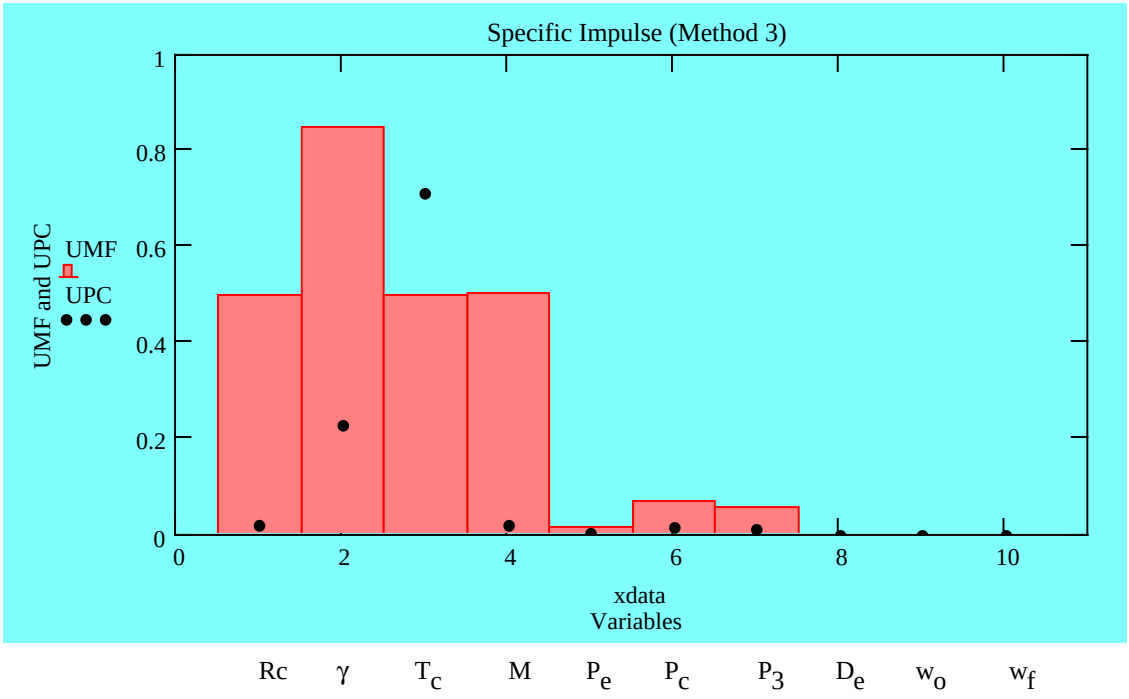

Figure D-3: UMF and UPC Values for Specific Impulse Method III

SPECIFIC IMPULSE METHOD IV

Nozzle divergence factor, $\lambda_N(\theta) := \frac{1}{2}\cdot(1 + \cos(\theta))$

$$Isp_4(\theta, Rc, \gamma, T_c, M, P_e, P_c, P_3, D_e, w_o, w_f, g_o, g_c) := \lambda_N(\theta)\cdot\sqrt{\frac{2\cdot Rc\cdot g_c}{g_o^{\,2}}\cdot\left(\frac{\gamma}{\gamma-1}\right)\cdot\left(\frac{T_c}{M}\right)\cdot\left[1-\left(\frac{P_e}{P_c}\right)^{\left(\frac{\gamma-1}{\gamma}\right)}\right]}\ldots + \frac{(P_e - P_3)\cdot\pi\cdot D_e^{\,2} g_c}{4\cdot(w_o + w_f)\cdot g_o}$$

Yellow boxes indicate input required from the user.

Light blue boxes indicate the results obtained.

User needs to update variable input values.

$lbmol := 1$ $ORIGIN := 1$

$\theta := 23.5deg$	Nozzle divergence angle
$Rc := 1.986\frac{BTU}{lbmol\cdot R}$	Universal gas constant
$\gamma := 1.2$	Specific heat ratio
$T_c := 5450R$	Chamber temperature
$M := 21.5\frac{lb}{lbmol}$	Molar mass/ molecular weight of exit fluid
$P_e := 14psi$	Nozzle exit pressure
$P_c := 1500psi$	Chamber pressure
$P_3 := 14psi$	Ambient pressure
$D_e := 0.87in$	Nozzle exit diameter
$w_o := 0.464\frac{lb}{sec}$	Oxidizer flow rate
$w_f := 0.066\frac{lb}{sec}$	Fuel flow rate

$g_c := 32.2 \frac{lb \cdot ft}{lbf \cdot s^2}$ Dimensionless conversion constant

$g_o := 32.2 \frac{ft}{s^2}$ gravitational acceleration at sea level

Uncertainty for each variable:

$\%U_\theta := 0.01$ uncertainty of nozzle divergence angle

$\%U_{Rc} := 0.005$ uncertainty of universal gas constant

$\%U_\gamma := 0.01$ uncertainty of specific heat ratio

$\%U_{Tc} := 0.03$ uncertainty of chamber temperature

$\%U_M := 0.005$ uncertainty of molar mass/ moleculer weight of exit fluid

$\%U_{Pe} := 0.03$ uncertainty of nozzle exit pressure

$\%U_{Pc} := 0.03$ uncertainty of chamber pressure

$\%U_{P3} := 0.03$ uncertainty of ambient pressure

$\%U_{De} := 0.01$ uncertainty of nozzle exit diameter

$\%U_{wo} := 0.01$ uncertainty of oxidizer flow

$\%U_{wf} := 0.01$ uncertainty of fuel flow

$$UMF = \frac{X_i}{r} \cdot \frac{dr}{dX_i}$$ Uncertainty Magnification Factors

$$UMF_{\theta} := \frac{\theta}{Isp_4(\theta, Rc, \gamma, T_c, M, P_e, P_c, P_3, D_e, w_o, w_f, g_o, g_c)} \cdot \frac{d}{d\theta} Isp_4(\theta, Rc, \gamma, T_c, M, P_e, P_c, P_3, D_e, w_o, w_f, g_o, g_c)$$

$$UMF_{Rc} := \frac{Rc}{Isp_4(\theta, Rc, \gamma, T_c, M, P_e, P_c, P_3, D_e, w_o, w_f, g_o, g_c)} \cdot \frac{d}{dRc} Isp_4(\theta, Rc, \gamma, T_c, M, P_e, P_c, P_3, D_e, w_o, w_f, g_o, g_c)$$

$$UMF_{\gamma} := \frac{\gamma}{Isp_4(\theta, Rc, \gamma, T_c, M, P_e, P_c, P_3, D_e, w_o, w_f, g_o, g_c)} \cdot \frac{d}{d\gamma} Isp_4(\theta, Rc, \gamma, T_c, M, P_e, P_c, P_3, D_e, w_o, w_f, g_o, g_c)$$

$$UMF_{Tc} := \frac{T_c}{Isp_4(\theta, Rc, \gamma, T_c, M, P_e, P_c, P_3, D_e, w_o, w_f, g_o, g_c)} \cdot \frac{d}{dT_c} Isp_4(\theta, Rc, \gamma, T_c, M, P_e, P_c, P_3, D_e, w_o, w_f, g_o, g_c)$$

$$UMF_{M} := \frac{M}{Isp_4(\theta, Rc, \gamma, T_c, M, P_e, P_c, P_3, D_e, w_o, w_f, g_o, g_c)} \cdot \frac{d}{dM} Isp_4(\theta, Rc, \gamma, T_c, M, P_e, P_c, P_3, D_e, w_o, w_f, g_o, g_c)$$

$$UMF_{Pe} := \frac{P_e}{Isp_4(\theta, Rc, \gamma, T_c, M, P_e, P_c, P_3, D_e, w_o, w_f, g_o, g_c)} \cdot \frac{d}{dP_e} Isp_4(\theta, Rc, \gamma, T_c, M, P_e, P_c, P_3, D_e, w_o, w_f, g_o, g_c)$$

$$UMF_{Pc} := \frac{P_c}{Isp_4(\theta, Rc, \gamma, T_c, M, P_e, P_c, P_3, D_e, w_o, w_f, g_o, g_c)} \cdot \frac{d}{dP_c} Isp_4(\theta, Rc, \gamma, T_c, M, P_e, P_c, P_3, D_e, w_o, w_f, g_o, g_c)$$

$$UMF_{P3} := \frac{P_3}{Isp_4(\theta, Rc, \gamma, T_c, M, P_e, P_c, P_3, D_e, w_o, w_f, g_o, g_c)} \cdot \frac{d}{dP_3} Isp_4(\theta, Rc, \gamma, T_c, M, P_e, P_c, P_3, D_e, w_o, w_f, g_o, g_c)$$

$$UMF_{De} := \frac{D_e}{Isp_4(\theta, Rc, \gamma, T_c, M, P_e, P_c, P_3, D_e, w_o, w_f, g_o, g_c)} \cdot \frac{d}{dD_e} Isp_4(\theta, Rc, \gamma, T_c, M, P_e, P_c, P_3, D_e, w_o, w_f, g_o, g_c)$$

$$UMF_{wo} := \frac{w_o}{Isp_4(\theta, Rc, \gamma, T_c, M, P_e, P_c, P_3, D_e, w_o, w_f, g_o, g_c)} \cdot \frac{d}{dw_o} Isp_4(\theta, Rc, \gamma, T_c, M, P_e, P_c, P_3, D_e, w_o, w_f, g_o, g_c)$$

$$UMF_{wf} := \frac{w_f}{Isp_4(\theta, Rc, \gamma, T_c, M, P_e, P_c, P_3, D_e, w_o, w_f, g_o, g_c)} \cdot \frac{d}{dw_f} Isp_4(\theta, Rc, \gamma, T_c, M, P_e, P_c, P_3, D_e, w_o, w_f, g_o, g_c)$$

At this stage, the uncertainty of the specific impulse is

$$Isp_4 := Isp_4(\theta, Rc, \gamma, T_c, M, P_e, P_c, P_3, D_e, w_o, w_f, g_o, g_c)$$

$Isp_4 = 269.421s$ Specific Impulse, Isp

Let $\frac{U_{Isp}}{Isp} = \%U$ $\frac{U_\theta}{\theta} = \%\theta$ $\frac{U_{Rc}}{Rc} = \%Rc$ $\frac{U_\gamma}{\gamma} = \%\gamma$ $\frac{U_{Tc}}{T_c} = \%T_c$

$\frac{U_M}{M} = \%M$ $\frac{U_{Pe}}{P_e} = \%P_e$ $\frac{U_{Pc}}{P_c} = \%P_c$ $\frac{U_{P3}}{P_3} = \%P_3$

$\frac{U_{De}}{D_e} = \%D_e$ $\frac{U_{wo}}{w_o} = \%w_o$ $\frac{U_{wf}}{w_f} = \%w_f$

$$\%U := \sqrt{\begin{aligned}&\left(UMF_\theta \cdot \%U_\theta\right)^2 + \left(UMF_{Rc} \cdot \%U_{Rc}\right)^2 + \left(UMF_\gamma \cdot \%U_\gamma\right)^2 + \left(UMF_{Tc} \cdot \%U_{Tc}\right)^2 \ldots \\ &+ \left(UMF_M \cdot \%U_M\right)^2 + \left(UMF_{Pe} \cdot \%U_{Pe}\right)^2 + \left(UMF_{Pc} \cdot \%U_{Pc}\right)^2 + \left(UMF_{P3} \cdot \%U_{P3}\right)^2 \ldots \\ &+ \left(UMF_{De} \cdot \%U_{De}\right)^2 + \left(UMF_{wo} \cdot \%U_{wo}\right)^2 + \left(UMF_{wf} \cdot \%U_{wf}\right)^2\end{aligned}}$$

$\%U = 1.783\%$ Uncertainty of the specific impulse as in %

$U_{Isp4} := Isp_4 \cdot (\%U)$ $U_{Isp4} = 4.804s$ Uncertainty of Isp, sec.

$$UPC_X = \frac{\left(UMF_X \cdot U_X\right)^2}{U^2}$$ Uncertainty Percentage Contribution (UPC)

$$UPC_\theta := \frac{\left(UMF_\theta \cdot \%U_\theta\right)^2}{\%U^2}$$ $UPC_\theta = 0.229\%$

$$UPC_{Rc} := \frac{\left(UMF_{Rc} \cdot \%U_{Rc}\right)^2}{\%U^2}$$ $UPC_{Rc} = 1.966\%$

$$UPC_\gamma := \frac{\left(UMF_\gamma \cdot \%U_\gamma\right)^2}{\%U^2}$$ $UPC_\gamma = 22.651\%$

$$UPC_{Tc} := \frac{\left(UMF_{Tc} \cdot \%U_{Tc}\right)^2}{\%U^2}$$ $UPC_{Tc} = 70.771\%$

$$UPC_M := \frac{\left(UMF_M \cdot \%U_M\right)^2}{\%U^2}$$ $UPC_M = 1.966\%$

$$UPC_{Pe} := \frac{\left(UMF_{Pe} \cdot \%U_{Pe}\right)^2}{\%U^2}$$ $UPC_{Pe} = 0.044\%$

$$UPC_{Pc} := \frac{\left(UMF_{Pc} \cdot \%U_{Pc}\right)^2}{\%U^2}$$ $UPC_{Pc} = 1.413\%$

$$UPC_{P3} := \frac{\left(UMF_{P3} \cdot \%U_{P3}\right)^2}{\%U^2}$$ $UPC_{P3} = 0.96\%$

$$UPC_{De} := \frac{\left(UMF_{De} \cdot \%U_{De}\right)^2}{\%U^2}$$ $UPC_{De} = 0.00\%$

$$UPC_{wo} := \frac{\left(UMF_{wo} \cdot \%U_{wo}\right)^2}{\%U^2}$$ $UPC_{wo} = 0.00\%$

$$UPC_{wf} := \frac{\left(UMF_{wf} \cdot \%U_{wf}\right)^2}{\%U^2}$$ $UPC_{wf} = 0.00\%$

$$UPC_{Rc} + UPC_\gamma + UPC_{Tc} + UPC_M + UPC_{Pe} + UPC_{Pc} + UPC_{P3} + UPC_{De} + UPC_{wo} + UPC_{wf} = 100\%$$

$$UMF := \begin{pmatrix} |UMF_{\theta}| \\ |UMF_{Rc}| \\ |UMF_{\gamma}| \\ |UMF_{Tc}| \\ |UMF_{M}| \\ |UMF_{Pe}| \\ |UMF_{Pc}| \\ |UMF_{P3}| \\ |UMF_{De}| \\ |UMF_{wo}| \\ |UMF_{wf}| \end{pmatrix}$$

$UMF =$

	1
1	0.085
2	0.5
3	0.849
4	0.5
5	0.5
6	0.012
7	0.071
8	0.058
9	0
10	0
11	0

$$UPC := \begin{pmatrix} UPC_{\theta} \\ UPC_{Rc} \\ UPC_{\gamma} \\ UPC_{Tc} \\ UPC_{M} \\ UPC_{Pe} \\ UPC_{Pc} \\ UPC_{P3} \\ UPC_{De} \\ UPC_{wo} \\ UPC_{wf} \end{pmatrix} \qquad xdata := \begin{pmatrix} 1 \\ 2 \\ 3 \\ 4 \\ 5 \\ 6 \\ 7 \\ 8 \\ 9 \\ 10 \\ 11 \end{pmatrix}$$

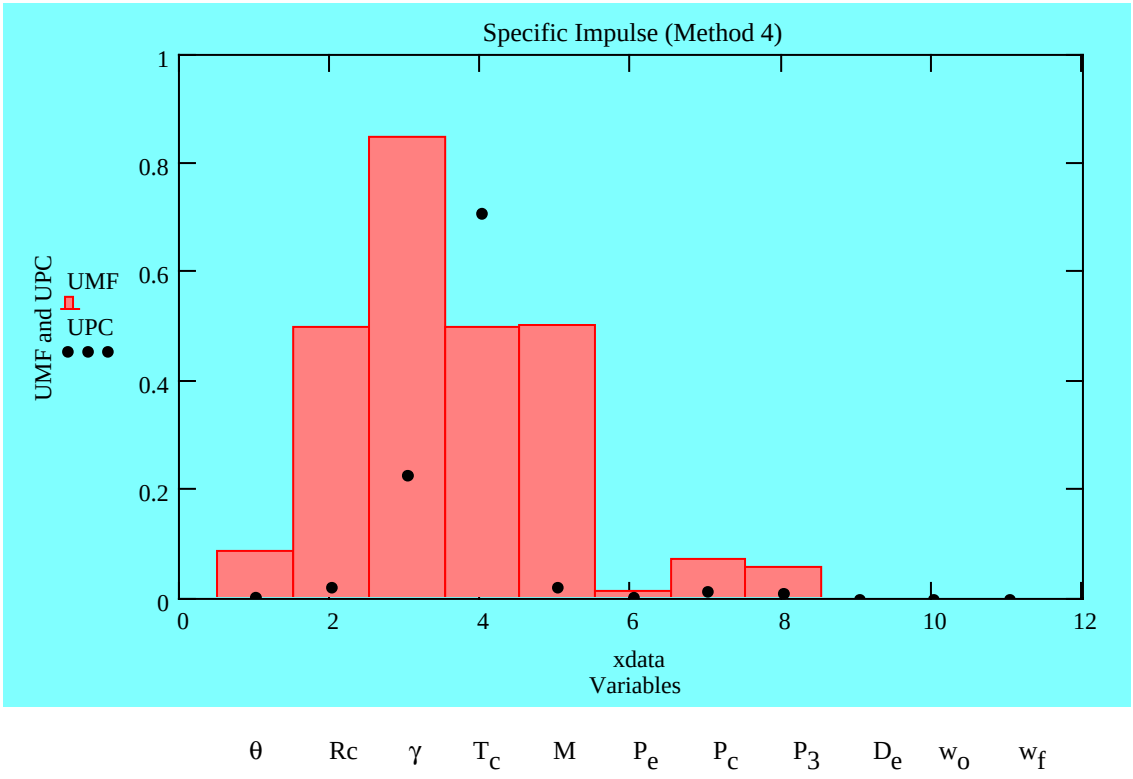

Figure D-4: UMF and UPC Values for Specific Impulse Method IV

SPECIFIC IMPULSE METHOD V

$$Isp_5(Cp_{eff}, T_c, T_e, M, P_e, P_3, D_e, w_o, w_f, g_o, g_c) := \sqrt{\frac{2 \cdot Cp_{eff} \cdot g_c}{g_o^{\,2}} \cdot \left(\frac{T_c - T_e}{M}\right)} \ldots + \frac{(P_e - P_3) \cdot \pi \cdot D_e^{\,2} g_c}{4 \cdot (w_o + w_f) \cdot g_o}$$

Yellow boxes indicate input required from the user.

Light blue boxes indicate the results obtained.

User needs to update variable input values.

$lbmol := 1$ ORIGIN:= 1

$Cp_{eff} := 11.916 \frac{BTU}{lbmol \cdot R}$ Effective specific heat constant

$T_c := 5450R$ Chamber temperature

$T_e := 2500R$ Temperature of fluid at the nozzle exit

$M := 21.5 \frac{lb}{lbmol}$ Molar mass/ molecular weight of exit fluid

$P_e := 14psi$ Nozzle exit pressure

$P_3 := 14psi$ Ambient pressure

$D_e := 0.87in$ Nozzle exit diameter

$w_o := 0.464 \frac{lb}{sec}$ Oxidizer flow rate

$w_f := 0.066 \frac{lb}{sec}$ Fuel flow rate

$g_c := 32.2 \frac{lb \cdot ft}{lbf \cdot s^2}$ Dimensionless conversion constant

$g_o := 32.2 \frac{ft}{s^2}$ gravitational acceleration at sea level

Uncertainty for each variable:

$\%U_{Cpeff} := 0.01$	uncertainty of universal gas constant
$\%U_{Tc} := 0.03$	uncertainty of chamber temperature
$\%U_{Te} := 0.03$	uncertainty of temperature of fluid at the nozzle exit
$\%U_{M} := 0.005$	uncertainty of molar mass/ moleculer weight of exit fluid
$\%U_{Pe} := 0.03$	uncertainty of nozzle exit pressure
$\%U_{P3} := 0.03$	uncertainty of ambient pressure
$\%U_{De} := 0.01$	uncertainty of nozzle exit diameter
$\%U_{wo} := 0.01$	uncertainty of oxidizer flow
$\%U_{wf} := 0.01$	uncertainty of fuel flow

$$UMF = \frac{X_i}{r} \cdot \frac{dr}{dX_i}$$ Uncertainty Magnification Factors

$$UMF_{Cpeff} := \frac{Cp_{eff}}{Isp_5\left(Cp_{eff}, T_c, T_e, M, P_e, P_3, D_e, w_o, w_f, g_o, g_c\right)} \cdot \frac{d}{dCp_{eff}} Isp_5\left(Cp_{eff}, T_c, T_e, M, P_e, P_3, D_e, w_o, w_f, g_o, g_c\right)$$

$$UMF_{Tc} := \frac{T_c}{Isp_5\left(Cp_{eff}, T_c, T_e, M, P_e, P_3, D_e, w_o, w_f, g_o, g_c\right)} \cdot \frac{d}{dT_c} Isp_5\left(Cp_{eff}, T_c, T_e, M, P_e, P_3, D_e, w_o, w_f, g_o, g_c\right)$$

$$UMF_{Te} := \frac{T_e}{Isp_5\left(Cp_{eff}, T_c, T_e, M, P_e, P_3, D_e, w_o, w_f, g_o, g_c\right)} \cdot \frac{d}{dT_e} Isp_5\left(Cp_{eff}, T_c, T_e, M, P_e, P_3, D_e, w_o, w_f, g_o, g_c\right)$$

$$UMF_{M} := \frac{M}{Isp_5\left(Cp_{eff}, T_c, T_e, M, P_e, P_3, D_e, w_o, w_f, g_o, g_c\right)} \cdot \frac{d}{dM} Isp_5\left(Cp_{eff}, T_c, T_e, M, P_e, P_3, D_e, w_o, w_f, g_o, g_c\right)$$

$$UMF_{Pe} := \frac{P_e}{Isp_5\left(Cp_{eff}, T_c, T_e, M, P_e, P_3, D_e, w_o, w_f, g_o, g_c\right)} \cdot \frac{d}{dP_e} Isp_5\left(Cp_{eff}, T_c, T_e, M, P_e, P_3, D_e, w_o, w_f, g_o, g_c\right)$$

$$UMF_{P3} := \frac{P_3}{Isp_5\left(Cp_{eff}, T_c, T_e, M, P_e, P_3, D_e, w_o, w_f, g_o, g_c\right)} \cdot \frac{d}{dP_3} Isp_5\left(Cp_{eff}, T_c, T_e, M, P_e, P_3, D_e, w_o, w_f, g_o, g_c\right)$$

$$UMF_{De} := \frac{D_e}{Isp_5\left(Cp_{eff}, T_c, T_e, M, P_e, P_3, D_e, w_o, w_f, g_o, g_c\right)} \cdot \frac{d}{dD_e} Isp_5\left(Cp_{eff}, T_c, T_e, M, P_e, P_3, D_e, w_o, w_f, g_o, g_c\right)$$

$$UMF_{wo} := \frac{w_o}{Isp_5\left(Cp_{eff}, T_c, T_e, M, P_e, P_3, D_e, w_o, w_f, g_o, g_c\right)} \cdot \frac{d}{dw_o} Isp_5\left(Cp_{eff}, T_c, T_e, M, P_e, P_3, D_e, w_o, w_f, g_o, g_c\right)$$

$$UMF_{wf} := \frac{w_f}{Isp_5\left(Cp_{eff}, T_c, T_e, M, P_e, P_3, D_e, w_o, w_f, g_o, g_c\right)} \cdot \frac{d}{dw_f} Isp_5\left(Cp_{eff}, T_c, T_e, M, P_e, P_3, D_e, w_o, w_f, g_o, g_c\right)$$

At this stage, the uncertainty of the specific impulse is

$$Isp_5 := Isp_5(Cp_{eff}, T_c, T_e, M, P_e, P_3, D_e, w_o, w_f, g_o, g_c)$$

$Isp_5 = 281.113s$ Specific Impulse, Isp

Let $\frac{U_{Isp}}{Isp} = \%U$ $\frac{U_{Cpeff}}{Cp_{eff}} = \%Cp_{eff}$ $\frac{U_{Tc}}{T_c} = \%T_c$ $\frac{U_{Te}}{T_e} = \%T_e$

$\frac{U_M}{M} = \%M$ $\frac{U_{Pe}}{P_e} = \%P_e$ $\frac{U_{P3}}{P_3} = \%P_3$ $\frac{U_{De}}{D_e} = \%D_e$

$\frac{U_{wo}}{w_o} = \%w_o$ $\frac{U_{wf}}{w_f} = \%w_f$

$$\%U := \sqrt{\left[\left(UMF_{Cpeff}\cdot\%U_{Cpeff}\right)^2 + \left(UMF_{Tc}\cdot\%U_{Tc}\right)^2 + \left(UMF_{Te}\cdot\%U_{Te}\right)^2 + \left(UMF_{M}\cdot\%U_{M}\right)^2\right] \ldots + \left(UMF_{Pe}\cdot\%U_{Pe}\right)^2 + \left(UMF_{P3}\cdot\%U_{P3}\right)^2 + \left(UMF_{De}\cdot\%U_{De}\right)^2 \ldots + \left(UMF_{wo}\cdot\%U_{wo}\right)^2 + \left(UMF_{wf}\cdot\%U_{wf}\right)^2}$$

$\%U = 3.10869\%$ Uncertainty of the specific impulse as in %

$U_{Isp5} := Isp_5\cdot(\%U)$ $U_{Isp5} = 8.739s$ Uncertainty of Isp, sec.

$$UPC_X = \frac{(UMF_X \cdot U_X)^2}{U^2}$$ Uncertainty Percentage Contribution (UPC)

$$UPC_{Cpeff} := \frac{(UMF_{Cpeff} \cdot \%U_{Cpeff})^2}{\%U^2}$$ $UPC_{Cpeff} = 2.587\%$

$$UPC_{Tc} := \frac{(UMF_{Tc} \cdot \%U_{Tc})^2}{\%U^2}$$ $UPC_{Tc} = 79.465\%$

$$UPC_{Te} := \frac{(UMF_{Te} \cdot \%U_{Te})^2}{\%U^2}$$ $UPC_{Te} = 16.721\%$

$$UPC_{M} := \frac{(UMF_{M} \cdot \%U_{M})^2}{\%U^2}$$ $UPC_{M} = 0.647\%$

$$UPC_{Pe} := \frac{(UMF_{Pe} \cdot \%U_{Pe})^2}{\%U^2}$$ $UPC_{Pe} = 0.29\%$

$$UPC_{P3} := \frac{(UMF_{P3} \cdot \%U_{P3})^2}{\%U^2}$$ $UPC_{P3} = 0.29\%$

$$UPC_{De} := \frac{(UMF_{De} \cdot \%U_{De})^2}{\%U^2}$$ $UPC_{De} = 0.00\%$

$$UPC_{wo} := \frac{(UMF_{wo} \cdot \%U_{wo})^2}{\%U^2}$$ $UPC_{wo} = 0.00\%$

$$UPC_{wf} := \frac{(UMF_{wf} \cdot \%U_{wf})^2}{\%U^2}$$ $UPC_{wf} = 0.00\%$

$$UPC_{Cpeff} + UPC_{Tc} + UPC_{Te} + UPC_{M} + UPC_{Pe} + UPC_{P3} + UPC_{De} + UPC_{wo} + UPC_{wf} = 100\%$$

$$UMF := \begin{pmatrix} |UMF_{Cpeff}| \\ |UMF_{Tc}| \\ |UMF_{Te}| \\ |UMF_{M}| \\ |UMF_{Pe}| \\ |UMF_{P3}| \\ |UMF_{De}| \\ |UMF_{wo}| \\ |UMF_{wf}| \end{pmatrix} \quad UMF = \begin{pmatrix} 0.5 \\ 0.924 \\ 0.424 \\ 0.5 \\ 0.056 \\ 0.056 \\ 0 \\ 0 \\ 0 \end{pmatrix} \quad UPC := \begin{pmatrix} UPC_{Cpeff} \\ UPC_{Tc} \\ UPC_{Te} \\ UPC_{M} \\ UPC_{Pe} \\ UPC_{P3} \\ UPC_{De} \\ UPC_{wo} \\ UPC_{wf} \end{pmatrix} \quad xdata := \begin{pmatrix} 1 \\ 2 \\ 3 \\ 4 \\ 5 \\ 6 \\ 7 \\ 8 \\ 9 \end{pmatrix}$$

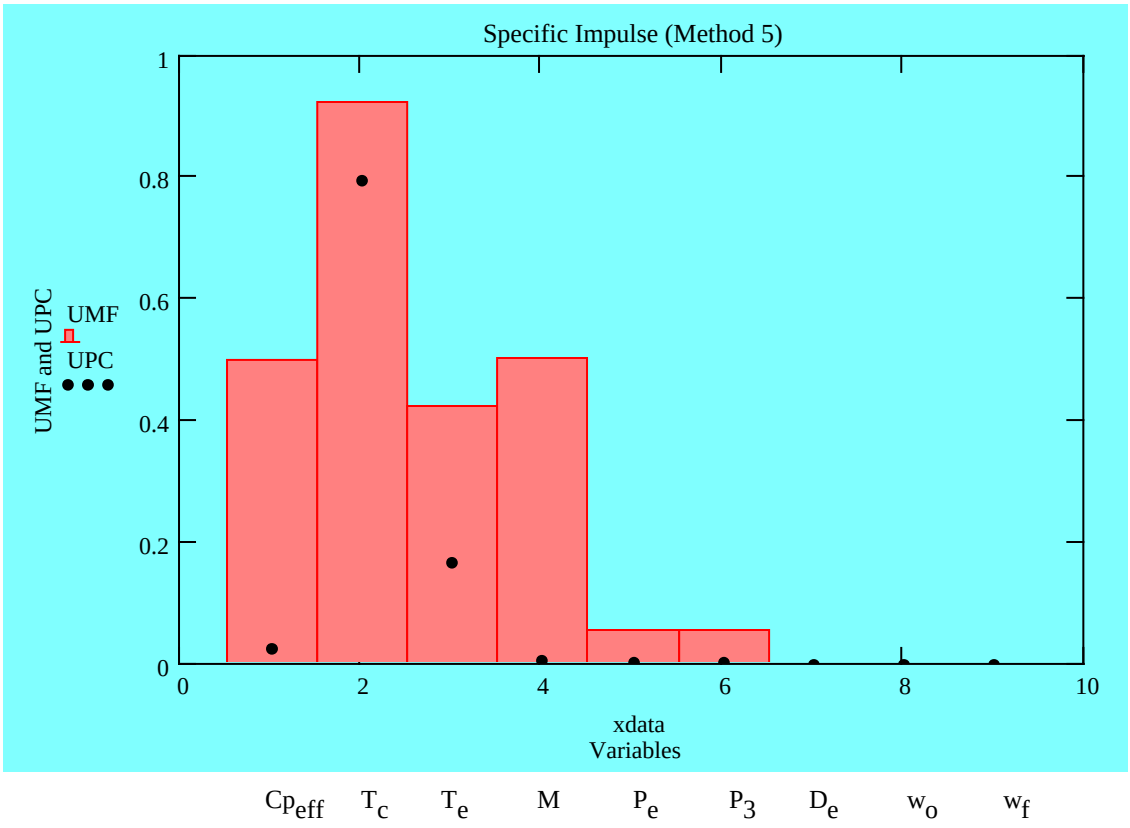

Figure D-5: UMF and UPC Values for Specific Impulse Method V